T.R.

GEBZE TECHNICAL UNIVERSITY

GRADUATE SCHOOL OF NATURAL AND APPLIED SCIENCES

DESIGN AND IMPLEMENTATION OF A NEW BATTERY TOPOLOGY FOR ELECTRIC VEHICLES: HYBRID BATTERY SYSTEM

TÜREV SARIKURT

A THESIS SUBMITTED FOR THE DEGREE OF

DOCTOR OF PHILOSOPHY

DEPARTMENT OF ELECTRONIC ENGINEERING

GEBZE

2016

T.R.

GEBZE TECHNICAL UNIVERSITY

GRADUATE SCHOOL OF NATURAL AND APPLIED SCIENCES

DESIGN AND IMPLEMENTATION OF A NEW BATTERY TOPOLOGY FOR ELECTRIC VEHICLES: HYBRID BATTERY SYSTEM

TÜREV SARIKURT

A THESIS SUBMITTED FOR THE DEGREE OF

DOCTOR OF PHILOSOPHY

DEPARTMENT OF ELECTRONIC ENGINEERING

THESIS SUPERVISOR

ASSOC. PROF. DR. ABDULKADİR BALIKÇI

GEBZE

2016

T.C.

GEBZE TEKNİK ÜNİVERSİTESİ

FEN BİLİMLERİ ENSTİTÜSÜ

ELEKTRİKLİ ARAÇLAR İÇİN YENİ BİR BATARYA TOPOLOJİSİ GELİŞTİRME VE UYGULAMA: HİBRİD BATARYA SİSTEMİ

TÜREV SARIKURT

DOKTORA TEZİ

ELEKTRONİK MÜHENDİSLİĞİ ANABİLİM DALI

DANIŞMANI

DOÇ. DR. ABDULKADİR BALIKÇI

GEBZE

2016

GEBZE TEKNİK ÜNİVERSİTESİ	**DOKTORA JÜRİ ONAY FORMU**

GTÜ Fen Bilimleri Enstitüsü Yönetim Kurulu'nun 27/06/2016 tarih ve 2016/43 sayılı kararıyla oluşturulan jüri tarafından 26/07/2016 tarihinde tez savunma sınavı yapılan Türev SARIKURT'un tez çalışması Elektronik Mühendisliği Anabilim Dalında DOKTORA tezi olarak kabul edilmiştir.

JÜRİ

ÜYE
(TEZ DANIŞMANI) : Doç. Dr. Abdulkadir BALIKÇI

ÜYE : Prof. Dr. Mehmet Hakan HOCAOĞLU

ÜYE : Doç. Dr. Ahmet Faruk BAKAN

ÜYE : Yrd. Doç. Dr. Tuba GÖZEL

ÜYE : Yrd. Doç. Dr. Uğur HASIRCI

ONAY

Gebze Teknik Üniversitesi Fen Bilimleri Enstitüsü Yönetim Kurulu'nun

...../...../..... tarih ve ...../..... sayılı kararı.

İMZA/MÜHÜR

SUMMARY

In this work, a new energy management system called Hybrid Battery System (HBS) is proposed in order to recommend a solution to drawbacks of battery electric vehicles, which are short driving range and low performance. Existing battery models are investigated, and a novel analytical battery model is proposed to use in simulations. The model is validated by experiments. Furthermore another model which indicates the relative capacity is also developed in the study. But this model become redundant because of the energy management strategy of HBS.

In general HBS consists of two different cells where one of them has high energy and the other has high power densities. Hybrid Battery concept is based on simultaneous use of the cells and the major task is to control energy share between the cells. At first a passive energy management system is proposed and constructed. However an active energy management system with battery voltage balancing feature is designed, analysed, simulated and built as the objective.

Key Words: Battery Electric Vehicles, Lithium-Ion Cells, Battery Model, Relative Capacity Estimation, Energy Management System.

ÖZET

Bu çalışmada tam elektrikli araçların düşük performans, kısa menzil gibi problemlerinin çözümü için Hibrid Batarya Sistemi olarak adlandırılan bir enerji sistemi önerilmiştir. Benzetimlerde kullanılmak üzere batarya modelleri incelenmiş özgün sayısal bir batarya modeli önerilmiş, önerilen modelin geçerliliği deneyler yardımıyla gösterilmiştir. Ayrıca çalışma kapsamında bataryanın kullanılabilir kapasitesini gösteren bir model daha geliştirilmiştir. Ancak tercih edilen enerji yönetim stratejileri nedeniyle bu model çalışmanın ilerleyen bölümlerinde kullanılmamıştır.

Genel olarak Hibrid Batarya konsepti birisi yüksek enerji yoğunluğuna, diğeri yüksek güç yoğunluğuna sahip iki farklı bataryanın birlikte kullanılmasına dayanmaktadır ve temel amaç bataryalar arasındaki enerji dağılımının kontrol edilmesidir. Tez kapsamında öncelikle pasif bir enerji yönetim sistemi tasarlanmış ve gerçekleştirilmiştir. Ancak nihai hedef olarak dengeleme özelliğine de sahip aktif bir enerji yönetimi önerilmiş, tasarımı ve analizi yapılmış ve gerçekleştirilmiştir.

Anahtar Kelimeler: Tam Elektrikli Araçlar, Lityum-İyon Bataryalar, Batarya Modeli, Kullanılabilir Kapasite Kestirimi, Enerji Yönetim Sistemi.

ACKNOWLEDGEMENTS

I would like to express my deep gratitude to my supervisor and research guide, Assoc. Prof. Dr. Abdulkadir BALIKÇI, for his support, immense knowledge, motivation and obviously patience. His suggestions and valuable supervision helped me in all the time of this research.

Besides my advisor, I would like to thank the rest of my thesis committee, Prof Dr. M. Hakan. HOCAOĞLU, for his sincere counsel and guidance, and Assoc. Prof. Dr. A. Faruk BAKAN, for his insightful comments and encouragement.

I thank to my fellow colleagues and friends, M. Burak ÖZAKIN, Murat CEYLAN and Umut ÖNDİN, whom I gained a lot from, through their personal and scholarly interactions, their recommendations and our constructive discussions. I also thank to all the lab mates in Power Systems Laboratory.

I owe a lot to my parents, who encouraged and helped me at every stage of my personal and academic life, and longed to see this achievement come true. I thank them for their persistent support and prayers.

Finally, I want to thank my wife, Derya AYDIN SARIKURT, for the inspiration she has been to me through her perspective on life, for her love and support.

This thesis study is supported by TUBİTAK under 2211-C programme. Battery modeling and SoH estimation parts are also supported by TUBİTAK project number of 110E209.

TABLE of CONTENTS

LIST of ABBREVIATIONS and ACRONYMS

Abbreviations and Acronyms		Explanations
BEV	:	Battery Electric Vehicle
BMS	:	Battery Management System
CN	:	Cycle Number
EMS	:	Energy Management System
EV	:	Electric Vehicle
HBS	:	Hybrid Battery System
HEV	:	Hybrid Electric Vehicle
LTO	:	Lithium Titanate
NMC	:	Lithium Nickel-Manganese-Cobalt-Oxide
PHEV	:	Plug-in Hybrid Electric Vehicles
RC	:	Relative Capacity
RCN	:	Reference Cycle Number
SC	:	Supercapacitor
SoC	:	State of Charge
SoH	:	State of Health

LIST of FIGURES

LIST of TABLES

1. INTRODUCTION

Dependency on fossil fuels is the main reason of most of environmental problems today. The effects of fossil fuel usage in conventional transportation can be divided as direct and indirect effects. Increase in air and noise pollution are direct effects. Indirect effects can be listed as decrease the soil and water quality, appearance of oil spills and acid rains, shifting the reduction of biodiversity, and obviously global warming and climate change. Air pollutants are substances that adversely affect the environment by interfering with climate, the physiology of plants, animal species, entire ecosystems, as well as with human property in the form of agricultural crops or man-made structures [1].

Resulting pollutants of fossil fuel usage are investigated under four headlines, which are gaseous pollutants (including lead (Pb), carbon monoxide (CO), carbon dioxide (CO2; not a pollutant), methane (CH4), nitrogen oxides (NOx), nitrous oxide (N2O), chlorofluorocarbons (CFCs), perfluorocarbons (PFCs), silicon tetraflouride (SF6), benzene and volatile components (BTX), ozone), persistent organic pollutants (e.g. dioxins), heavy metals (e.g. lead, mercury, zinc, chrome, copper and cadmium) and particulate matter (ash, dust) [2], [3]. Gaseous pollutants such as carbon monoxide (CO), sulfur dioxide (SO2), nitrogen oxides (NOx), volatile organic compounds (VOCs), ozone (O3) are mainly due to combustion of fossil fuels [4]. Respiratory, cardiovascular, nervous, urinary and digestive systems are directly affected by the high air pollution concentration. Long-term exposure to lower pollutant concentrations have similar effects as well. Air pollution can also has hazardous effects during pregnancy because pollutants affect the developing foetus. Besides hazardous effects of air pollutants in cellular basis are also proven where a review is available in [2].

Furthermore, security of future oil supply and its price stability are uncertain. 900.000.000 vehicles in all around the earth consumes 20.000.000 barrels of crude oil per day according to 2012 report of IEA named world energy outlook. Furthermore according to the same report the vehicle count is expected to be 1.7 billion by the year 2035 [5]. For this purpose hybrid electric vehicles must be accepted as transition

phase as battery electric vehicles are the ultimate solution. According to Turkish Statistical Institute (TUIK), by January 2016 there are 20.098.994 vehicles exist in Turkey [6]. Also, again according to a report prepared by TUIK which ended in 2015, carbon dioxide emissions are 459.1 million tonnes per year for 2013. 82.2 % of this amount is because of energy production and distribution [7]. Also according to another local report 12% of total carbon emissions are caused from road transportation [8]. According to an investigation of IEA among EVI (Electric Vehicles Initiative) member countries, the ratio of electric vehicles over all vehicles is 0.08% [9]. In Turkey, in 2015 the amount of total automobiles sold is 725.596 where only 120 of them are electric vehicles [10]. 38 of them have under 85 kW and 82 of them have over 121 kW battery capacity. As a result the ratio of electric vehicles sold in Turkey in 2015 over all road vehicles is 0.0165 %.

1.1. Motivation

Electric vehicles (EV) are important alternatives on clean transportation and expected to gain significant market share in near future [11]. Electric vehicles (EVs) can be classified as Hybrid Electric Vehicles (HEVs) in which an electric motor is used alongside an internal combustion engine, Plug-in Hybrid Electric Vehicles (PHEVs) which can be charged externally and Battery Electric Vehicles (BEVs) in which only propulsion mechanism is an electric motor. Main deficiencies of BEVs are short driving range with single charge, low life span of battery stacks and low performance.

BEVs are the optimum way of clean transportation without any pollutant emission. The power source of a BEV needs to have both high power and high energy densities in order to extend driving range and increase performance. Lithium-Ion, is the most energy and power dense battery type when compared with the other types, however none of commercial batteries provide both energy and power ratings together. Therefore mostly battery-supercapacitor (SC) hybrid systems including high energy batteries and high power SCs are used. SCs have higher power densities and longer cycle life than batteries, however they are heavy, have longer charge and discharge times, high self-discharge rates, and low energy densities [12], [13]. By 2013 average energy densities for SC are 05 to 15 Wh/kg. Life cycle of SCs is around

several 100000s and power density is around 15 kW/kg. There are numbers of lithium cells and SCs which are commercially available. Hence Ragone plots or charts are used to indicate for comparison of energy and power densities of electrical sources. A recent example of Ragone chart is shown in Figure 1.1.

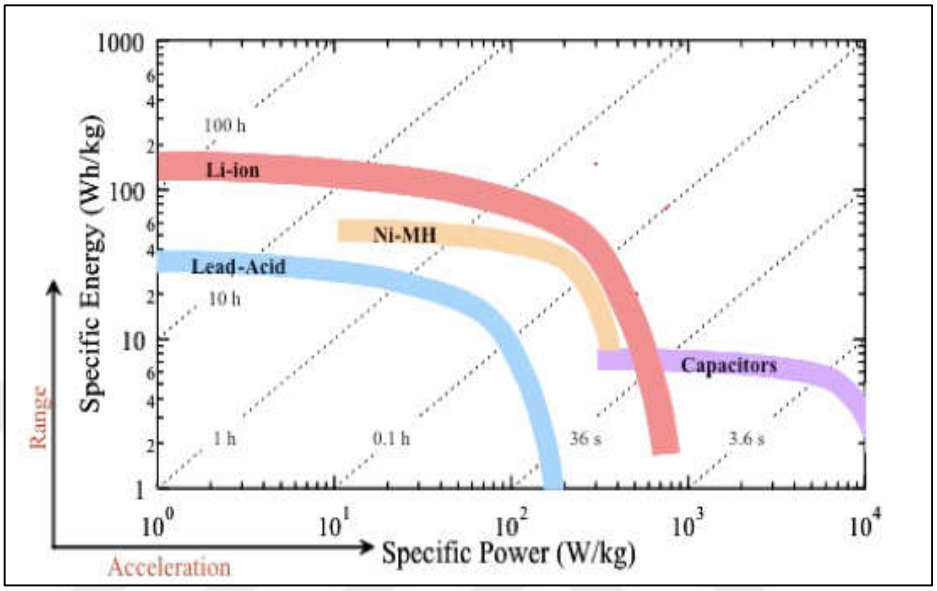

Figure 1.1: A Ragone chart.

Besides, following the development in lithium battery technologies, features of lithium batteries are improving while the prices decrease. Thus a suitable battery can be used rather than a SC in order to maintain high power.

The main purpose of this study is to develop an energy system formed by a battery-battery hybrid. This concept is named as Hybrid Battery System (HBS). HBS consists of two different battery types. One type should have high energy density and the other should have high power density. For this purpose, in this study power dense LTO [14] and energy dense NMC [15] cells are used. Energy share between these batteries is arranged such that the LTO cell supplies most of the charge in power demanding parts of the course, and NMC cell supports the LTO cell. With this arrangement the drawn current from energy dense cell is limited. Hence, high power will be drawn from power dense cell and the power dense cell is supported by energy dense cell, consequently the overall performance of the vehicle will be increased and driving range will be extended.

1.2. Objectives

In EVs energy management is a complicated task. Many approaches which have different purposes for different vehicle types exist in the literature. For example in HEVs main objective is to decrease fuel consumption, while in SC-battery hybrids the goal is to extend battery range by drawing high transient currents from the SC which has higher power density. A comprehensive review is provided in Section 4.1. Voltage imbalances between cells which form a battery pack is also a problem. In order to increase efficiency, this situation should be resolved by a method which is not based on energy dissipation.

Energy management of HBS is mainly based of determining the level of shared load current between different cell types. There are different approaches to follow for this purpose. For most of these alternatives battery state parameters such as SoH or SoC must be estimated accurately.

Simulations have great importance in EV studies. The most important components of these applications are batteries and to develop accurate battery models is crucial. One of the objectives of this study is to investigate existing battery models in the literature and develop different battery models for different purposes. Also another objective is to investigate SoH estimation methods and propose a simple and accurate method.

Main objective of this thesis is to introduce the hybrid battery concept and show the feasibility of Hybrid Battery System with application. For this purpose the energy management. For this purpose investigation of existing energy management strategies and implementation of a novel system, which is designed according to the specifications of the cells and requirements of the HBS, is aimed. Also battery voltage imbalances needs to be handled by the system. In this way validity of the hybrid battery concept and success of the HBS with suitable components will be demonstrated.

1.3. Thesis structure and content

Thesis report is divided to 4 sections. In the next section battery modelling studies and a detailed review about modelling approaches are provided. Firstly a novel analytical battery model is introduced. Model is based on capacity estimation. Therefore it is capable of SoC estimation. This study is accepted to be presented in ECRES 2016 conference. Another model which was introduced is an electric equivalent circuit model. This model was proposed in several symposiums and conferences, such as EVK [16], ISIE [17] and ENERGYCON [18]. The model is used in SoH estimation studies. A third model which is introduced in this section is a generic model, provided by Simulink software. This model modified in order to represent batteries and used in energy management simulations. Both of the three models are validated with experiments.

In the third section battery SoH estimation method is introduced. First a detailed review is presented about SoH estimation approaches. Proposed method is based on representing SoH by using relative capacity (RC) of a battery. Hence, a parametric RC model is proposed for SoH estimation, which is also presented in several symposiums or conferences such as ISIE [17] and ENERGYCON [18]. Also, in the context of this thesis the RC model is edited and simplified. This version is presented as the slope approach. Both RC models are validated with experiments.

The fourth section is about HBS. In this section firstly the hybrid battery concept is introduced. As the main objective is to develop an EMS for HBS, EMS approaches are investigated in the study. A detailed review of the literature is also provided in this section. Two different EMS approaches are proposed in the thesis. The first one, the passive approach is based on direct, parallel connection of different type cells. In this approach none active components are used. This study is published as a chapter in the book, Progress in Clean Energy [19]. The second EMS approach is an active EMS. A bidirectional converter is used for energy transfer between two cells. A research on bidirectional DC/DC converters is done for this purpose, and a literature review is presented within this section. Later on, first a single level then a two level system is designed, simulated and implemented.

2. BATTERY MODELLING

When compared to other secondary battery types, a lithium-ion battery has relatively higher volumetric energy and power densities, low self-discharge rate and very small memory effect. Therefore, they are preferred and used in a wide scale of applications such as home and portable electronics or EVs [20]–[24]. Battery models are important in design and simulation stages of these applications.

Two type of lithium-ion batteries with different anode structures are used in this study. Both batteries are automotive grade and in pouch type. The chemistries of the batteries are lithium-titanate – LTO ($Li_4Ti_5O_{12}$) [14], and lithium-nickel-manganese-cobalt-oxide – NMC ($LiNiMnCoO_4$) [15]. The properties of the batteries are compared in Table 2.1.

Two basic routines, which have to be mentioned separately, are commonly used during the study. First is the charging and discharging routines during aging. Especially NMC cells are subjected to this routines during aging process. The details of this process is provided by the manufacturer and following rules are followed:

- Charge: Batteries are charged with constant 11 A (1 C) until the terminal voltage reaches 4.2 V (Constant current mode). Than charging continued in the same terminal voltage until charging current stays in 0. 55 A (0.05 C) for a specific time (Constant voltage mode)
- Discharge: Batteries are discharged with constant 11 A (1 C) until the terminal voltage drops down to 3.0 V.
- Rest time: Batteries are rested between charge and discharge processes for 10 minutes [15].

The other routine is capacity tests. To obtain actual capacities of batteries, a fully charged battery is totally discharged with 1 C constant current (11 A for NMC and 13 A for LTO). The discharge time is recorded and compared with 3600 seconds.

Table 2.1: Comparison of the properties of the batteries.

Properties	**Battery Model**	
Model name	Kokam SLBP55205130H	Altairnano 13Ah
Type	NMC	LTO
Chemistry	$LiNiMnCO_4$	$Li_4Ti_5O_{12}$
Nominal voltage	3.7 V	2.25 V
Nominal capacity	11 Ah	13 Ah
Maximum continuous charge current	33 A	130 A
Maximum continuous discharge current	88 A	130 A
Maximum peak discharge current	110 A	260 A
Weight	280 g	400 g
Energy	42 Wh	29 Wh
Maximum power (at 50% SoC)	380 W	670W
Energy density	150 Wh/kg	73 Wh/kg
Power density	1357 W/kg	1675 /kg
Length of life (Cycles)	1400	16000

2.1. Background

A lithium-ion battery has complex electrochemical structure and nonlinear characteristics. Therefore, modelling of a battery is a tedious task. The criteria for designing a battery model and comparing it with existing models can be summarized as; accuracy of the model, length of calculations used for model, the number of parameters and contribution required from other scientific disciplines [16], [17], [25]. In addition, the duration of repeating experiments also increases the difficulty of modelling. For example, for health modelling, the experiments continue until the end of battery life, which may last for months.

Battery models may be classified as electrochemical, statistical, analytical and electrical equivalent circuit models according to the available literature [25]–[27].

Electrochemical or physical models are based on internal chemical reactions of batteries. Therefore these models are highly accurate and complicated. An electrochemical model requires long computational time because it includes several number of nonlinear equations. Electrochemical models are very detailed but some of these details are unnecessary for some studies [25], [26], [28]–[30].

Statistical or stochastic models are based on extracting meaningful information from experiments instead of using internal chemical characteristics [31]. They require less computational time although they are not as accurate as physical models. Statistical data for these type of models are collected through several experimental scenarios. Accuracy of these models decrease when tested within conditions different than experimental scenarios. There are different examples of this type of modelling including stochastic [32] or semi-empirical approaches [33], statistical analysis [34] and fuzzy neural network [35].

Analytical modelling can be accepted to begin with a pseudo-two-dimensional model [36] or a kinetic battery model in which the recovery effect is mainly investigated [37]. Besides, early examples of analytical models are based on indicating remaining charge of batteries [38]. In analytical models battery condition and characteristics are indicated as analytical expressions. Because of the analytical structure, these models need less computational time. However, analytical models generally represent the fundamental principles of electrochemistry [39]–[41].

The most important advantage of modelling batteries as electrical circuits is capability to make mathematical extractions by using circuit analysis theories. Therefore these models are used successfully in several areas including EV applications. Battery parameters are represented as circuit elements or subcircuits in this approach. Values for parameters can be evaluated either by advanced chemical techniques such as EIS (Electrochemical impedance spectrometry) [42] or experimental data [17], [43], [44]. Complexity of the model increases with detail level. An equivalent circuit battery model may include even a single [17], [45] or two resistor-capacitor subcircuits [46], [47] or more subcircuits including more RC pairs [48] depending on detail level.

Within the scope of this thesis two different battery models are investigated and proposed. One of the proposed model is a simple analytical model. This model

includes just a couple of equations, representing charge and discharge models of the battery. Accuracy of the model is around 4%. The purpose of the analytical model was to use it with metaheuristic methods and optimisation algorithms, for a smart energy management system. During the process of thesis, the idea of a smart energy management system is abandoned. Therefore this modelling method isn't preferred in any stage of the study. Yet a comprehensive infrastructure about analytical modelling is built. The modelling method, which is also very simple, is introduced in details in this thesis either. The method is validated by modelling different types of lithium model.

Second model is an electric equivalent circuit model which was proposed in earlier studies [16], [17] and used in several other studies [18], [49]. The model includes a single R/C pair. The parameters of the model are derived from several experiments. Both details of experimental study and validation of the model is included to this chapter.

Generally a thermal management system exists in EVs. Thus the battery temperature is limited in a desired band. Both of two proposed models are designed for EV applications, consequently none of them reflects neither the ambient or cell temperature nor thermal effects. Analytical model is needed. For this reason no aging experiments were conducted during building of the model and is based on representing the change in battery capacity under different circumstances. The electric equivalent circuit is suitable for health applications and includes aging effects. But only NMC cells could be modelled because of long experimental study required. Therefore another model is needed for some phases of the study. For this reason a generic battery model of Matlab/Simulink is arranged to represent existing batteries. The accuracy of generic models are also presented in this chapter.

2.2. Analytical Battery Model

In general, analytical battery models are based on representing state of charge or capacity of a battery as a mathematical function. A simple analytical model can be easily implemented in EV applications, especially in energy management studies, where the main objective is to control the energy share between sources. For this

purpose, numerical analysis methods or heuristic optimization techniques may be preferred more, if a simple model, which is suitable to be embedded in algorithms or iterative solution methods, is used. As a result, solution accuracy may be increased while calculation time may be decreased.

A healthy and unaged battery will be totally discharged in 1 hour, if it is discharged with its nominal current. The charge which is consumed in 1 hour by drawing nominal current is called the nominal capacity. Nominal capacities of the LTO and NMC cells are 13 Ah and 11 Ah respectively [14], [15]. According to Peukert's law, available capacity of a battery decreases as discharge rate increases [50]. Because of this fact, an acception about linear relationship between battery capacity and discharge current is not proper. Therefore, in this study, the effect of different charge or discharge rates on battery capacity is investigated and the capacity change in any discharge or charge current rates is modelled. Thus the analytical battery model consist of two components, charge and discharge models.

To generate the discharge model, fully charged batteries are totally discharged with various load currents, and the discharge durations are recorded. By using this time values, three individual equations for battery discharge time (depending on discharge current) are generated. Than the discharge model is created by modifying the most accurate equation. The model gives the amount of capacity used, after discharging the battery with a specific current for a specific time. Charge model is also created in the same way. Batteries are charged with various currents and charging durations are recorded. This model gives the amount of capacity increased, after charging with a specific current for a specific time.

2.2.1. Modelling of LTO Cell

Maximum and minimum voltage limits are 2.8 V and 1.9 V in 30oC, respectively for LTO cells. Discharge experiments are conducted with constant currents of 6.5 A (0.5 C), 13 A (1 C), 26 A (2 C), 39 A (3 C), 52 A (4 C), 65 A (5 C), 78 A (6 C) and 100 A, as the nominal current of an LTO cell is 11 A. Maximum discharge current is chosen as 100 A because of the limitations of DC power source. Similarly charge experiments are also operated with same current levels. Discharge and charge curves for every

current level are given respectively in Figure 2.1 and Figure 2.2. Discharge and charge durations corresponding these experiments are given in Table 2.2.

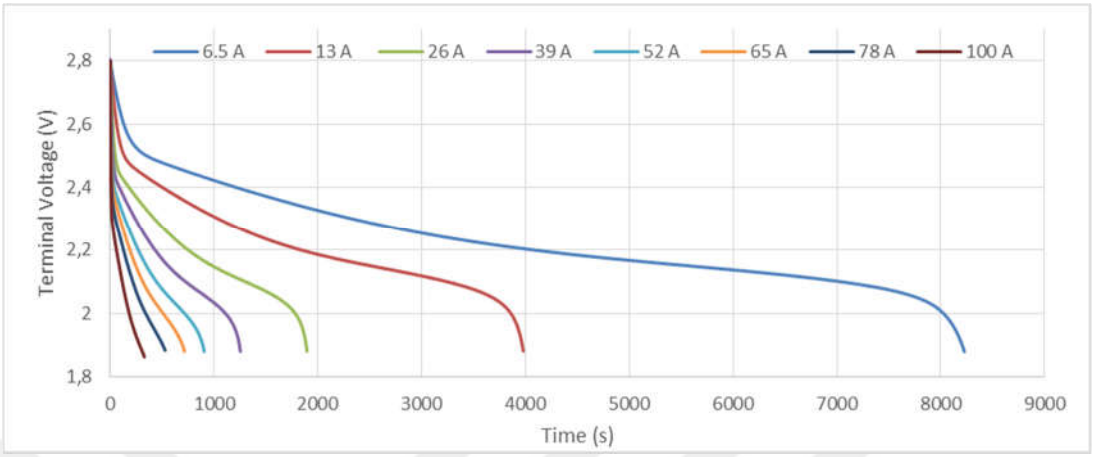

Figure 2.1: Discharge curves of LTO cell for different current rates.

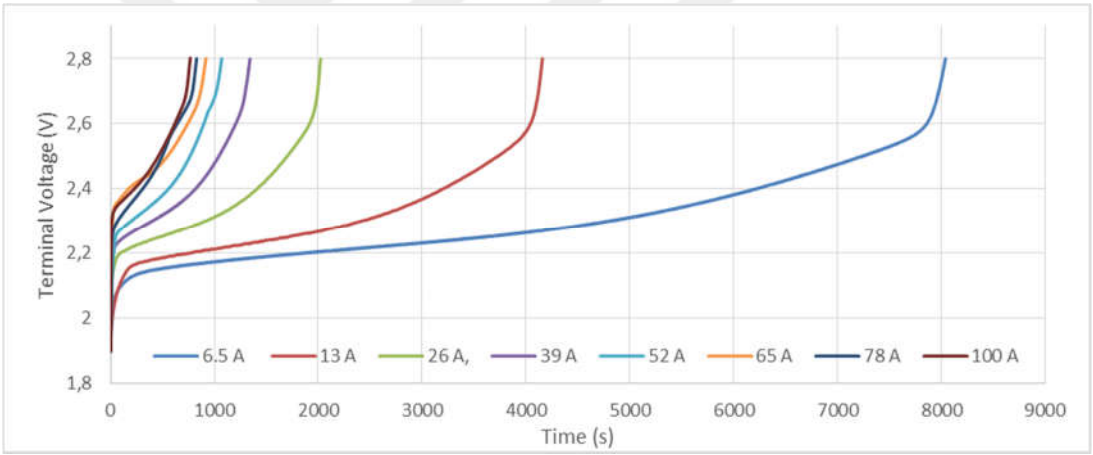

Figure 2.2: Charge curves of LTO cell for different current rates.

Table 2.2: Charge and discharge durations of LTO cell for different current rates.

Current (A)	6,5	13	26	39	52	65	88	100
Charge Duration (s)	8033	4142	2022	1342	1066	917	823	766
Discharge duration (s)	8199	3970	1889	1245	893	697	505	286

2.2.1.1. Discharge Model of the LTO Cell

Three equations which give discharge durations $\left(t_{discharge}\right)$ depending on discharge currents are generated by using three different curve fitting scheme. These are:

$$t_{discharge1} = 60930\ I^{-1.07} \tag{2.1}$$

$$t_{discharge2} = 54570\ I^{-1.001} - 183.9 \tag{2.2}$$

$$t_{discharge3} = \frac{0.06066\ I^3 + 6.979\ I^2 - 560.7\ I + 52070}{I - 0.03522} \tag{2.3}$$

where I is the discharge current. Later these equation are modified to build a discharge model ($f_{cap_{discharge}}$) to show used capacity. These models are given in Eq. (2.4), (2.5), and (2.6).

$$f_{cap_{discharge1}} = \frac{13\ t}{60930\ I^{-1.07}} \tag{2.4}$$

$$f_{cap_{discharge2}} = \frac{13\ t}{54570\ I^{-1.001} - 183.9} \tag{2.5}$$

$$f_{cap_{discharge3}} = \frac{13\ t\ (I - 0.03522\ )}{0.06066\ I^3 + 6.979\ I^2 - 560.7\ I + 52070} \tag{2.6}$$

Models give the used capacity in terms of Ah if current I is drawn from the battery for t seconds.

Each of three models are evaluated with discharge durations given in

Table 2.2. Results of the models are compared with nominal capacity of the LTO cell. Comparison of the models are given in Figure 2.3. Average errors are 928 mAh and 6.78 % for the first, 604 mAh and 4.65 % for the second, and 143 mAh and

1.1 % for the third models. From the errors it can be said that the third model is the most accurate one.

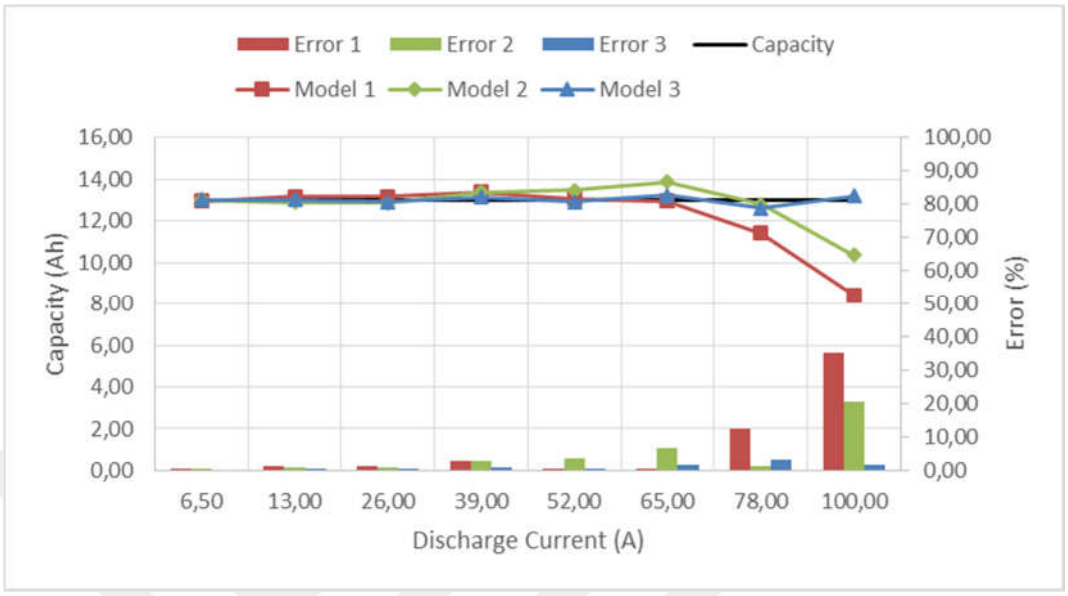

Figure 2.3: Comparison of the discharge models for LTO cell.

2.2.1.2. Charge Model of the LTO Cell

Three equations are also generated by using three different curve fitting scheme for charge model. These are:

$$t_{charge1} = 48410\, I^{-0.9602} \tag{2.7}$$

$$t_{charge2} = 54590\, I^{-1.036} + 203.3 \tag{2.8}$$

$$t_{charge3} = \frac{0.04527\, I^3 + 13.34\, I^2 - 780.8\, I + 67260}{I + 1.31} \tag{2.9}$$

where I is the charge current. The charge models ($f_{cap_{charge}}$) derived from above equations are given in Eq. (2.10), (2.11) and (2.12).

$$f_{cap_{charge1}} = \frac{13\ t}{48410\ I^{-0.9602}} \tag{2.10}$$

$$f_{cap_{charge2}} = \frac{13\ t}{54590\ I^{-1.036} + 203.3} \tag{2.11}$$

$$f_{cap_{deşarj3}} = \frac{13\ t\ (I + 1.31)}{0.04527\ I^3 + 13.34\ I^2 - 780.8\ I + 67260} \tag{2.12}$$

Models give the charged capacity in terms of Ah if current I is applied to the battery for t seconds.

Each of three models are evaluated with charge durations given in Table 2.2. Results of the model is compared with nominal capacity of the LTO cell. Comparison of the models are given in Figure 2.4.

Average errors are 3.95 Ah and 30.39 % for the first, 1.17 Ah and 8.91 % for the second, and 4.02 Ah and 30.92 % for the third models. From the errors it can be said that for charging simulations the second model is the most accurate one.

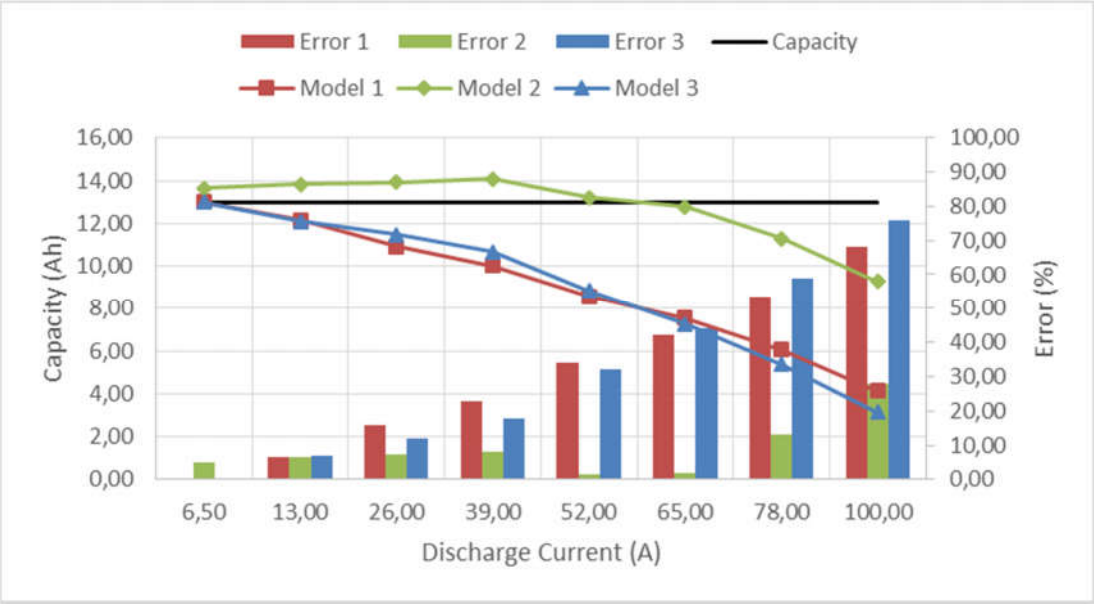

Figure 2.4: Comparison of the charge models for LTO cell.

2.2.2. Modelling of NMC Cell

The same procedure with LTO cells is followed for NMC cells. Maximum and minimum voltage limits are 4.2 V and 2.7 V [15], and discharge experiments are conducted with constant currents of 5.5 A (0.5 C), 11 A (1 C), 22 A (2 C), 33 A (3 C), 44 A (4 C), 55 A (5 C), 66 A (6 C) and 88 A (8 C), as the nominal current of an NMC cell is 11 A and maximum continuous discharge current is 88 A. Similarly charge experiments are also operated with same current levels. Discharge and charge curves for every current level are given respectively in Figure 2.5 and Figure 2.6. Note that the maximum continuous charge current of the NMC cell is 33 A, and inevitably the cell is damaged during charge tests.

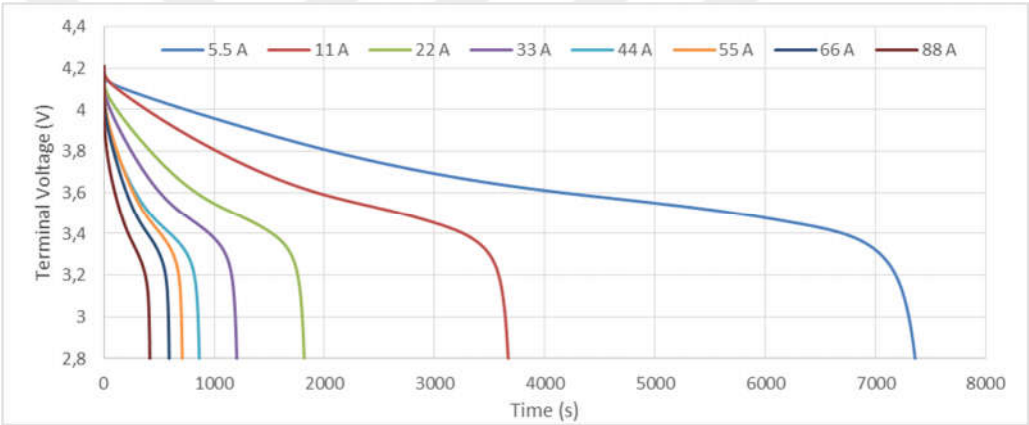

Figure 2.5: Discharge curves of NMC cell for different current rates.

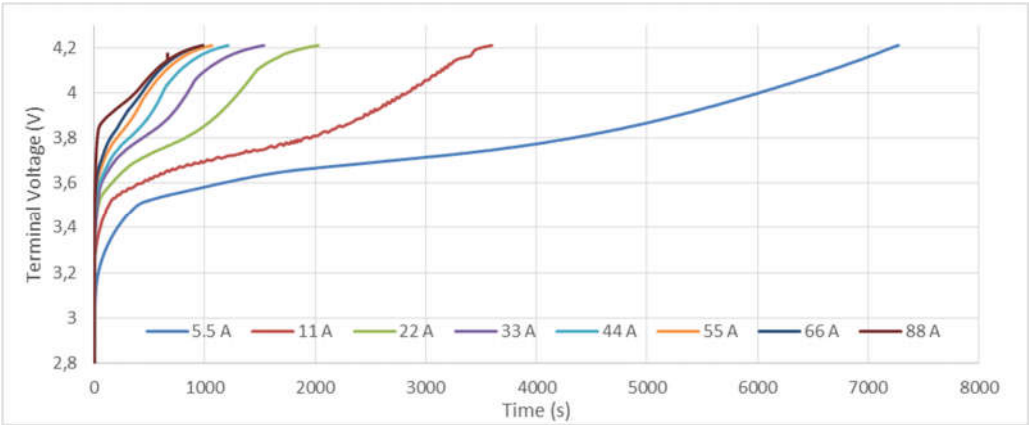

Figure 2.6: Charge curves of NMC cell for different current rates.

Discharge and charge durations corresponding these experiments are given in Table 2.3

Table 2.3: Charge and discharge durations of NMC cell for different current rates.

Current (A)	5.5	11	22	33	44	55	66	88
Charge Duration (s)	7274	3697	2029	1537	1214	1066	987	983
Discharge duration (s)	7316	3658	1811	1201	862	709	590	415

2.2.2.1. Discharge Model of NMC Cell

Three equations which gives discharge durations depending on discharge currents ($t_{discharge}$) are generated by using three different curve fitting scheme. These are:

$$t_{discharge1} = 41130\, I^{-1.012} \tag{2.13}$$

$$t_{discharge2} = 39940\, I^{-0.9914} - 51.49 \tag{2.14}$$

$$t_{discharge3} = \frac{-0.01352\, I^3 + 1.94\, I^2 - 123.5\, I + 40950}{I + 0.1485} \tag{2.15}$$

where I is the discharge current. Later, these equation are modified to build a discharge model ($f_{cap_{discharge}}$) to show used capacity. These models are given in Eq. (2.16), (2.17), and (2.18).

$$f_{cap_{discharge1}} = \frac{11\, t}{41130\, I^{-1.012}} \tag{2.16}$$

$$f_{cap_{discharge2}} = \frac{11\, t}{39940\, I^{-0.9914} - 51.49} \tag{2.17}$$

$$f_{cap_{discharge3}} = \frac{11\ t\ (I + 0.1485\ )}{-0.01352\ I^3 + 1.94\ I^2 - 123.5\ I + 40950} \tag{2.18}$$

Models give the used capacity in terms of Ah, if current I is drawn from the battery for t seconds.

Each of three models are evaluated with discharge durations given in Table 2.3. Results of the model is compared with nominal capacity of the NMC cell. Comparison of the models are given in Figure 2.7.

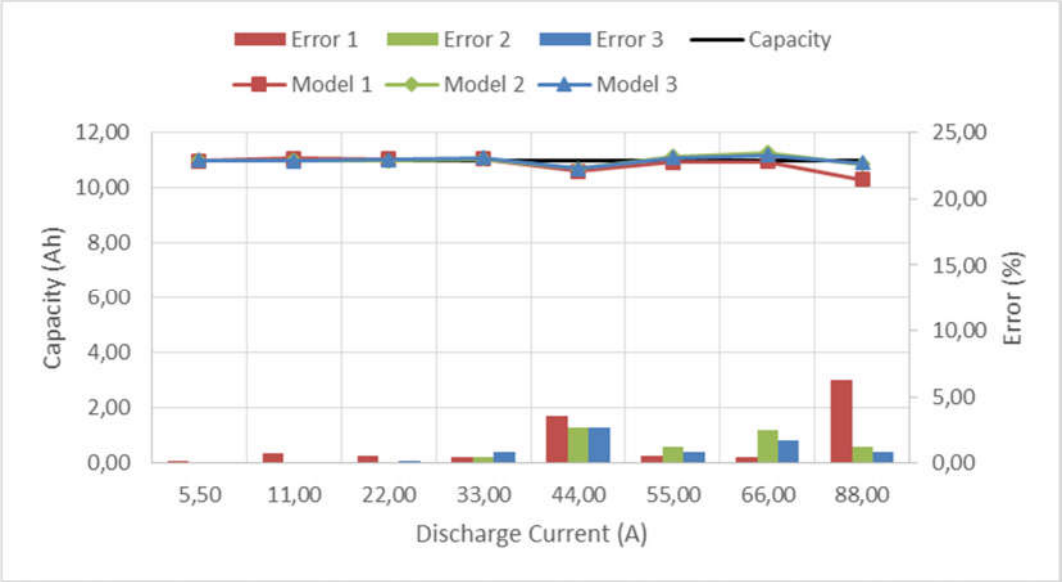

Figure 2.7: Comparison of the discharge models for NMC cell.

Average errors are 175 mAh and 1.59 % for the first, 81 mAh and 1.25 % for the second, and 79 mAh and 0.9 % for the third models. From the errors it can be said that the third model is the most accurate one.

2.2.2.2. Charge Model of NMC Cell

Three equations are also generated by using three different curve fitting scheme for charge model. These are:

$$t_{charge1} = 30960\ I^{-0.8593} \tag{2.19}$$

$$t_{charge2} = 44540\, I^{-1.113} + 597.5 \tag{2.20}$$

$$t_{charge3} = \frac{0.1087\, I^3 - 11.98\, I^2 + 849.2\, I + 29660}{I - 0.8687} \tag{2.21}$$

where I is the charge current. The charge models ($f_{cap_{charge}}$) derived from above equations are given in Eq. (3.22), (3.23) and (3.24):

$$f_{cap_{charge1}} = \frac{11\, t}{30960\, I^{-0.8593}} \tag{2.22}$$

$$f_{cap_{charge2}} = \frac{11\, t}{44540\, I^{-1.113} + 597.5} \tag{2.23}$$

$$f_{cap_{charge3}} = \frac{11\, t\, (I - 0.8687)}{0.1087\, I^3 - 11.98\, I^2 + 849.2\, I + 29660} \tag{2.24}$$

where t is the charge duration and I is charge current. Models give the charged capacity in terms of Ah if current I is applied to the battery for t seconds.

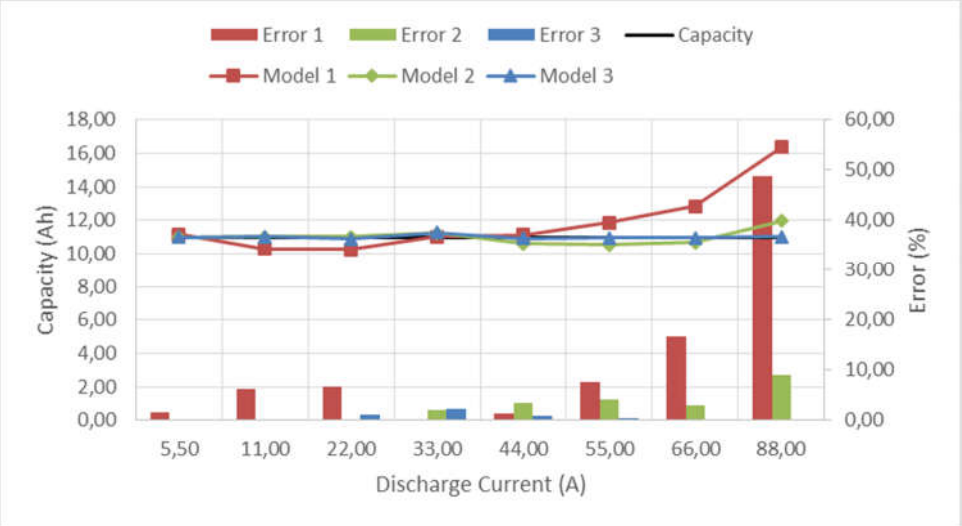

Figure 2.8: Comparison of the charge models for NMC cell.

Each of three models are evaluated with charge durations given in Table 2.3. Results of the model is compared with nominal capacity of the NMC cell, 11 A. Comparison of the models are given in Figure 2.8.

Average errors are 1.23 Ah and 11.16 % for the first, 303 mAh and 2.75 % for the second, and 75 mAh and 0.68 % for the third models. From the errors it can be said that for charging simulations the third model is the most accurate one.

For LTO cell Eq. (2.6) and Eq. (2.11) is chosen as discharge and charge models respectively. On the other hand Eq. (2.18) and Eq. (2.24) are chosen as the discharge and charge models, respectively for NMC cell.

2.2.3. Validation of the Models

For validation of the models, a load cycle, which reflects both peak discharge and charge situations, is used. The test cycle includes both charging and discharging parts. The profile of the load signal is shown in Figure 2.9. The cycle lasts for 360 seconds with maximum load current of 80 A and maximum charge current of 20 A.

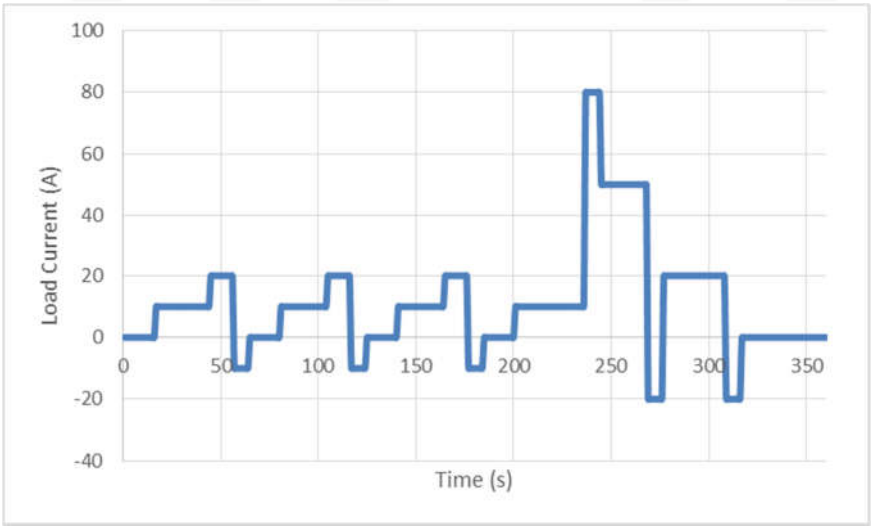

Figure 2.9: The test cycle which is used in validation experiments.

The test cycle is applied to fully charged and new LTO and NMC cells repetitively until they are fully discharged. The voltage outputs and the SoCs of the cells are given in Figure 2.10. From the Figure 2.10 it can be noticed that LTO and NMC cells are totally discharged in 4574 and 3482 seconds respectively.

Test cycle is divided into 20 sequences, in order to implement charge and discharge models. The simulations are performed by summing capacity values calculated by using corresponding model for each sequence. According to the simulation results, discharge times are 3613.16 and 4758.32 seconds for NMC and LTO cells respectively. The error between the experimental discharge time and simulations are 131 seconds and 3.7 % for NMC and 184 s. and 4 % for LTO cells.

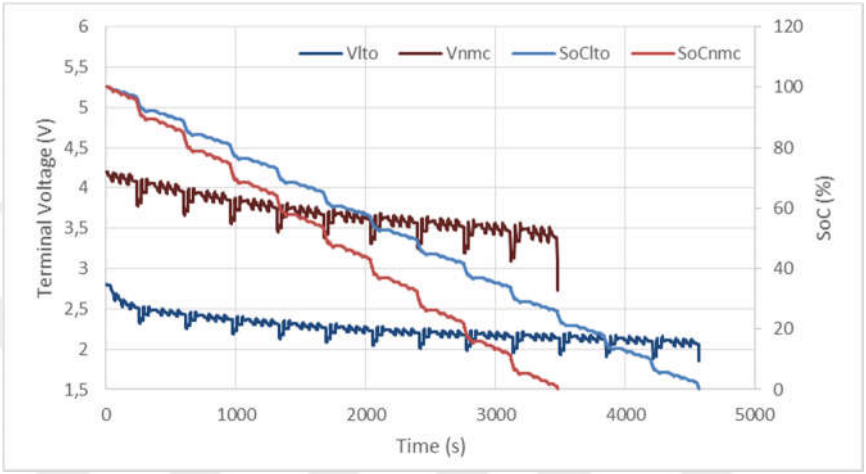

Figure 2.10: SoC and terminal voltage changes of both cells under test cycle.

The most important feature of analytical modelling is the simplicity. Although battery modelling is a time consuming task, this method enables to build a battery model following a small number of experiments. The proposed model is not detailed. Temperature or aging effects are not reflected. Yet the model is capacity model and the accuracy of the two models are around 96%. Furthermore analytical model gives consumed capacity during time “t” under the load current of “I” amperes. Hence the model can be used as a SoC estimation method.

2.3. Electric Equivalent Circuit Battery Model

Another modelling approach which was adopted in the study is electric equivalent circuit modelling. Battery model is more detailed than the analytical model. For this purpose a previously proposed electric equivalent circuit are enhanced to reflect aging effects of a battery.

The model, which was proposed earlier [16], [17], consists mainly of an internal resistance and a parallel R/C block. The change of V_{OC} depends on SoC and an analytical V_{OC} model derived from series of experiments are as;

$$V_{OC} = -1.035e^{-25SoC} + 0.325\,SoC^2 - 0.495\,SoC + 3.575 \tag{2.29}$$

The model is validated in Simulink environment. Comparison simulation and experimental results for the model is given in Figure 2.11. As seen from the Figure 2.11 average error is 0.422 % and the maximum error is 3.642 %.

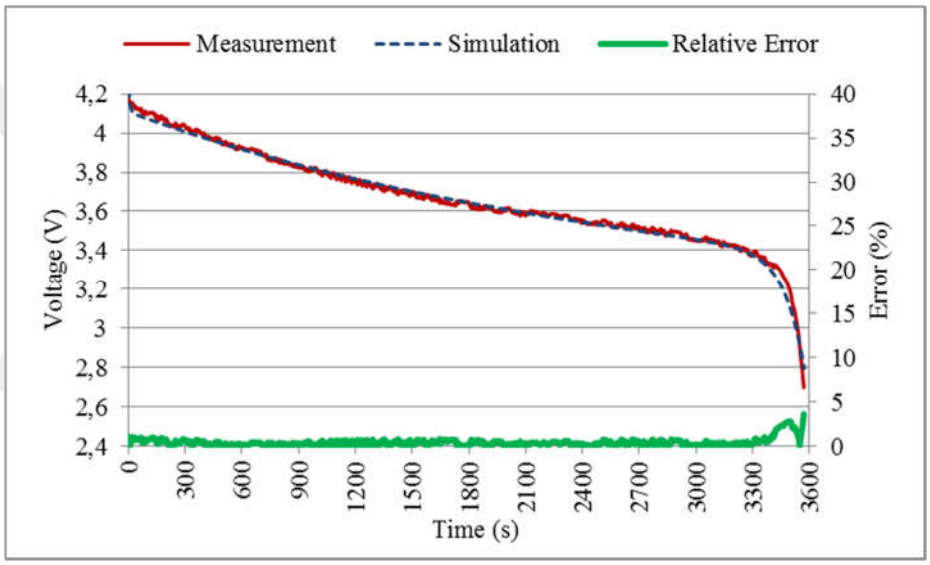

Figure 2.11: Validation of the battery model.

Aging of a battery is simulated by using relative capacity. Model is modified in order to reflect aging effects by using relative capacity – cycle number information which was provided by manufacturer. A graphic which indicates this relationship is given in Figure 2.12.

Change in the relative capacity of the battery can be reflected to the maximum capacity. As a result SoC is affected by this capacity degradation in the model. The model are tested with constant 11 A current and the results of aging simulations are displayed in a 3d surface plot as in Figure 2.13. The axes indicate battery voltage, discharge time and the cycle age of the battery, respectively.

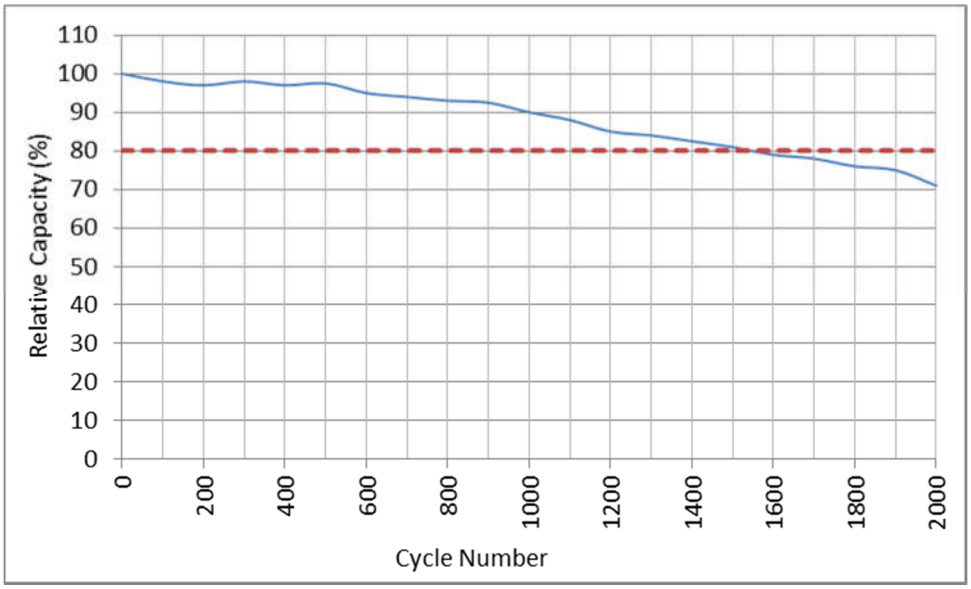

Figure 2.12: Change of relative capacity with age.

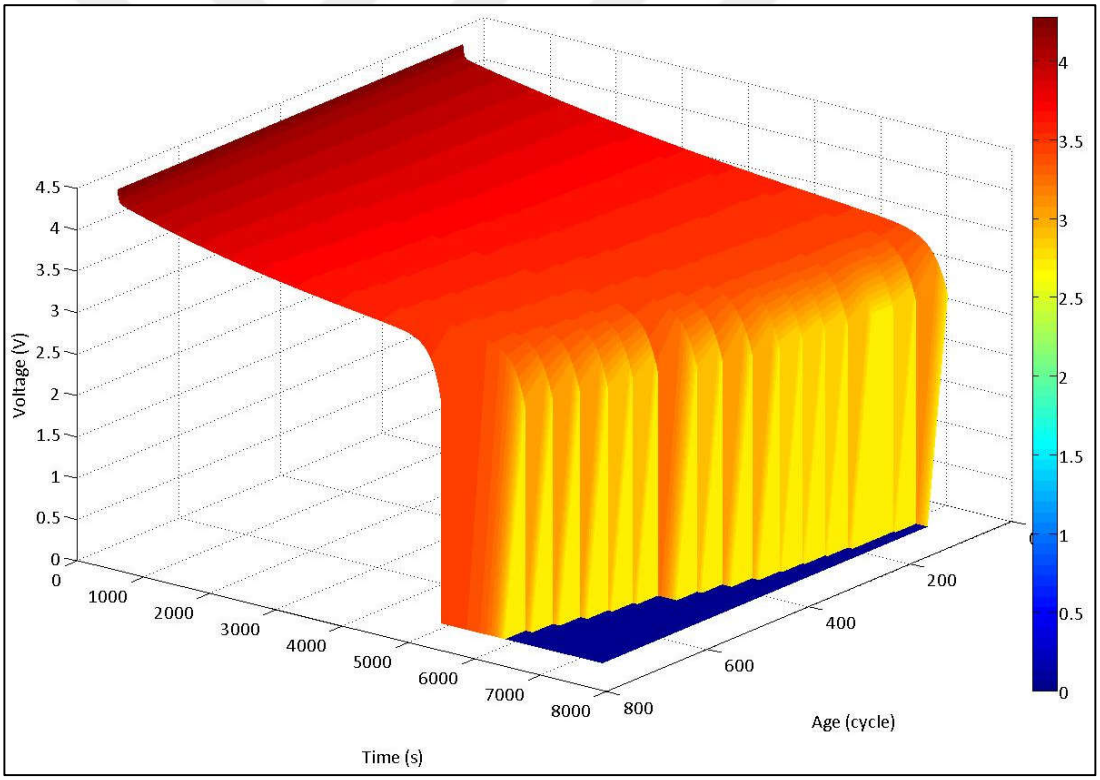

Figure 2.13: Results of aging simulations of a battery.

2.4. Generic Battery Model

Although each of the previously introduced models are successful they can't be used in energy management studies. Analytical model is suitable to use with

numerical methods. Yet it only represents the capacity change and incapable of reflecting other battery parameters such as terminal voltage. Electric equivalent circuit model is capable of reflecting the changes in terminal voltage. But it is difficult to embed the tools shown in a complicated simulation environment. Although the model is only available for NMC cells. Therefore it is not possible to use electric equivalent circuit model in energy management studies but in health estimation.

The generic battery model in Matlab is used in this study. There are several advantages of the generic model over other models for energy management studies. First of all generic model is a block in Simulink library and easy to implement any simulation circuit. Second the model can easily be modified to reflect actual LTO and NMC cells. Drawbacks of the model are, it doesn't reflect any temperature changes and aging effects.

In Figure 2.14 and Figure 2.15 generic model parameters and the discharge characteristics of the NMC and LTO cells are given respectively.

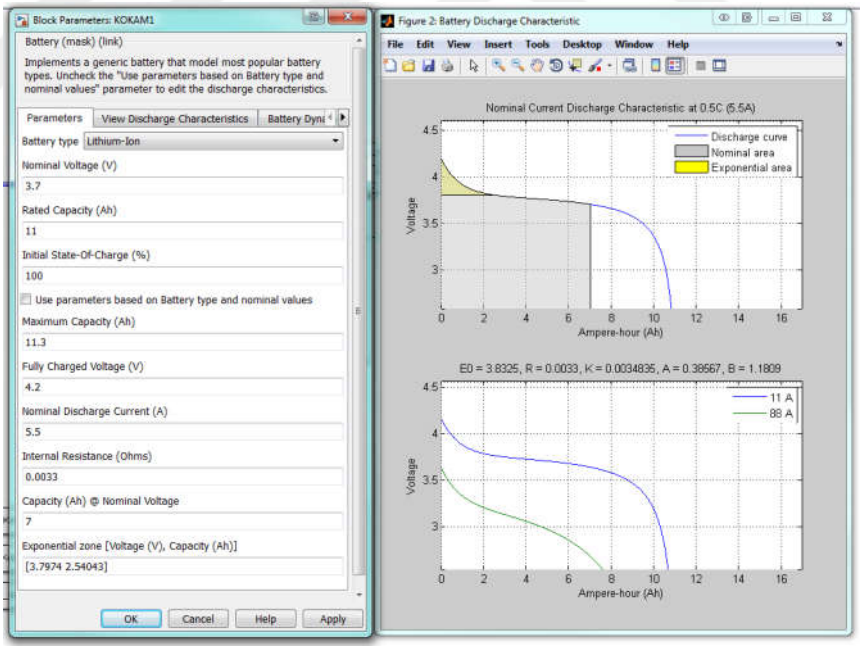

Figure 2.14: Generic model parameters and discharge characteristics of NMC cell.

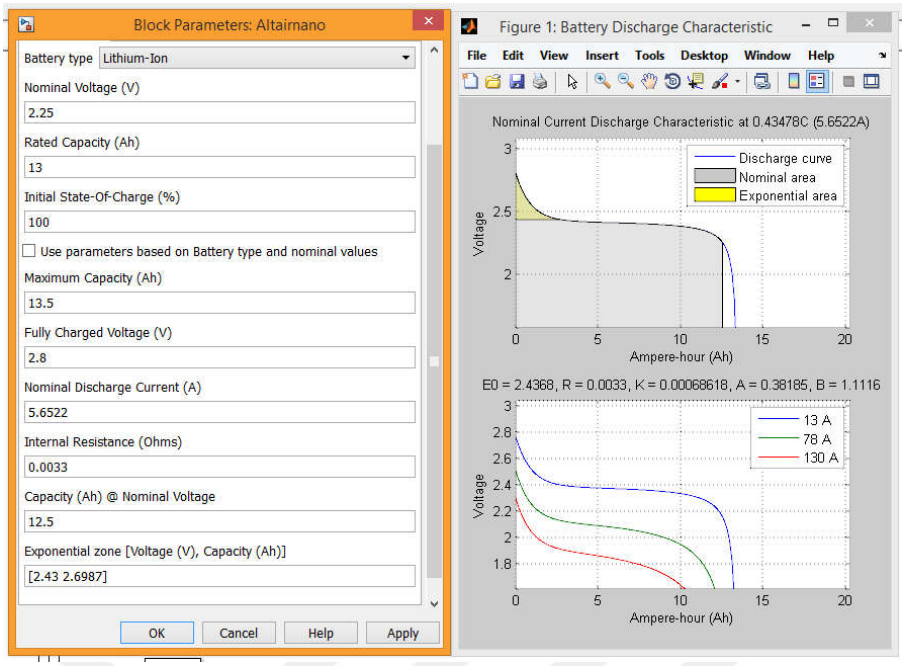

Figure 2.15: Generic model parameters and discharge characteristics of LTO cell.

For validation, generic models are conducted to the driving cycle (Figure 2.9) and the results are compared with actual outputs of batteries, which were given in Figure 2.10.

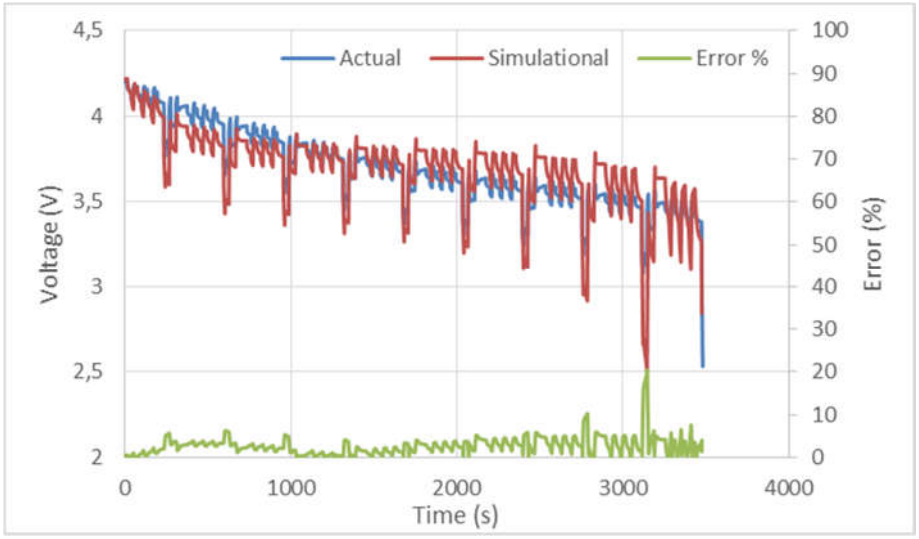

Figure 2.16: Comparison of generic model results of NMC cell.

Comparison of actual and simulation results of NMC and LTO cells are given in Figure 2.16 and Figure 2.17 respectively. Maximum error for generic model of NMC cell is 0.7 V and 20.42 % where the average error is 0.097 V and 2.69 %. Discharge

time of the model is 3119 seconds where the actual battery discharges in 3482 seconds.

Maximum error for generic model of LTO cell is 0.42 V and 17.35 % where the average error is 0.149 V and 6.24 %. Discharge time of the model is 4207 seconds where the experimental discharge time is 4574 seconds.

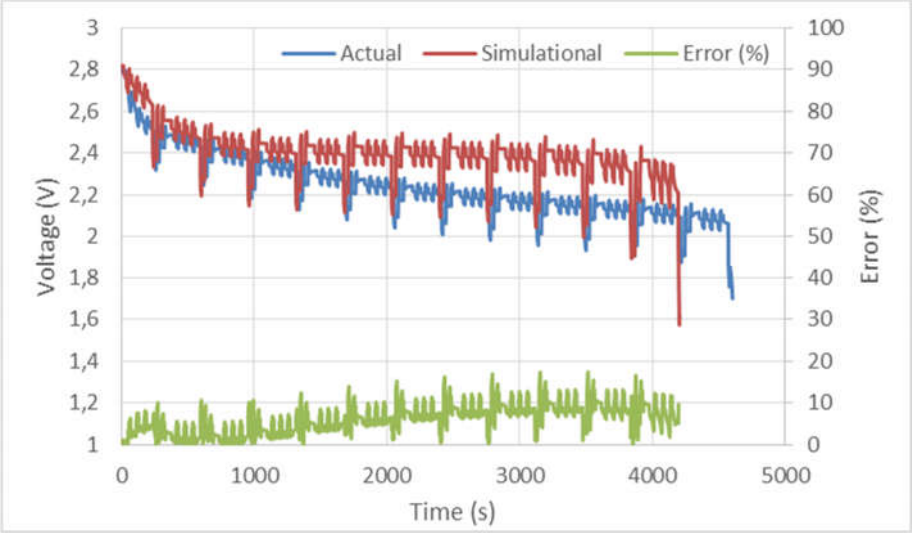

Figure 2.17: Comparison of generic model results of LTO cell.

3. BATTERY STATE OF HEALTH ESTIMATION

Performance of a battery decreases with age. The reason of this decrease can be a number of intertwined complex processes which occur in similar instances. Therefore it is difficult to determine the level of this decrease [51]. Remaining battery life information is important for reliable operation in EV applications. For this reason a parameter called state of health (SoH) which indicates actual health condition of battery is defined. SoH is the comparison between initial and the actual conditions of a battery, and 100 % SoH indicates an unused battery.

There is a multiplicity in the definition of SoH. SoH may be obtained by different approaches and different variables [52]. Studies to obtain SoH can be divided into two categories which are experimental approaches and adaptive approaches [53]. In adaptive approaches, model parameters which define SoH or battery health condition itself, are obtained by using adaptive algorithms or methods. Also on-line SoH estimation is possible with adaptive approaches. Kalman filter variations [54]–[57], observers [58], and fuzzy logic applications [59], [60] may be included to this category. Experimental approaches may also be divided into two categories. These are measurement based and model based approaches. Measurement based approaches include measuring internal resistance or impedance of a battery, which increase with age. By using this increment, an estimation can be made about SoH [42], [61]–[67]. In model based studies experimental data is used to develop a model. There are studies in which data fitting techniques [68], [69], probabilistic methods [70] and coulomb counting [71] are used. Experimental approaches based on measurement of internal resistance or impedance of batteries are the most accurate approaches but not capable of online estimation. It is difficult to establish a detailed model in both probabilistic and experimental approaches and excessive computational effort is needed during operation. Furthermore, for the models which were developed by using experimental data, the accuracy decrease at different conditions than their experimental conditions.

In this study SoH is represented in terms of relative capacity (RC). RC is the comparison between actual and nominal capacity values of a battery. There is a

capacity fade in an aging battery, which is the decrease of charge-discharge capacity of the battery [72]. In this study capacity fade is used to estimate RC. RC is related with the cycle number (CN), which represents the age of the battery. In order to investigate CN-RC relationship a battery should be aged until it is out of service (SoH < 80%) This is a repetitive task and takes a long period of time. Manufacturers usually provide CN-RC information to the end user. In this study NMC cell and the information provided for this cell are used [15]. The CN-RC relationship for NMC cell is shown in Figure 2.12, where the red dotted line is the 80% limit. Manufacturers use specific charge-discharge routines during the aging process of a battery. In this study I named a single cycle with manufacturer's charge-discharge routine as "reference cycle" (RCN). Therefore, the information provided by manufacturer, gives the relationship between RC and RCN of a battery. As a result, RC can be estimated by this relationship if age of a battery can be obtained in terms of RCN.

Performance degradation of aging batteries can be used to determine reference cycle number. This degradation can be observed by using terminal voltage of battery. When a current is drawn from a battery, terminal voltage decreases. This decrease is different for different aged batteries under same load signal.

In the context of this thesis a simple method for RC estimation by using RCN is proposed. For this purpose two different RCN models, which are both based on the change of terminal voltage under a significant load signal, is developed. The electric equivalent circuit battery model which was introduced in section 3.3 is used for this purpose. The maximum error of the battery model is less than 4 %. Behaviours of batteries in different reference cycles are simulated. Different responses of batteries to the same load signal, by means of differences in terminal voltages are investigated. These differences are transformed to numerical quantities to develop RCN models and thereafter RC is estimated by using the relationship between RCN and RC. Both models are validated with two groups of experiments.

3.1. The Relative Capacity Models

As mentioned before battery reactions differ in different age and health conditions. This difference can be noticed below in Figure 3.1 and Figure 3.2. Terminal

voltage graphics of two different aged batteries are given in Figure 3.2 after a specific load profile, ECE 15 (Figure 3.1) is applied to them. These batteries are aged with manufacturer's procedures as given in details in Section 2. Therefore the ages of these batteries can be noted as 100 and 700 RCNs.

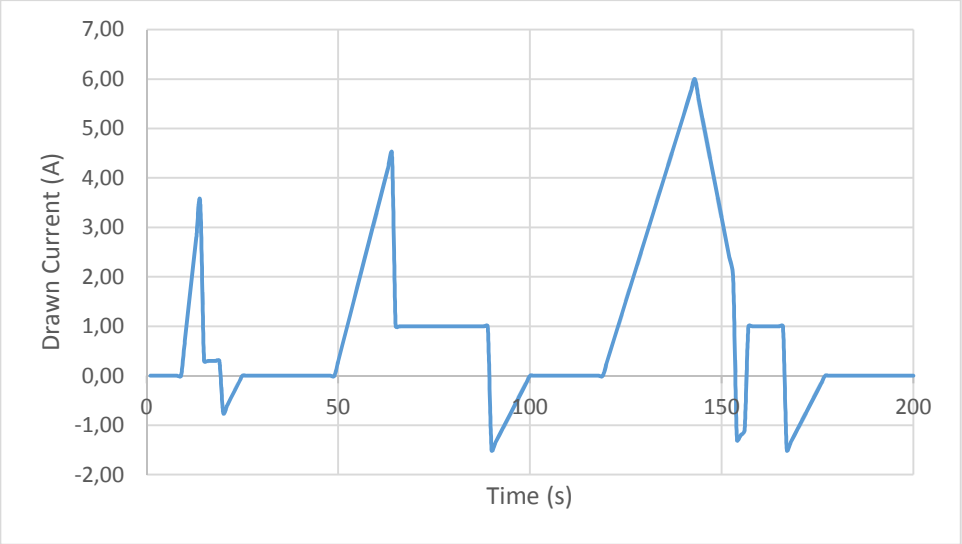

Figure 3.1: ECE 15 driving cycle profile.

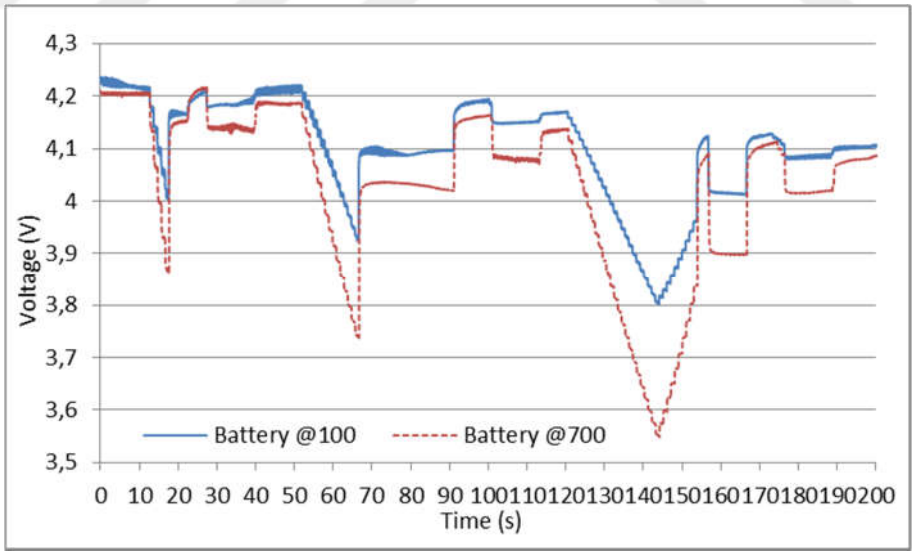

Figure 3.2: Reactions of batteries in different RCNs to the same load profile.

As seen from Figure 3.2. the differences of battery responses depending on health-age condition may be used to determine RC of a battery. Therefore the proposed method is based on determining the change of terminal voltages by age

under same load conditions. In order obtain this difference two similar methods are use during the thesis. In both methods three zones with downward slopes which may easily be recognized from the figure are used. The object was to represent the difference in numbers. In first method a couple of variable parameters (a and b) are defined and values of one of them is used for identification. This method is named as "parametric approach". In the second method the slopes of the different voltage signals are used for this purpose and this approach is named as "slopes approach".

The three indicative zones in the cycle is selected and used as load signals. In order to clarify the test signals, this zones are shown in Figure 3.3. Amplitudes of these signals increase in time and all three signals have different slopes. Peak amplitudes are 40 A, 50 A and 65 A, and durations are 5 s, 15 s, and 25 s for first, second and third signals respectively. In the simulations the signals are generated by "controlled current source block" where in experiments they are generated by a programmable DC power source.

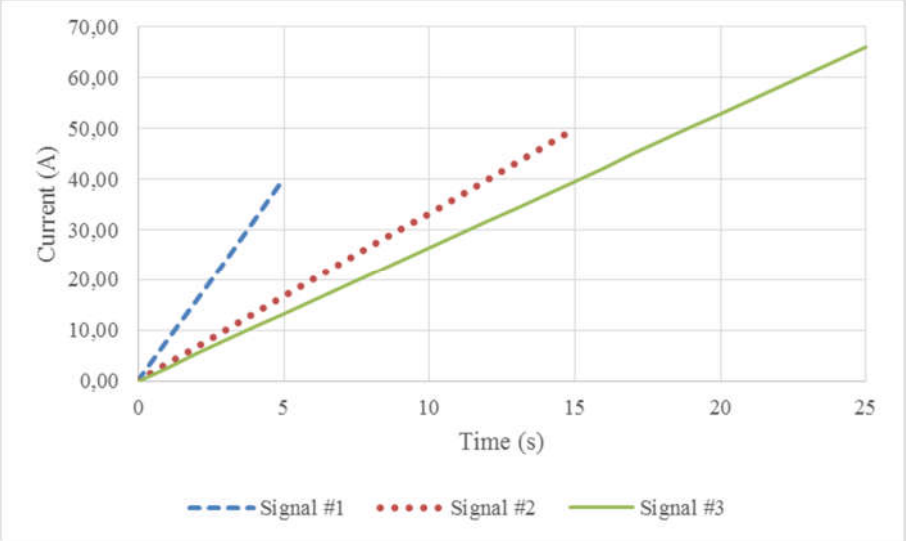

Figure 3.3: Test signals.

3.1.1. The Parametric Approach

A linear voltage signal can be represented as in equation (3.1) where α and b are the parameters, V_t is voltage and t is the corresponding time value.

$$V_t = \frac{b}{a+t} \tag{3.1}$$

The parameters α and b reflects the difference between the slopes of lines. These parameters can be obtained by using two voltage values during the slope.

$$a = \frac{V_2 t_2 - V_1 t_1}{V_1 - V_2},\ b = \frac{V_1 V_2 (t_2 - t_1)}{V_1 - V_2} \tag{3.2}$$

In equation (4.2), V_1 and V_2 are the voltage values observed at t_1 and t_2 instances, which are the starting and finishing instances of slopes respectively. Because these two parameters are dependent on each other they will give same results.

$$RCN(a_1) = -0.001371a_1^3 + 0.4846a_1^2 - 58.15a_1 + 2579 \tag{3.3}$$

$$RCN(b_1) = -0.001713b_1^3 + 0.02631b_1^2 - 13.71b_1 + 2637 \tag{3.4}$$

$$RCN(a_2) = -0.0003195a_2^3 + 0.179a_2^2 - 35.28a_2 + 2642 \tag{3.5}$$

$$RCN(b_2) = -4.019 \times 10^{-6}b_2^3 + 0.009731b_2^2 - 8.29b_2 + 2678 \tag{3.6}$$

$$RCN(a_3) = -1.612 \times 10^{-4}a_3^3 + 0.1074a_3^2 - 25.82a_3 + 2233 \tag{3.7}$$

$$RCN(b_3) = -2.055 \times 10^{-6}b_3^3 + 0.005887b_3^2 - 6.09b_3 + 2259 \tag{3.8}$$

Time values are accepted as $t_1 = 1$, $t_2 = 6$ seconds for the first zone, $t_1 = 1$, $t_2 = 16$ seconds for the second zone and $t_1 = 1$ and $t_2 = 26$ seconds for the third zone. The simulation results of a battery for every centenary cycles of age for first signal is given as an example in Table 3.1. In the table given quantities are the recorded voltage values in corresponding seconds of simulation

Table 3.1: Simulation results of the battery for the first signal for every centenary cycle.

Time (s)	Vt_1	Vt_{100}	Vt_{200}	Vt_{300}	Vt_{400}	Vt_{500}	Vt_{600}
1	4,310	4,310	4,310	4,310	4,310	4,310	4,310
2	4,294	4,291	4,287	4,273	4,269	4,261	4,257
3	4,274	4,267	4,257	4,230	4,221	4,204	4,196
4	4,249	4,238	4,222	4,181	4,167	4,142	4,128
5	4,219	4,204	4,183	4,127	4,108	4,073	4,053
6	4,187	4,167	4,140	4,069	4,045	4,000	3,975
	Vt_{700}	Vt_{800}	Vt_{900}	Vt_{1000}	Vt_{1100}	Vt_{1200}	Vt_{1300}
1	4,310	4,310	4,310	4,310	4,310	4,310	4,310
2	4,252	4,244	4,235	4,226	4,217	4,207	4,196
3	4,185	4,169	4,151	4,132	4,113	4,093	4,071
4	4,112	4,086	4,059	4,030	4,001	3,970	3,936
5	4,032	3,996	3,959	3,920	3,881	3,838	3,792
6	3,947	3,903	3,855	3,806	3,756	3,702	3,644
	Vt_{1400}	Vt_{1500}	Vt_{1600}	Vt_{1700}	Vt_{1800}	Vt_{1900}	Vt_{2000}
1	4,310	4,310	4,310	4,310	4,310	4,310	4,310
2	4,185	4,173	4,161	4,149	4,136	4,123	4,108
3	4,048	4,024	3,999	3,974	3,948	3,920	3,892
4	3,901	3,865	3,827	3,788	3,749	3,707	3,663
5	3,745	3,696	3,644	3,591	3,538	3,480	3,421
6	3,584	3,522	3,457	3,389	3,323	3,251	3,175

For given simulation results in Table 3.1, a and b can be obtained as given in Table 3.2, by using equation (3.2). Time values are normalized as $t_1 = 1, t_2 = 6$ for the first, $t_1 = 1, t_2 = 16$ for the second and $t_1 = 1, t_2 = 26$ for the third zone for this calculations.

The change in the values of parameters are taken in to account to generate a function for RCN. By using curve fitting and the parameter values given in Table 3.2, equations (3.3) and (3.4) are generated to calculate the value of RCN depending on

parameter a and b respectively, where the subscript represents the signal which the parameter belongs. Equations for the other signals were also generated with the same logic by using Table 3.1.

Parameter values for second and third signals obtained with same procedures are given in Table 3.3 and Table 3.4, respectively. As seen from Table 3.4 there are no available parameter values for third signal, for the battery over 900 cycles. Because batteries over 900 cycles are totally discharged in simulations of the third signal.

Table 3.2: Values of a and b parameters for the first signal.

Param.	Vt_1	Vt_{100}	Vt_{200}	Vt_{300}	Vt_{400}	Vt_{500}	Vt_{600}
a	169,284	144,728	120,665	83,433	75,351	63,545	58,398
b	733,923	628,087	524,374	363,905	329,074	278,189	256,006
	Vt_{700}	Vt_{800}	Vt_{900}	Vt_{1000}	Vt_{1100}	Vt_{1200}	Vt_{1300}
a	53,424	46,907	41,412	36,733	32,923	29,419	26,369
b	234,567	206,481	182,794	162,630	146,210	131,108	117,962
	Vt_{1400}	Vt_{1500}	Vt_{1600}	Vt_{1700}	Vt_{1800}	Vt_{1900}	Vt_{2000}
a	23,698	21,345	19,262	17,408	15,837	14,342	12,995
b	106,449	96,308	87,328	79,339	72,567	66,122	60,318

SoH of a battery can be estimated by using value of the RCN of the battery and the correlation between RCN and capacity which was given in Figure 2.12. The RC-RCN relationship in the figure is smoothened by moving average method and the RC model is derived as a 6th order polynomial in terms of RCN, as given in equation (3.9)

$$RC\ (\%) = 1.165 \times 10^{-17} RCN^6 - 8.103 \times 10^{-14} RCN^5 + 2.15 \times 10^{-10}\ RCN^4 - 2.66x10^{-7} RCN^3 + 1.441 \times 10^{-4} RCN^2 - 0.3418 RCN + 99.95 \quad (3.9)$$

As a result, in order to obtain remaining capacity of a battery this procedure should be followed.

- A specific test signal is applied to the battery,
- The value of the parameter, a is calculated by using appropriate equation.
- RCN value is obtained by using appropriate model.
- RC is obtained by using equation (3.9)

Table 3.3: Values of a and b parameters for the second signal.

Param.	Vt_1	Vt_{100}	Vt_{200}	Vt_{300}	Vt_{400}	Vt_{500}	Vt_{600}
a	255,764	223,348	191,527	142,023	128,823	110,579	101,736
b	1104,08	964,696	827,867	615,001	558,239	479,790	441,763
	Vt_{700}	Vt_{800}	Vt_{900}	Vt_{1000}	Vt_{1100}	Vt_{1200}	Vt_{1300}
a	93,270	82,608	73,434	65,483	58,868	52,732	47,319
b	405,361	359,515	320,068	285,877	257,430	231,046	207,774
	Vt_{1400}	Vt_{1500}	Vt_{1600}	Vt_{1700}	Vt_{1800}	Vt_{1900}	Vt_{2000}
a	42,521	38,248	34,426	30,993	28,047	25,234	22,681
b	187,142	168,766	152,330	137,569	124,903	112,806	101,828

Table 3.4: Values of a and b parameters for the third signal.

Param.	Vt_1	Vt_{100}	Vt_{200}	Vt_{300}	Vt_{400}
a	169,284	144,728	120,665	83,433	75,351
b	733,923	628,087	524,374	363,905	329,074
	Vt_{500}	Vt_{600}	Vt_{700}	Vt_{800}	Vt_{900}
a	63,545	58,398	53,424	46,907	41,412
b	278,189	256,006	234,567	206,481	182,794

3.1.2. The Slope Approach

Slope of the terminal voltage during a period of time can be calculated by using (3.10) where V_1 and V_2 are the voltage values which were recorded at t_1 and t_2 instances respectively during the slope.

$$m = \frac{v_2 - v_1}{t_2 - t_1} \tag{3.10}$$

Reactions of different aged batteries is simulated by using battery model and the simulation setup. In simulations the slope of a battery terminal voltage is recorded for every centenary reference cycles for each of the three test signals. In Table 3.5, Table 3.6, and Table 3.7 below slope values, respectively for the first, second, and third signals are listed. Like in the parametric approach, there are no available slope values for 3rd signal for a battery over 900 cycles, which is shown in Table 3.7.

Table 3.5: Slope values for the first signal.

Slope	Vt_1	Vt_{100}	Vt_{200}	Vt_{300}	Vt_{400}	Vt_{500}	Vt_{600}
m	-0.025	-0.029	-0.034	-0.048	-0.053	-0.062	-0.067
	Vt_{700}	Vt_{800}	Vt_{900}	Vt_{1000}	Vt_{1100}	Vt_{1200}	Vt_{1300}
m	-0.073	-0.081	-0.091	-0.101	-0.111	-0.122	-0.133
	Vt_{1400}	Vt_{1500}	Vt_{1600}	Vt_{1700}	Vt_{1800}	Vt_{1900}	Vt_{2000}
m	-0.145	-0.158	-0.171	-0.184	-0.197	-0.212	-0.227

Table 3.6: Slope values for the second signal.

Slope	Vt_1	Vt_{100}	Vt_{200}	Vt_{300}	Vt_{400}	Vt_{500}	Vt_{600}
m	-0.016	-0.018	-0.021	-0.027	-0.030	-0.034	-0.037
	Vt_{700}	Vt_{800}	Vt_{900}	Vt_{1000}	Vt_{1100}	Vt_{1200}	Vt_{1300}
m	-0.039	-0.044	-0.048	-0.053	-0.057	-0.063	-0.068
	Vt_{1400}	Vt_{1500}	Vt_{1600}	Vt_{1700}	Vt_{1800}	Vt_{1900}	Vt_{2000}
m	-0.073	-0.079	-0.085	-0.092	-0.098	-0.104	-0.111

Table 3.7: Available slope values for the third signal.

Slp.	Vt_1	Vt_{100}	Vt_{200}	Vt_{300}	Vt_{400}	Vt_{500}	Vt_{600}	Vt_{700}	Vt_{800}	Vt_{900}
m	-0.017	-0.019	-0.024	-0.026	-0.030	-0.032	-0.034	-0.038	-0.041	-0.045

The changing pattern of slope values used to form an equation by using curve fitting. As a result cycle number is modelled depending on slope. Three models for three test signals are achieved and listed below. In the equations RCN is the reference cycle number, m_n is the slope of the n^{th} test signal.

$$RCN = -6.243\ 10^4 m_1^3 - 4.613\ 10^4 m_1^2 - 1.783\ 10^4 m_1 - 402.2 \quad (3.11)$$

$$RCN = -4.384\ 10^5 m_2^3 - 1.78\ 10^5 m_2^2 - 3.718\ 10^4 m_2 - 540.3 \quad (3.12)$$

$$RCN = 2.836\ 10^7 m_3^3 + 2.628\ 10^6 m_3^2 + 4.444\ 10^4 m_3 + 155.7 \quad (3.13)$$

Slope of any battery can be obtained by equation (3.10) after applying test signal. Then cycle number of the battery can be calculated by using corresponding equation for the applied test signal.

In the next step relative capacity is estimated by using RCN. For this purpose relationship given in Figure 2.12 and equation (3.9) is used. As a result in order to obtain remaining capacity of a battery, the procedure of the slope approach may be summarized as below.

- A test signal is applied to the battery,
- The value of the slope is calculated by using appropriate equation (equation (3.10)).
- RCN value is obtained by using appropriate model (equations (3.11), (3.12), or (3.13)).
- RC is obtained by using equation (3.9)

3.2. Validation of the RC Modelling Methods

Two different groups of experiments are conducted to validate the method and determine the accuracy. For the first group of experiments, method is tested on batteries which were aged with manufacturer's charge-discharge procedures.

Therefore ages of these batteries can be represented in terms of RCN. This group of experiments is called “controlled tests”, since these batteries are aged in a controlled manner. Second group of experiments are conducted with randomly aged batteries which were used in different applications. Since these batteries are not aged in a specific routine, this group of experiments is called “uncontrolled experiments”.

A fully charged battery with relative capacity of 100 % is expected to be fully discharged in 1 hour if it is discharged with 1 C. After testing the batteries with test signals (slope test), fully charged batteries are discharged with 11 A (1 C) and the discharge time is recorded. Discharge time is compared with 3600 s in order to calculate RC (capacity test).

3.2.1. Validation of the Parametric Approach

3.2.1.1. Controlled Tests

In Table 3.8, experimental results for every 100 cycles of the battery is given, where V_1 and V_2 are the voltage values recorded in t_1 and t_2, which are the starting and ending instances of slopes respectively.

Comparison between calculated and known cycle numbers is given in Table 3.9 and a comparison between estimated RC and the actual capacity values is given in Table 3.10. As seen from the Table 3.10 average error in RC estimation is 2.14 %, 2.022 %, and 1.908 % for the first, second, and the third signals respectively. Summary of the errors for controlled tests are listed in Table 3.11 .

3.2.1.2. Uncontrolled Tests

Uncontrolled tests were undertaken with five different batteries which were previously employed in several applications and tests. Thus these batteries are not aged with standard procedures and their cycle numbers are unknown. In the first phase, experimental results of the batteries under the test driving cycle were used in the proposed method. Then RCN and SoH estimations are performed. In the second phase capacities of tested batteries are measured and compared with estimated

values. In Table 3.12 experimental results of 5 different batteries are given for all three zones.

Table 3.8: Experimental data of the batteries which were aged with catalogue procedures.

Signal	Cycle num.	100	200	300	400	500
1	V_1	4.209	4.214	4.188	4.207	4.201
	V_2	4.048	3.982	3.902	3.871	3.815
	t_1	12.058	10.9	12.4	10.579	13.519
	t_2	17.868	16.858	18.68	16.809	19.505
2	V_1	4.209	4.183	4.168	4.188	4.172
	V_2	3.931	3.845	3.784	3.753	3.698
	t_1	51.337	51.099	52.819	52.578	53.499
	t_2	67.326	67.798	67868	66.99	67.455
3	V_1	4.176	4.146	4.146	4.137	4.13
	V_2	3.698	3.589	3.477	3.405	3.367
	t_1	121.87	121.39	122.51	120.75	120.63
	t_2	146.78	146.09	147.08	145.57	144.77

Table 3.9: Comparison between the calculated and the known cycle numbers in controlled tests.

Signal	Cycle number	100	200	300	400	500
1	Value of the Parameter a	148.72	103.72	87.359	72.685	59.852
	Calculated Cycle Number	139.43	231.15	283.31	386.09	540.61
	Error (%)	39.43	15.57	5.56	3.47	8.12
2	Value of the Parameter a	230.32	183.02	152.46	127.05	11.649
	Calculated Cycle Number	108.16	222.19	291.63	393.80	489.68
	Error (%)	8.16	11.10	2.79	1.55	2.06
3	Value of the Parameter a	197.11	157.84	131.61	119.31	110.27
	Calculated Cycle Number	75.95	194.64	323.64	403.87	472.29
	Error (%)	24.050	2.68	7.90	0.99	5.52

Table 3.10: Comparison between estimated RC and measured capacity values in controlled tests.

Signal	Cycle number	100	200	300	400	500
1	Estimated RC (%)	97.342	97.025	97.027	97.047	96.472
	Measured Capacity (%)	102.167	100.667	98.167	97.694	97
	Error (%)	4.723	3.617	1.162	0.663	0.535
2	Estimated RC (%)	97.631	97.033	97.031	97.039	96.774
	Measured Capacity (%)	102.167	100.667	98.167	97.694	97
	Error (%)	4.440	3.609	1.157	0.671	0.233
3	Estimated RC (%)	98.076	97.082	97.049	97.027	96.085
	Measured Capacity (%)	102.167	100.667	98.167	97.694	97
	Error (%)	4.004	3.561	1.139	0.683	0.155

Table 3.11: Summary of errors in the controlled tests.

	Signal 1	Signal 2	Signal 3	Average
RCN Prediction Error (cycles)	28,35	11,02	16,93	18,77
RCN Prediction Error (%)	14,43	5,13	8,23	9,26
Capacity Estimation Error (%)	2,14	2,02	1,91	2,02

As seen from Table 3.12, there is no available voltage or time values for the battery #3. The reason of this situation is that the battery is totally discharged during or before the third signal applied and no available parameter could be measured.

In Table 3.13, value of parameter, a, value of the calculated cycle number belonging to a, estimated capacity and measured capacity values are listed for each batteries listed.

As seen from Table 3.13 average errors of RC estimation with the parametric approach is 3.016 %, 2.749 % and 2.704 % for first, second, and third signals respectively.

Table 3.12: Experimental data of the 5 batteries without aging information.

Signal	Battery ID	#1	#2	#3	#4	#5
1	V_1	4.216	4.216	4.193	4.205	4.186
	V_2	4.054	4.014	3.166	4.005	4.005
	t_1	12.45	12.47	11.939	13.758	12.918
	t_2	17.87	17.218	16.518	20.238	17.781
2	V_1	4.214	4.195	4.136	4.191	4.171
	V_2	3.944	3.815	2.651	3.904	3.828
	t_1	51.937	51.658	82.039	53.778	52.5
	t_2	66.857	66.558	66.349	68.793	68.089
3	V_1	4.17	4.169	N/A	4.162	4.141
	V_2	3.67	3.569	N/A	3.65	3.585
	t_1	122.157	122.257	N/A	124.356	122.739
	t_2	146.28	146.446	N/A	147.404	145.629

Table 3.13: Comparison of estimated and measured capacity values in controlled tests.

Signal	Cycle number	#1	#2	#3	#4	#5
1	Value of parameter (a)	137.77	95.375	13.638	132.16	109.91
	Calculated Cycle Number	180.53	251.61	1872.6	193.30	221.47
	Estimated RC (%)	97.124	97.018	74.808	97.085	97.034
	Measured Capacity (%)	99.722	98.583	77.666	101.33	100.05
	Error (%)	2.605	1.587	3.679	4.192	3.0193
2	Value of parameter (a)	221.69	152.70	26.126	208.94	178.84
	Calculated Cycle Number	136.93	290.92	1836.7	170.67	230.01
	Estimated RC (%)	97.360	97.031	75.452	97.162	97.026
	Measured Capacity (%)	99.722	98.583	77.666	101.33	100.05
	Error (%)	2.179	1.574	2.850	4.116	3.027
3	Value of parameter (a)	180.37	147.35	N/A	168.61	152.31
	Calculated Cycle Number	114.577	240.10	N/A	155.00	217.69
	Estimated RC (%)	97.549	97.021	N/A	97.241	97.038
	Measured Capacity (%)	99.722	98.583	77.666	101.33	100.05
	Error (%)	2.179	1.584	N/A	4.038	3.015

3.2.2. Validation of the Slope Approach

3.2.2.1. Controlled Tests

The slope values extracted from slope tests are used in RCN model to validate the RCN estimation. Since test batteries in controlled experiments are aged with manufacturer's procedures, estimated RCN values can directly be compared to actual ages of the batteries. Results are given in Table 3.14, (a), (b) and (c) for the first, second, and third signals respectively.

Table 3.14: RCN estimation results for controlled experiments.

Test signal ID	Cycle Number	Value of "m"	Calculated Cycle Number	Error (Cycle Number)	Error (%)
1	100	-0,0277	57,790	42,210	42,21
	200	-0,0389	225,827	25,827	12,91
	300	-0,0455	320,025	20,025	6,67
	400	-0,0539	435,032	35,032	8,75
	500	-0,0645	572,470	72,470	14,49
2	100	-0,017	54,641	45,359	45,36
	200	-0,022	182,051	17,949	8,97
	300	-0,026	299,797	0,203	0,07
	400	-0,030	431,803	31,803	7,95
	500	-0,034	534,322	34,322	6,86
3	100	-0,019	70,293	29,707	29,71
	200	-0,023	188,829	11,171	5,59
	300	-0,027	321,533	21,533	7,18
	400	-0,029	403,302	3,302	0,83
	500	-0,032	480,994	19,006	3,80

As it can be seen from Table 3.14, average errors are 37.646, 24.193, and 17.911 cycles and 14.897%, 11.906%, and 8.391% for first, second, and third signals respectively.

In the next phase relative capacity of the batteries are estimated by using RCN values. The estimated values are compared with actual RC values which were extracted from capacity tests. The results are given in Table 3.15. As it can be seen from Table 3.15, maximum errors are 3.680%, 3.617%, and 3.910% and average errors are 1.744%, 1.690%, and 1.683% for first, second, and third signals respectively.

Table 3.15: RC estimation results for controlled experiments.

Test Signal ID	Cycle Number	Estimated Cycle number	Estimated Capacity (%)	Measured Capacity (%)	Error (%)
1	100	57,790	98,407	102,167	3,680
	200	225,827	97,030	100,667	3,613
	300	320,025	97,047	98,167	1,141
	400	435,032	96,969	97,694	0,743
	500	572,470	96,223	97,000	0,802
2	100	54,641	98,471	102,167	3,617
	200	182,051	97,119	100,667	3,524
	300	299,797	97,036	98,167	1,152
	400	431,803	96,977	97,694	0,735
	500	534,322	96,516	97,000	0,499
3	100	70,293	98,172	102,167	3,910
	200	188,829	97,097	100,667	3,546
	300	321,533	97,048	98,167	1,140
	400	403,302	97,028	97,694	0,682
	500	480,994	96,813	97,000	0,192

3.2.2.2. Uncontrolled Tests

In these experiments five different batteries are used. These batteries were already employed in different applications such as electric vehicles tests or competition robots. Therefore, neither there are not much information about conditions of these batteries (such as their cycle numbers), nor are they aged by manufacturer's aging procedures. At first, these batteries are subjected to slope tests and their slopes are measured. Then by using these slope values their RCN obtained and by using the model their relative capacities are calculated. Meanwhile capacity tests are applied to the batteries and their actual capacities are measured.

The comparison between measured and estimated capacities of these batteries are given in Table 3.16 Since the third battery is fully discharged during the test with third signal, there is no available data for slope test of third signal for third battery.

Table 3.16: Capacity results for uncontrolled tests.

Test Signal ID	Bat. ID	m	RCN	Estimated Cap. (%)	Measured Cap.		Error (%)
					(s)	(%)	
1	#1	-0,03	91,18	97,844	3590	99,722	1,883
	#2	-0,043	278,83	97,025	3549	98,583	1,580
	#3	-0,224	1980,6	70,935	2796	77,666	6,091
	#4	-0,031	106	97,655	3648	101,333	3,630
	#5	-0,037	200,86	97,067	3602	100,055	2,986
2	#1	-0,018	76,834	98,061	3590	99.722	1.665
	#2	-0,026	299,41	97,036	3549	98.583	1.569
	#3	-0,104	1891,1	74,478	2796	77.666	4.105
	#4	-0,019	108,4	97,628	3648	101.333	3.656
	#5	-0,022	196,26	97,077	3602	100.055	2.976
3	#1	-0,021	111,08	97,598	3590	99.722	2.129
	#2	-0,025	237,5	97,022	3549	98.583	1.583
	#3	N/A	N/A	N/A	N/A	N/A	N/A
	#4	-0,022	154,47	97,244	3648	101.333	4.035
	#5	-0,024	220,36	97,035	3602	100.055	3.018

As it can be seen from the Table 3.16, maximum errors are 6.091%, 4.105%, 4.035 % and average errors are 3.234%, 2.794%, and 2.691 % for first and second signals respectively.

3.3. Conclusion

The proposed RC estimation methods, which are different variations of the same approach and very similar, may be used for RC estimation for high accuracy. The basic drawbacks of the methods are that they need a specific test signal and online estimation is not possible. But these methods may be implemented to any vehicle with a simple initialization procedure. After the battery of the vehicle is fully charged, following a test signal RC or SoH of a vehicle may be obtained. The conference proceedings published from these study exists in the literature.

4. HYBRID BATTERY SYSTEM

Although BEVs are the most clean transportation alternatives, they have some drawbacks such as short driving range with single charge, low life span of battery stacks, voltage imbalances in a battery stack and low performance. To overcome these disadvantages and to improve performance using SCs with batteries is a common strategy for BEVs [23]. But SCs also have drawbacks when compared to batteries, such as, low energy densities, high self-discharge rates, and to be more prone to voltage imbalances [12], [13].

In this study a new approach, Hybrid Battery Concept is proposed. This concept includes a battery-battery hybrid energy system instead of battery-SC hybrid. The Hybrid Battery Concept in this study consists of two different of batteries instead of a battery-SC hybrid. One of these batteries has high energy density and the other one has high power density. The battery with high power density will be employed in high performance (hence high power) demanding conditions and the battery with high energy density will help to increase the driving distance. LTO battery is being operated in demanding conditions meanwhile NMC battery is subjected to support LTO without exceeding a current limit. Consequently lifetimes of both batteries are increased. In this study a Kokam SLPB55205130H model $\mathrm{LiNiMnCo_4}$ battery [15] is chosen as the energy dense cell with energy density of 160 Wh/kg and lifespan of 1400 cycles and the Altairnano 13Ah model $\mathrm{Li_4Ti_5O_{12}}$ battery [14] is chosen as the power dense cell with power density of 1675 W/kg and a lifespan of 16000 cycles. A general block diagram of a hybrid battery system can be seen in Figure 4.1.

4.1. Background

Energy management systems (EMS) are computer aided tools which handles basic tasks in order to control and optimize the performance of the system. Generally in electric vehicles EMS takes on the coordination of the energy supplied by several sources which exist in the vehicle and the recovery of the energy which is generated by regenerative braking system. This coordination can be achieved by the use of some

factors such as driving cycles, charge and discharge characteristics and energy storage parameters [73]. Basically EMSs are the tools which decide when and which source to use.

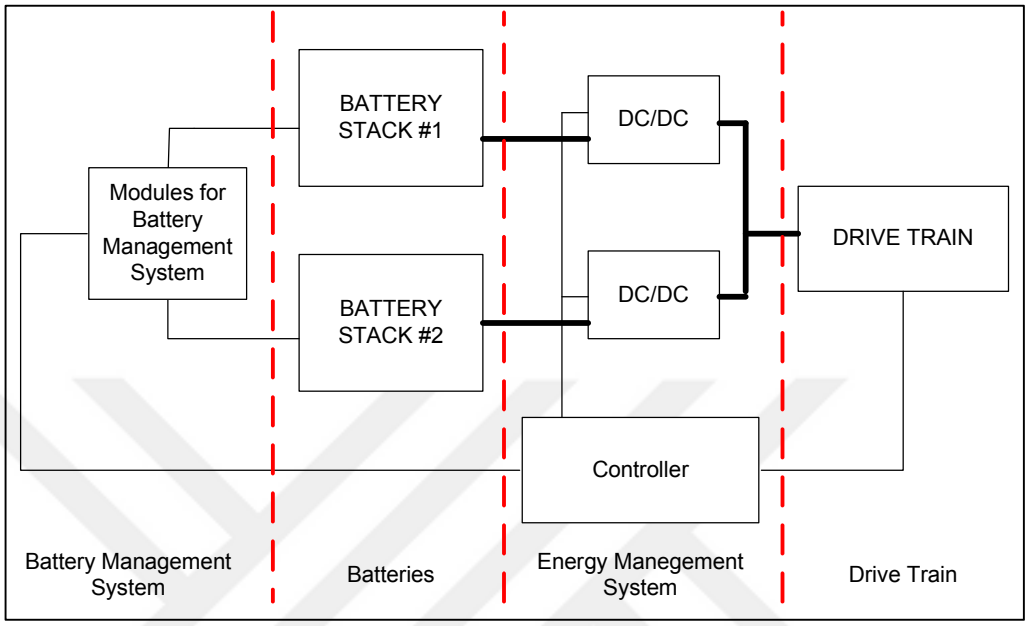

Figure 4.1: General block diagram of HBS.

As an energy management system for FEVs, in Hybrid Battery Systems (HBS) the task of EMS is determination of which battery to be used and amount of energy to be drawn depending on the driving and route conditions. In contrast with FEVs, in HEVs EMSs are mostly used for determination of the ratio and frequency of employment of internal combustion engine or electric motor. The main motivations of energy management strategies for HEVs are decreasing the fuel consumption and/or reducing the carbon monoxide emissions. The objective is to use electric energy more efficiently. For instance an internal combustion engine has low torque values in low speeds meanwhile an electric motor can generate high torques. In this manner, a general strategy is using the electric motor until a specific speed limit, then switching to the engine [74]. Gonder and Markel described three different strategies, a strategy where only the electric motor is employed, the electric motor used dominantly and the internal combustion engine used dominantly [75].

Primarily numerical methods are preferred in energy management of hybrid vehicles. Commonly dynamic programming is used for optimization in a particular

time period. A-ECMS (Adaptive Equivalent Consumption Minimization Strategy) is used [76] but numerical analysis takes long time. In another study target routes are divided into a series of time segments and optimized separately [77]. By this approach also the solution duration is shorter but the solution itself is suboptimal. Also in [78] a simple method based on static optimization is proposed. Another approach to decrease the effort for calculations is based on Hamilton-Jacobi-Bellman equations and principles [79]. Some heuristic algorithms in which Boolean or fuzzy rules were employed also used for the same purpose [80]. For this purpose rule based strategies developed in [81] and fuzzy logic is used in [82]. In order to obtain a global and optimal solution linear [83] and dynamic programming methods [84], [85] are studied. Drawback of these methods is that an online solution can't be obtained because the proposed strategies are performed for known driving cycles. Thereby in these approaches the whole route information is assumed to be known. Nevertheless solutions of these studies may be used as a benchmark while developing a different strategy, or used while generating rules for a rule-based method.

To avoid this [86] used an alternative driving cycle, which is a combination of several driving cycles instead of a single cycle. Although these methods use independent driving cycles, still it will be difficult to cover a real life driving situation. In some studies the current conditions of the vehicle and route are taken into consideration by EMS [87]–[89]. Some methods in which the EMS predicts future conditions and events such as model predictive control [90], stochastic control [91] or global optimization [92], [93] methods are also studied. Thus a connection between the upcoming situations and EMS can be established. These approaches have heavy computational work as a result of advanced control techniques. Estimation accuracy and estimation duration are the parameters to determine the success of the strategy. Estimation of conditions of near future allows the EMS to perform optimization even in small time frames and gives good results [94]. For these approaches the benefits of the control strategy directly depends on the accuracy of estimations. In some studies the required parameters for optimization were obtained by using pattern recognition [95], collected continuously during the ride [87] or battery state of charge as a parameter [96].

However in HBS these motivations and objective are invalid. Therefore the studies about battery-SC hybrids are also examined. In applications of battery-SC hybrids the main motivation is reducing the usage frequency of battery thus reducing the number charge-discharge cycles and increasing the battery life. The basic principle is supplying power demand by employing the SC while supplying energy demand by employing the battery [97]. With this approach fast charge and discharge cycles and high power to be drawn from the battery can be limited. Besides there are also ongoing studies about satisfying the energy demand of oscillating loads and optimizing the parameters and ratio of the SC.

Battery-SC hybrids can be divided into three categories as passive, semi-active and active [98]. In passive topology battery and SC are connected in parallel and directly coupled to the load. Although the semi-active topology is more successful then the passive, a dc/dc converter is needed. In active hybridization two dc/dc converters are needed which makes this topology complicated [98], [99]. In passive hybridization both battery and the SC are connected in parallel with load [98]–[102]. Semi-active hybrids include a DC/DC converter in order to adjust voltage of a source with respect to other. There are three different configurations for semi-active hybrids. In battery semi-active hybrid battery and SCs are cascaded where the converter is placed between the battery and the load. The purpose of this configuration is to control battery current [103]–[105]. In capacitor semi-active hybridization DC/DC converter is placed between SC and the load to improve usage of SC energy [106]–[108]. The third configuration is called parallel or load semi-active hybridization. In this topology, battery and the SC are connected in parallel where the DC/DC converter is placed between this parallel block and the load. This structure enables to satisfy high load demands with limited energy sources [108], [109]. Active hybridization topologies can also be categorized as series or parallel active hybrids. Series active hybrid topology can be achieved by adding another DC/DC converter to a semi-active hybrid where in parallel active hybrids all sources and the load are connected in parallel with DC/DC converters between each connection [108], [110]–[114].

The advantage of the passive topology is its simple structure without a control circuit or power electronics. Thus both the price and the volume of the system

decreases while durability and reliability increases. Also the regenerative breaking is possible without spending extra effort. Major drawback of this topology is that the load sharing between the battery and the SC is totally uncontrolled. General approach in passive hybridization is deciding the voltage and capacitance values of the capacitor by using a load profile of a specific pulse train [98]–[102]. Although this approach gives a good point of view about steady state operation of the system, it is insufficient for transient process [99]. Generally in passive hybridization studies it is shown that the driving distance increases when compared with a system without capacitors [115]–[117]. E.g. [117] hybridized a 600 mAh lithium battery with a 600 mF SC, used a load profile of 2 A, proven that the driving distance is increased without giving any analytical explanation. [102], [118], [119] also made similar studies however [119] made assumptions by using chemical inner structure and simulated in time domain and by a pulse train. [120] uses ECE 15 driving cycle and a novel driving cycle which they have generated in Warsaw including effect of temperature.

In this study two different topologies are investigated, passive and semi-active topologies. First a parallel battery-battery hybrid is proposed and implemented [19]. Unlikely battery-SC hybrids battery-battery hybrids requires high inductances in order to limit the drawn current from a specific selected battery. Another proposed strategy is a semi-active topology with a novel DC/DC converter. In this topology, active elements commutates with a constant duty ratio of 50% during whole operation any active control scheme is not needed, hence can be categorized as a passive topology.

4.2. The Passive EMS for HBS

A totally uncontrolled operation is not possible while using two different type of batteries instead of a battery-SC hybrid. In passive battery-SC hybrids the peak power demand is satisfied by the SC and the battery is used in order to provide longer system operation. In HBS the peak power demand is shared between both batteries although one of them has higher power density. To avoid this situation and to operate system likewise a battery SC hybrid an additional passive power electronics element, a Choke inductor is added to the system. The Choke inductor is connected in series

with the battery which has higher energy density to limit the drawn current from that battery during the peak power phases of the route. Circuit diagram of the passive HBS topology is given in Figure 4.2.

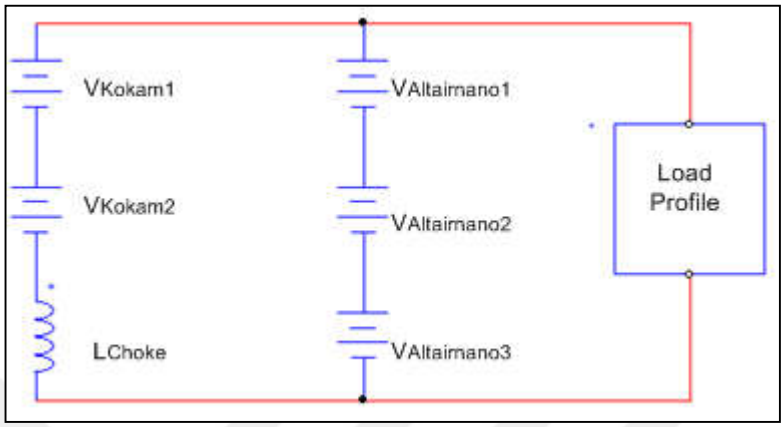

Figure 4.2: Circuit diagram of passive HBS.

NMC and LTO cells have maximum voltages of 4.2 V and 2.8 V depending on temperature conditions, respectively, as given in [14], [15]. Thus, in order to level branch voltages, NMC cells are used in a stack of two batteries connected in series and LTO cells are used in a stack of three batteries. Hence a bus voltage of 8.4 V is reached in both two branches.

An analytical explanation for the system couldn't be available for this stage of the study, because battery specifications given by the manufacturers is not sufficient Following results of simulations it is found that the value of Choke inductor is needed to be around 1H.

To validate the applicability of the proposed energy management strategy a series of experiments were conducted. In these experiments a choke inductor of 3mH is used instead of 1H because of size limitations, considering an average current of 50 A passing through the inductor.

The driving cycle which was given in Figure 2.9 is used in experiments. In the first experiment two batteries were connected in parallel with each other and directly coupled to a load of the driving cycle. The results of the first experiment can be seen in Figure 4.3, where the straight and dotted lines indicate the responses of batteries with high power and high energy densities, respectively.

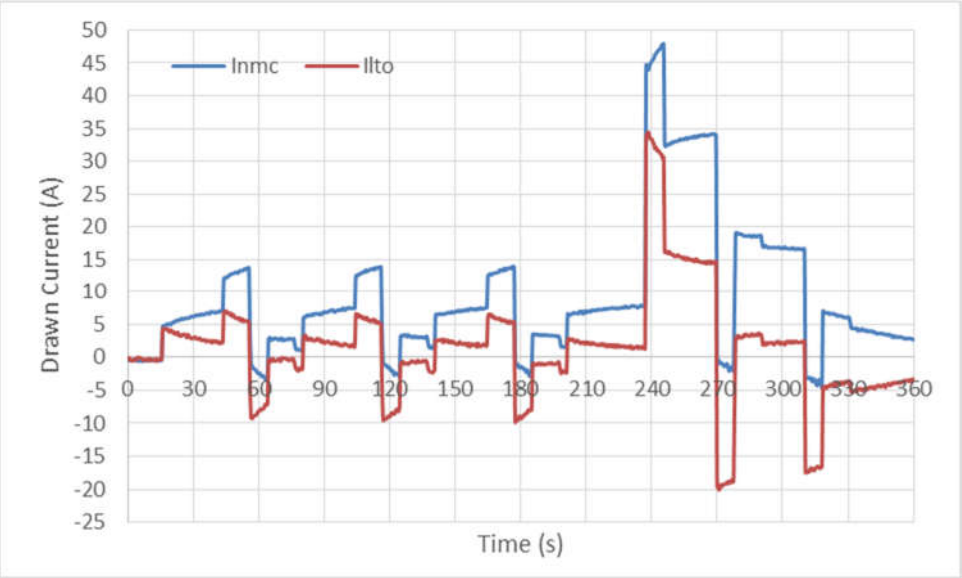

Figure 4.3: Results of experiments without inductor.

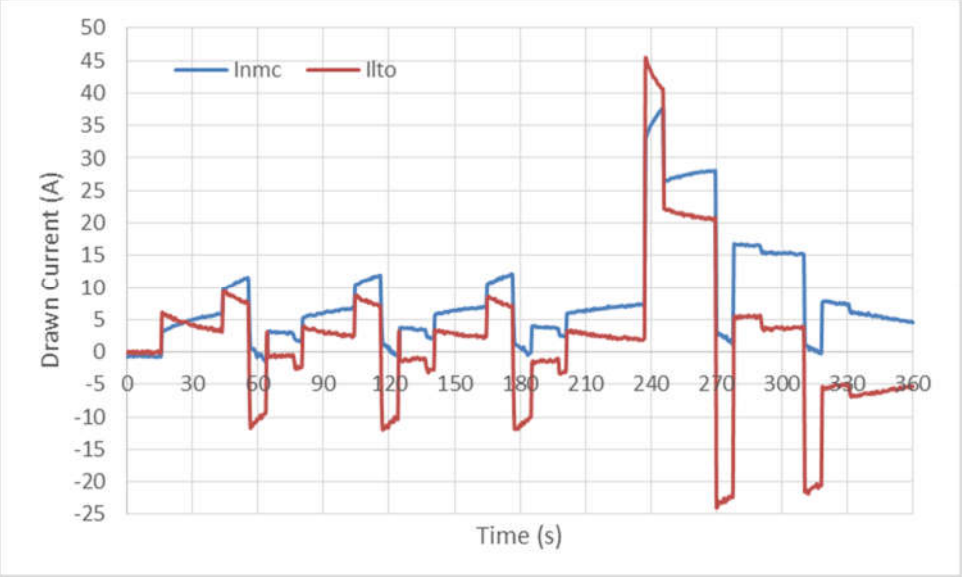

Figure 4.4: Results of experiments with 3 mH inductor.

In the next step the experiment was repeated by connecting a 3 mH inductor in series with the battery with high energy density. The results of the experiment can be seen in Figure 4.4, where the straight and dotted lines indicate the responses of batteries with high power and high energy densities, respectively.

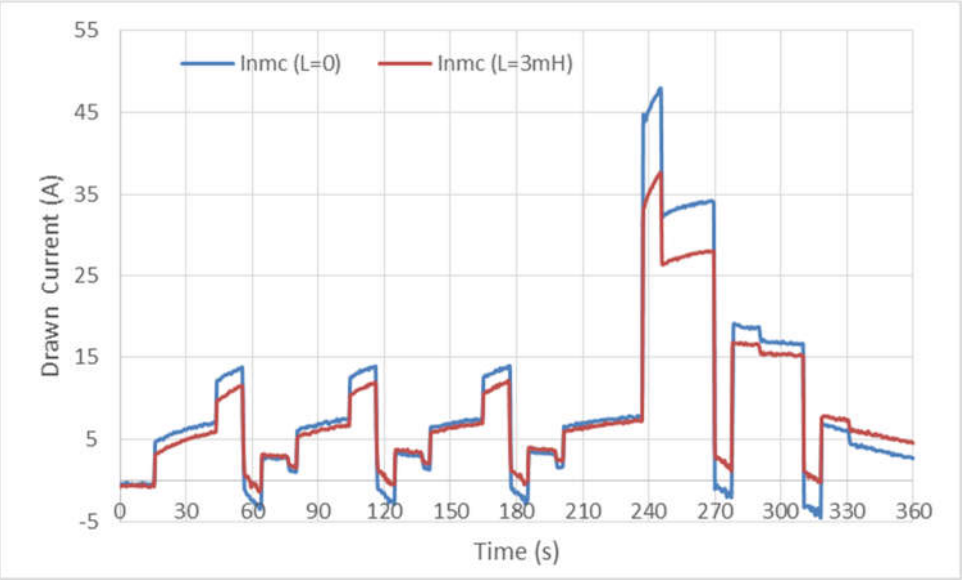

Figure 4.5: Comparison of responses of NMC battery.

Finally in Figure 4.5, the comparison of the results of battery with high energy density in both experiments are shown. The dotted and straight lines demonstrate the results with 3 mH inductor and without inductor, respectively.

Parallel hybridization of batteries has a different motivation when compared to battery-SC hybrids. Battery-SC hybrids are mainly based on calculating the desired parameters of suitable SC for operation [98]–[102]. In battery-battery hybrids, this approach is not possible in battery-battery hybrids, since there are limited battery types which are commercially available. Also many battery parameters are not available for end users or such information is very vague even if it is shared. Hence using a Choke inductor to limit the drawn current from high energy cell is a significant option. From Figure 4.3 it can be said that without any extra elements the drawn current from NMC cell higher than LTO cell. It must be limited around 2 C current (22A) to extend the life of NMC cell [15]. Therefore an inductor around 1 H is needed.

Experiments could only be performed with a 3 mH inductor. From Figure 4.5 it can be seen that there is already a difference between the responses of the batteries. Also the parallel inductor has a significant impact on the result of the battery with higher energy level. Considering that the main expectation is limiting the drawn current from the battery it can be said that passive hybridization with an inductor with the correct value can be used in control of HBS.

4.3. Active EMS for HBS

The proposed active energy management system has a cell scale structure and consists of several number of levels depending on current or power ratings. Every level includes an LTO and an NMC cells, and a bidirectional DC/DC converter between two cells for energy transfer. 5 level topology for the propose system is given in Figure 4.6. As seen from the Figure 4.6 LTO cells are connected in series and this packet is directly connected to the load. On the side of the converter NMC cells are cascaded to each other through a resistor. Anodes of parallel cells may be attached each other through a resistor in voltage balancing studies [121]. The structure including resistors and anodes are called share bus and the resistors are named as bus resistors. In this study the bus resistors are omitted assuming the voltage imbalances between cascaded will not be high and the energy transfer rate will be limited. DC/DC converter includes a transformer in this study. Hence the sides of the converter will be mentioned as primary and secondary respectively for the LTO and NMC cells.

4.3.1. Bidirectional converter

The most important component of the system is the bidirectional DC/DC converter. It is important to select or design appropriate topology for the success of the system. For this purpose the converters in the literature are investigated.

The bidirectional DC/DC converters in the literature may be divided into two categories, isolated and non-isolated converters.

Non-isolated converters are simple, economic and has high reliability. There are basic and derived non-isolated DC/DC converter topologies. Basic topologies include half bridge, Cûk, and SEPİC/Luo, and the derived topologies are cascaded buck-boost (cascaded full bridge), cascaded half bridge or interleaved half-bridge converters. Both six topologies can be seen in Figure 4.7.

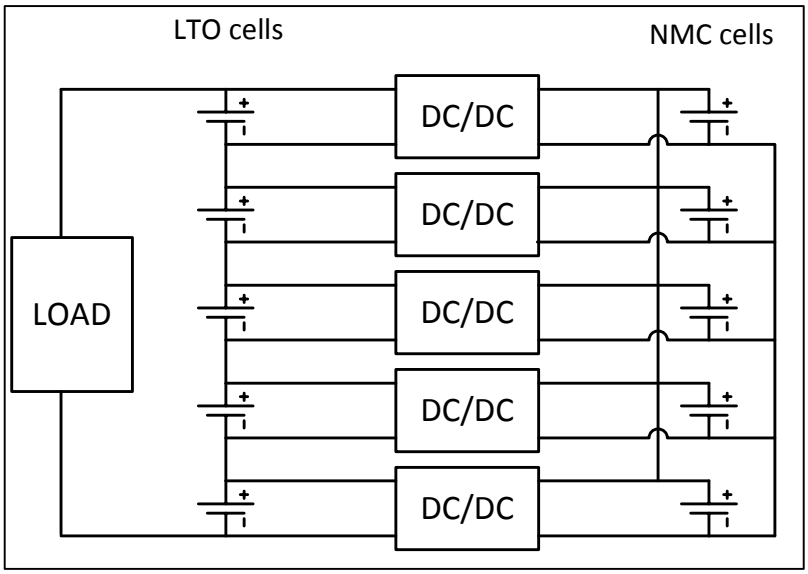

Figure 4.6: 5 level system topology.

In [122] bidirectional buck boost and bidirectional buck-boost cascaded converters are compared for a motor drive application which was powered by batteries. Although buck boost cascaded requires twofold components, their electric and thermal stresses are lower [122]. The stresses of switches are also same in half bridge converter, but this converter can only be operated as buck in one direction and boost in the other [123]. Bidirectional buck boost converter can also be operated in the same manner. The most significant advantage of Cûk converters are their low input-output current ripple [124]. SEPIC/Luo converter is combination of SEPIC (single ended primary inductor converter) and Luo converters. This converter works as SEPIC and step up converter in one direction and works as Luo and step down converter in the other. In [123] half bridge, combined SEPIC/Luo and Cûk converters are investigated and current stresses are compared for energy transfer between an ultacapacitor bank of 150/300 V and a 300 V DC link. In [125] basic converters are compared for a system of 750 V DC link voltage, 180/360 V battery pack voltage, 20K frequency, 30% maximum inductor current. It's denoted that the stress in switches and diodes of half bridge is lower than other topologies. It can be said that the efficiency of half bridge converter is higher where it requires less amount of active elements. But this efficiency decreases with battery voltage level.

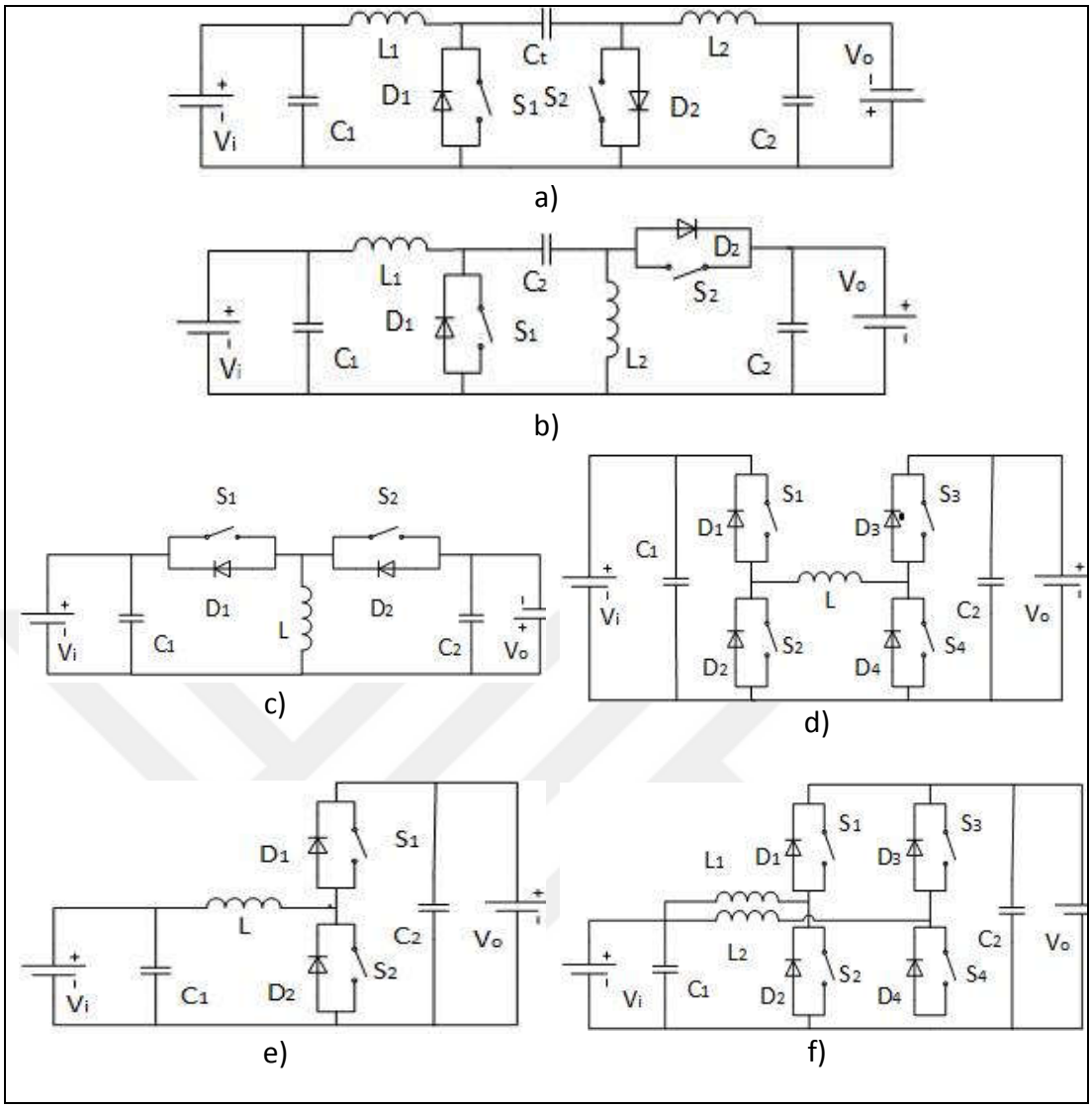

Figure 4.7: Basic non-isolated bidirectional DC/DC converter topologies. a) Cûk, b) SEPIC/Luo, c) bidirectional buck-boost, d) cascaded buck-boost, e) cascaded half bridge, f) interleaved half bridge.

In order to increase efficiency VFPWM (Variable frequency PWM) method is used. Also in [126] for a generator based interior permanent magnet machine which provides power from diesel, an energy management between battery and SC is operated by using a half bridge converter. In [127] 42-14 V DC/DC converter named 2-phase buck converter is proposed. The topology includes coupled inductors. Energy losses of the converter is low owing to low energy storage and it has better transient response. The cascaded buck boost converter topology which was given in Figure 4.7 (d) is called as cascaded buck boost – inductor in the middle (CCB-IIM). in some studies [128]. Also another version of this topology in which there is a capacitor in

the middle (CCB-CIM) is proposed [129]. In [130] these two topologies are modelled, analysed and compared.

Also in some studies three level converters, which can be categorized under multi-level converters are used [125], [131], [132]. In this converters switching stresses are low but high numbers of switching elements are needed. Using areas of three level converters are limited with the type of the topology. Simple reviews for non-isolated bidirectional converters can be found in [123], [125].

In isolated bidirectional converter studies the primary or secondary sides of topologies are divided as current fed or voltage fed. This topologies are beneficial depending on the application or used current or voltage source. This difference can be achieved by using a series inductor or a parallel capacitor to the related side [133], [134]. In [134] two different topologies to use between a 12 V battery and 300 V fuel cell link are compared. The high sides of the topologies are full bridge voltage fed and one of the low side is a half bridge current fed and the other is a full bridge current fed. In [135] a 15 KW prototype for motor drive of a hybrid vehicle is proposed. The primary side of the converter is a voltage fed full bridge and the secondary side is a current fed full bridge. This topology is not appropriate for high power applications because of the leakage inductance of the transformer. This leakage causes spikes on switches of the current fed side. In [136] an RCD snubber is used in secondary side in order to solve this problem. Also in [137] the primary side of the converter is designed as a half bridge instead of a full bridge for same reason. In [138] both sides are half bridges. There is no need for a snubber circuit in this topology, because there is no need to reduce the stresses on switches as the primary switch acts as an active clamp. Another topology is called dual active bridges in which both sides are voltage fed [139]. There is no need for snubber circuits as full bridges on each sides act as snubber. Switching stresses are low and the efficiency is high, however voltage range should be narrow for optimal operation. There are variations of dual bridge topology in which one side [140] or both sides [141] are half bridges. An extended review is given in [142].

Also a third type of bidirectional converters can be given as multiple port converters. These topologies are consist of cascaded isolated or non-isolated

converters. These converters are used in multiple input applications [133], [143]. These converters are also used in battery voltage balancing applications [144].

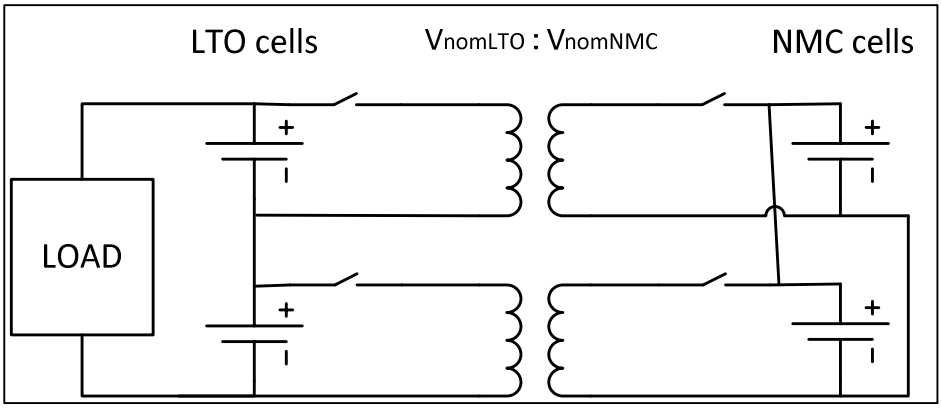

Figure 4.8: Circuit diagram of the proposed converter.

The isolated bidirectional DC/DC converter analysed and used in this study may be defined as a simple synchronous flyback converter. Some primitive variations of this topology exist in the literature, and mainly used in voltage balancing applications. [121], [145], [146]. The circuit diagram of the proposed converter is given in Figure 4.8.

The proposed converter topology consists of a transformer, switches, a snubber circuit and the cells. Although there are two switches in the circuits the duty ratios of the switches are constant at 50%. This duty ratio doesn't change during the whole process and independent from battery condition or operation mode Hence the system can be classified as a semi-active energy management system with passive control scheme. This simplicity is one of the major advantages of the system. A control scheme or feedback is not necessary during operation. Furthermore any route information is not required either.

4.3.1.1. Transformer

Another main component of the system is the transformer. It enables an isolated operation for the system. Also transformer is needed to establish a voltage balance between two different battery types. The voltages ratio of the transformer is 2.8V to 4.2 V, which are the maximum voltage values in room temperature of the

LTO and NMC cells, respectively [14], [15]. The switching frequency of the MOSFETs is 20 kHz. Core material is chosen as 3C90 considering the operating frequency of the system. Type of the core is ETD29T.

4.3.1.2. The snubber circuit

A resonance occurs between the output capacitor of the MOSFET (C_{om}) and leakage inductor of the transformer (L_{lk}), during system operation. Because of this resonance, a high voltage spike appears on the drain of the MOSFET when the MOSFET is switched off. As a result of this high voltage spike on the drain pin, a large current within the MOSFET is allowed, resulting low switching efficiency, even damaging the MOSFET. This phenomenon is called avalanche breakdown.

Input voltage, V_{in} and reflection of output voltage to the primary side, nV_o effects the MOSFET where n is the turns ratio of the transformer. When MOSFET is switched off, primary current of the system charges C_{om} in a very short instance. When the voltage of the output capacitor exceeds sum of input voltage and reflection of output voltage ($V_{in} + nV_o$), body diode of the MOSFET in the secondary side is turned on. Therefore the voltage across the magnetizing inductor of the transformer becomes equal to reflected output voltage, nV_o. As a result, a resonance between $C_{om}$and L_{lk} occurs. When the MOSFET is switched on, reverse recovery current of the body diode of the MOSFET on the secondary side of the system is added to the primary current and consequently a large current ripple occurs.

The excessive voltage should be supressed to protect the MOSFETs. Thus an RCD snubber circuit is designed. In the snubber circuit C_{snub} is assumed to be large that the voltage across the capacitor doesn't change during one period. When voltage across the output capacitor of the MOSFET exceeds $V_{in} + nV_o$, snubber diode, D_{snub} is turned on and primary current flows to C_{snub} through D_{snub}, resulting adsorption of the current in L_{lk}. Value of the snubber resistance can be calculated as in equation (5.1) [147]:

$$R_{snub} = \frac{V_{snub}^2}{\frac{1}{2} L_{lk} i_{peak}^2 \frac{V_{snub}}{V_{snub} - nV_o} f_s} \tag{4.1}$$

In the equation V_{snub} is the voltage across C_{snub}, $i_{peak}$is the peak value of the primary current, and f_s is the switching frequency of the system. V_{snub} is chosen as 3 times of nV_o. Switching frequency of the system, $f_s = 20000\ Hz$ and i_{peak} = 0.4 A. L_{lk} is measured as 1.64 μH. Consequently snubber resistance is obtained as $R_{snub} = 424.93\ \Omega$.

Snubber capacitor can be calculated by considering the ripple of the snubber capacitor voltage, where ΔV_{snub} is the change in snubber capacitor voltage.

$$C_{snub} = \frac{V_{snub}}{\Delta V_{snub} R_{snub} f_s} \tag{4.2}$$

By choosing the maximum ripple of the snubber capacitor voltage as 10%, value of the snubber capacitor can be obtained as $C_{snub} = 1176.7\ nF$.

In order to show the effect of snubber circuit an experiment is done. In the experiment, voltages of LTO and NMC cells are 2.7 V and 3.3 V, respectively. Thus the direction of energy transmission is from LTO to NMC cell. The voltages on the terminals of transformer is recorded for both without and with snubber circuits and given in Figure 4.9, a) and b), respectively.

4.3.1.3. Operation of the bidirectional converter

Simulations of the bidirectional converter is completed in Simulink using generic battery models, introduced in Section 3.4 and simulation diagram is shown in Figure 4.10.

In the first simulations SoC of the LTO cell is chosen as 100% while SoC of the NMC cell is 50%, in order to analyse energy transfer in LTO-NMC direction. In the beginning $V_{LTO} = 2.81\ V$ and $V_{NMC} = 3.67\ V$, where after the operation new values are $V'_{LTO} = 2.58\ V$ and $V'_{NMC} = 3.72\ V$. The voltage ratio between the cells is 1.44 and the error between this ratio and the voltage ratio of the transformer is 3.93%. The simulation results are given in Figure 4.11.

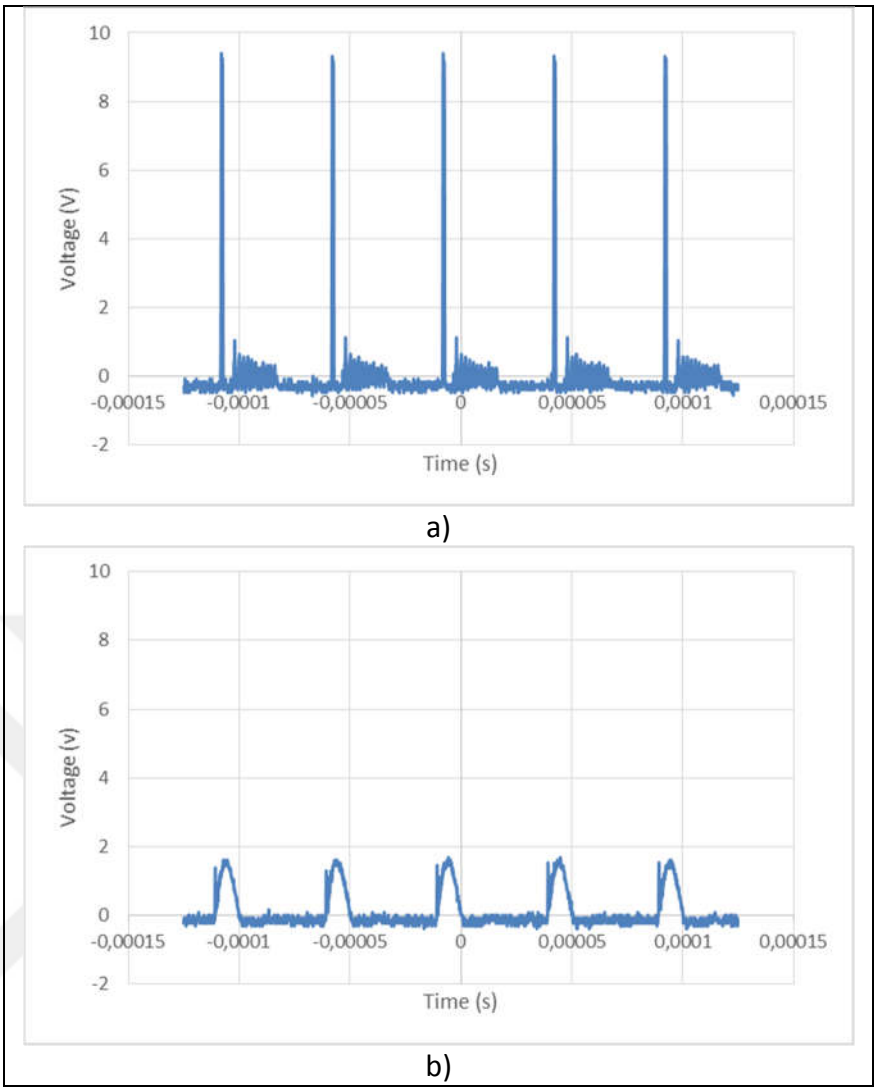

Figure 4.9: Transformer voltage a) without, b) with, snubber circuit.

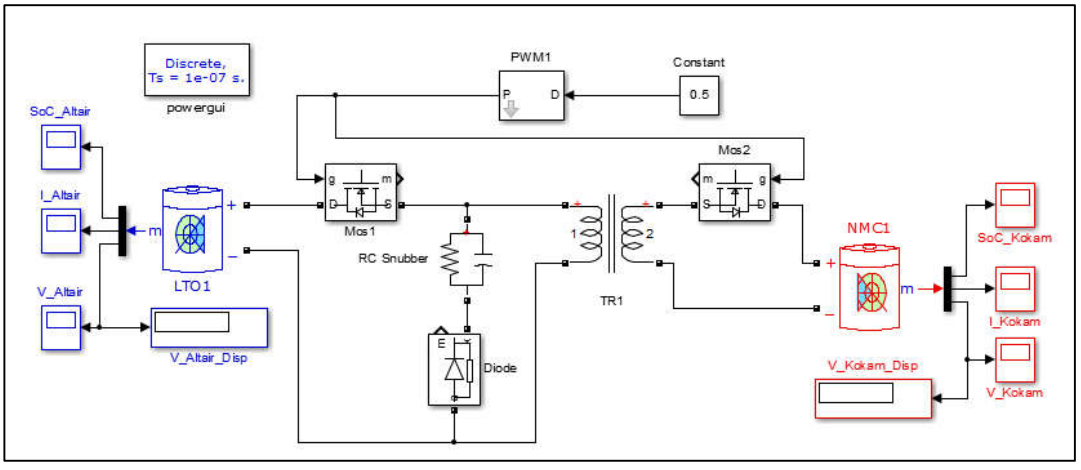

Figure 4.10: Simulation setup for the bidirectional converter.

The simulation is repeated with different conditions where SoC of the NMC cell is 100% and LTO cell is 50%, where $V_{NMC} = 4.218\,V$ and $V_{LTO} = 2.427\,V$. After operation new values for batttery voltages are, $V'_{NMC} = 3.798\,V$ and $V'_{LTO} = 2.646\,V$. The voltages ratio between two cells are 1.435 and the error is 4.29%. The simulation results are given in Figure 4.12 and the current waveforms are shown in Figure 4.13. Directions of the currents are from system to battery. Thus the graphic in Figure 4.13 can be interpreted as NMC cell is being discharged while LTO cell is being charged.

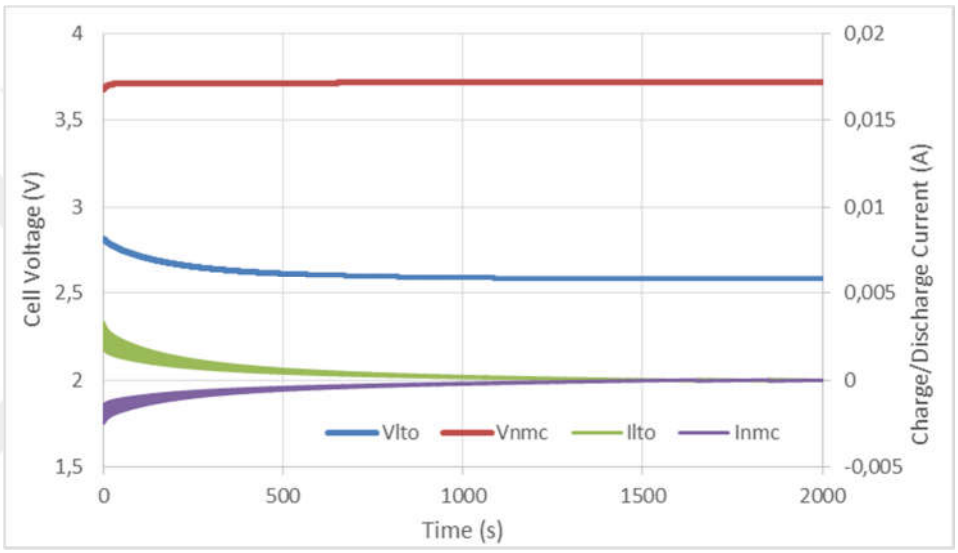

Figure 4.11: Simulation results of battery voltages and currents during energy transfer in LTO-NMC direction.

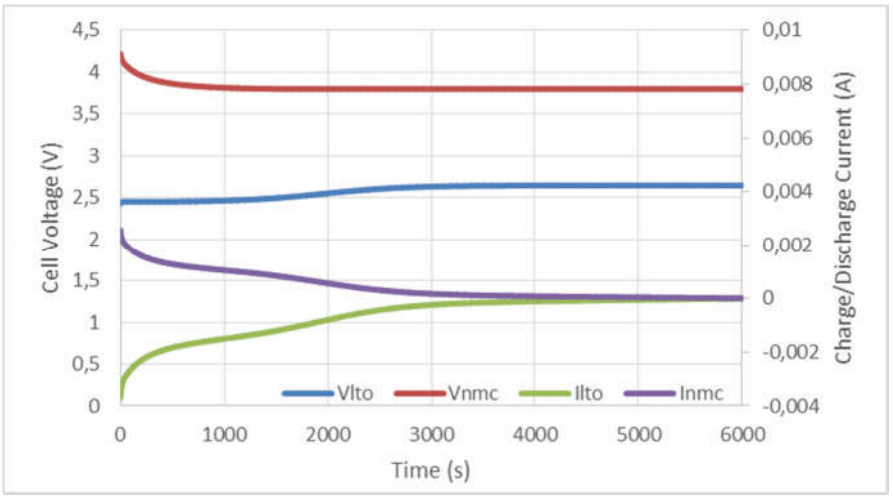

Figure 4.12: Simulation results of battery voltages and currents during energy transfer in NMC-LTO direction.

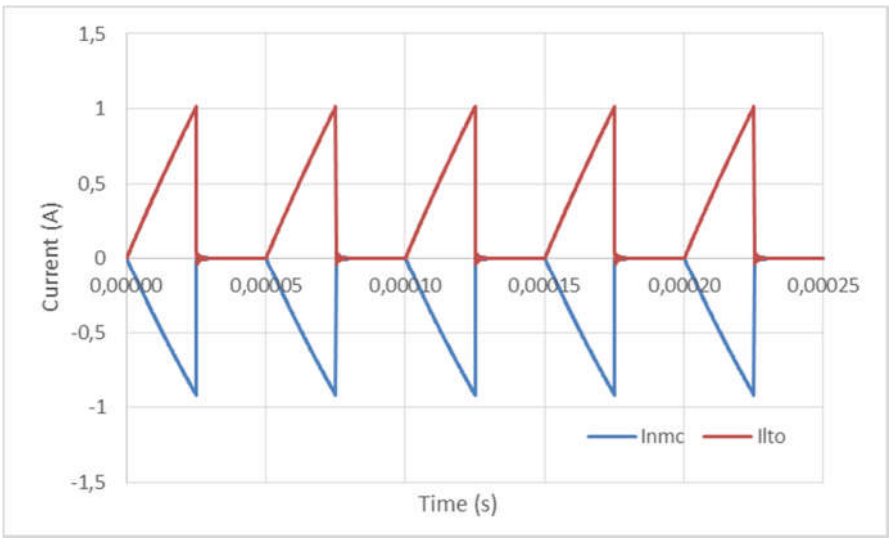

Figure 4.13: Simulation results of battery current waveforms during energy transfer in NMC-LTO direction.

Circuit diagram of the bidirectional converter can be seen in Figure 4.14. A prototype of the bidirectional converter, which is shown in Figure 4.15, is produced for experimental studies. IRL540N is chosen as MOSFET because of logic driving capability and economical reasons. Switching signal is produced by a signal generator and gates of two switches are insulated by using 1:1 isolation transformers. Frequency and duty ratio of the PWM signal is 20 KHz and 0.5 respectively. The transformer is build in the laboratory. Including the diode forward voltage of the MOSFETs the transformer is build as turn ratio, $a = 0.73$.

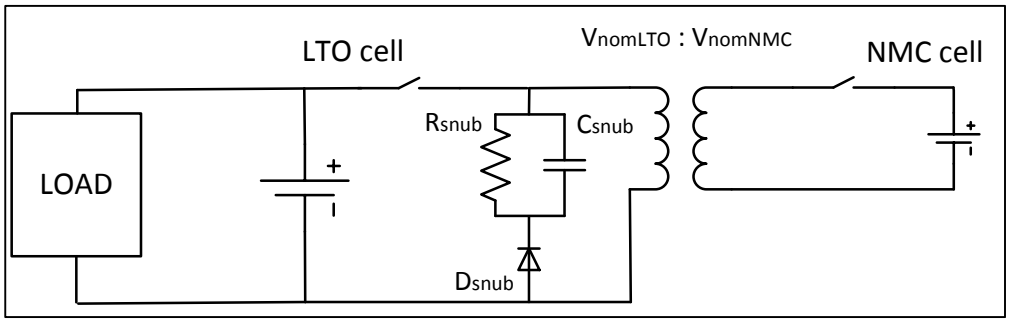

Figure 4.14: Bidirectional converter circuit.

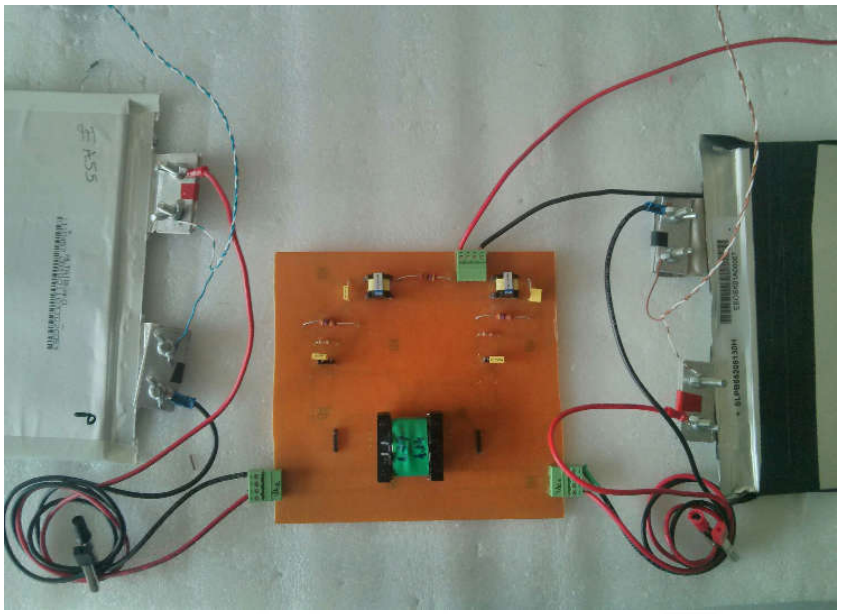

Figure 4.15: Prototype circuit of the bidirectional converter.

In the first experiment the energy transfer is in NMC-LTO direction. Battery voltagers are arranged as $V_{LTO} = 2.535\ V$ and $V_{NMC} = 4.047\ V$. The scope outputs of current waveforms for this experiment is given in Figure 4.16. The similarity between the simulation results which is given in Figure 4.13 can be recognized.

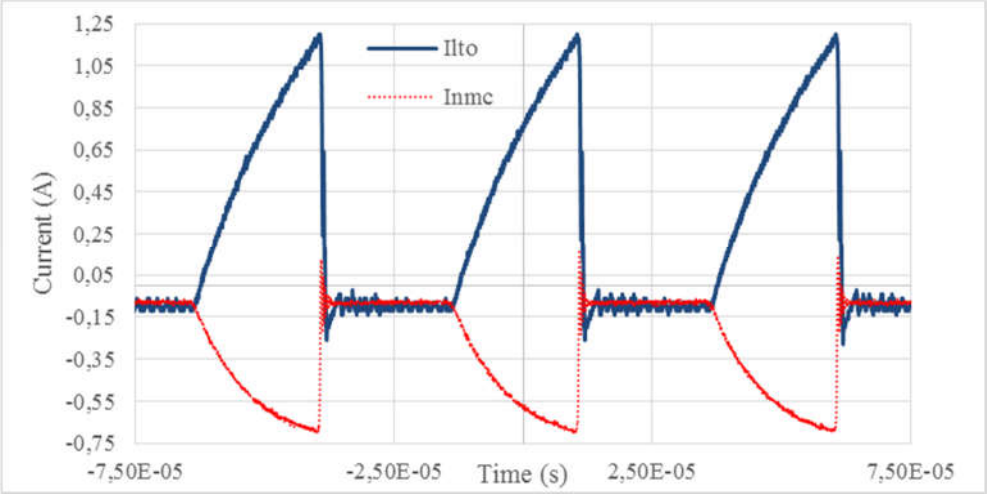

Figure 4.16: Scope outputs of the current waveforms for the first experiments.

As seen from the figure maximum value of the charge current of LTO cell is 1.16 A. Maximum value of the discharge current of NMC cell is 0.696 A. Although the maximum values of charge and discharge currents are different, the negative

component of the charge current of LTO cell must be noted. Because of this negative component, mean value of the current of LTO cell is 0.274 A where the mean value of current of NMC cell is -0.281 A Also saturation of the transformer is postponed because of this negative component. The value of the efficiency in energy transfer is 95.4%. Considering the system will mostly be used in discharge mode and direction of the energy transfer is from NMC to LTO cell, this efficiency value may be accepted as general system efficiency.

After balancing the new voltage values for the cells are $V_{NMC} = 3.952\,V$ and $V_{LTO} = 2.688\,V$. The ratio between cell voltages is 0.68. The error is 6.8 % when compared to transformer's voltage ratio. Battery voltages for this experiment is given in Figure 4.17.

For the second experiments voltages of NMC and LTO cells are set to 3.329 V and 2.669 V respectively. Direction of the energy transfer is from LTO cell to NMC cell. After operation the new values for the cell voltages are 3.374 V and 2.488 V respectively for NMC and LTO cells. The ratio of battery voltages is 0.73 and the error is around 1 %. Battery voltages for this experiment is given in Figure 4.18.

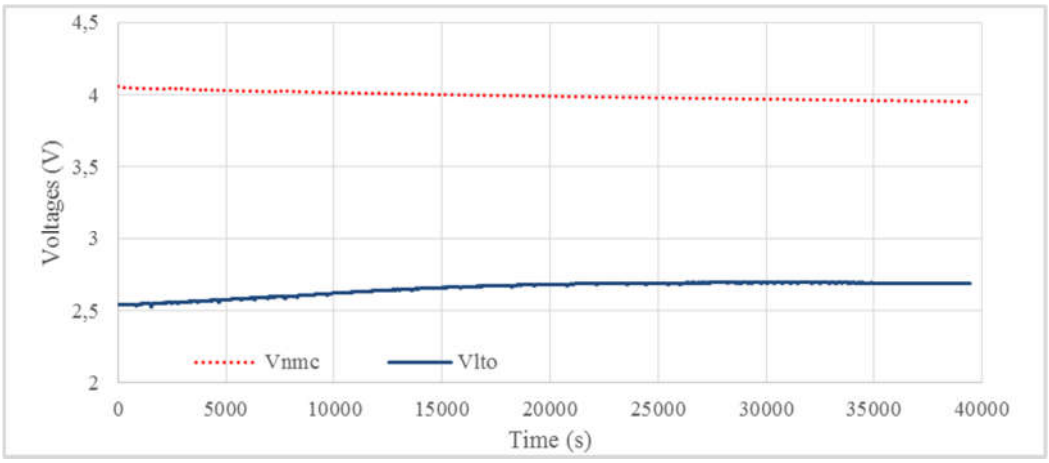

Figure 4.17: Experimental results of battery voltages for energy transfer in NMC-LTO direction.

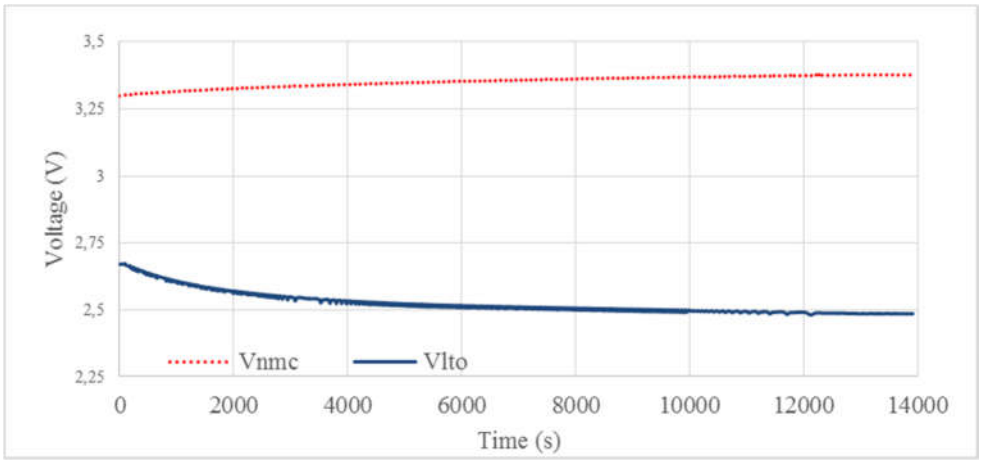

Figure 4.18: Experimental results of battery voltages for energy transfer in LTO-NMC direction.

4.3.2. Operation of the active EMS

4.3.2.1. Simulations

The operation of the proposed energy management system may be investigated under several headlines such as idle mode, charge or discharge modes. In both of the three modes simulations were done for a three level system. For idle mode operation battery voltages are set as: $V_{LTO_1} = 2.6166\,V$, $V_{LTO_2} = 2.5209$ V and $V_{LTO_3} = 2.4754\,V$, $V_{NMC_1} = 4.0283\,V$, $V_{NMC_2} = 3.9297\,V$, and $V_{NMC_3} = 3.8776\,V$. Average values are $V_{LTO_{ort}} = 2.5376\,V$ and $V_{NMC_{ort}} = 3.9452\,V$. After the operation new average values are $V_{NMC_{ort}} = 3.9452\,V$ and $V_{LTO_{ort}} = 2.5376\,V$. Voltage waveforms for simulation results are given in Figure 4.19 (a) and (b) respectively for LTO and NMC cells.

In discharge mode operation LTO cells are subjected to a load. In this mode both battery voltage imbalances are satisfied and LTO cells are supported by NMC cells. In simulations battery voltages are set as $V_{NMC_1} = 4.21\,V$, $V_{NMC_2} = 3.9297$ and $V_{NMC_3} = 3.8494\,V$ for NMC cells, and $V_{LTO_1} = 2.5547$, $V_{LTO_2} = 2.2569$, and $V_{LTO_3} = 2.1895\,V$ for LTO cells. The results are given in Figure 4.20.

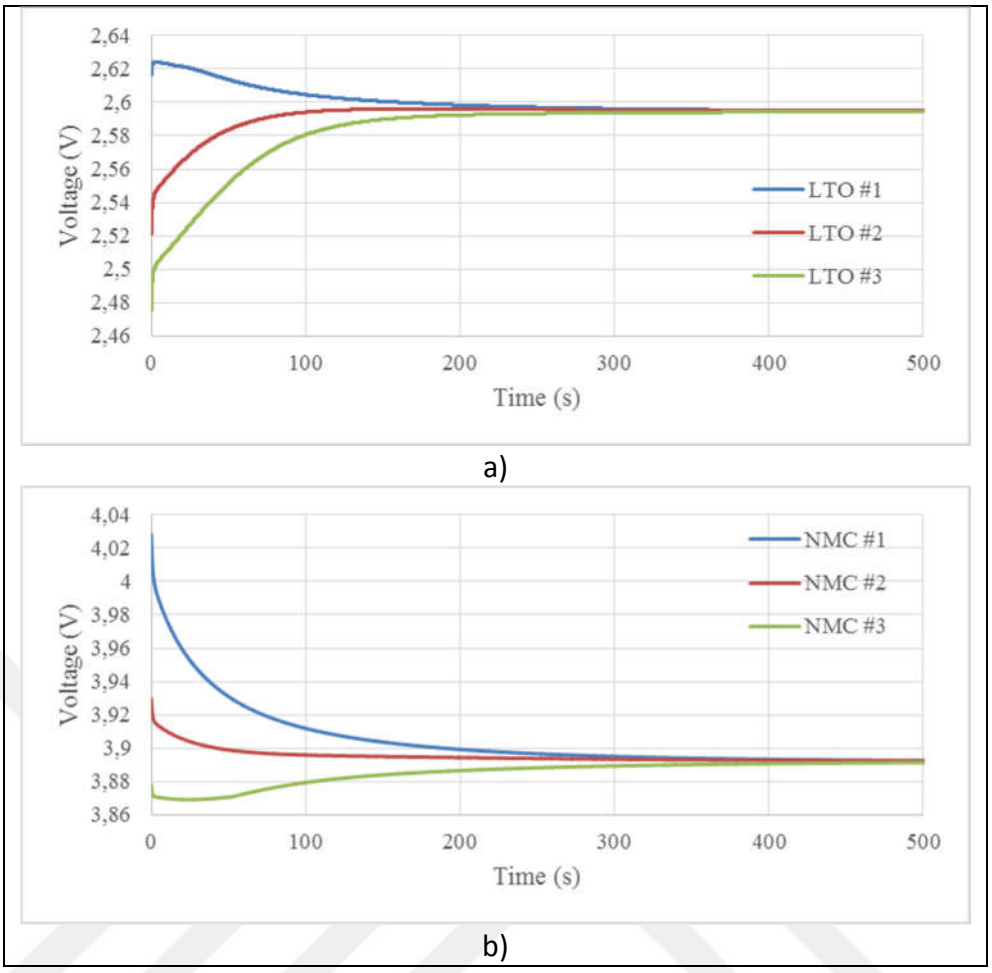

Figure 4.19: Simulation results for idle mode operation, a) for LTO, b) for NMC cells.

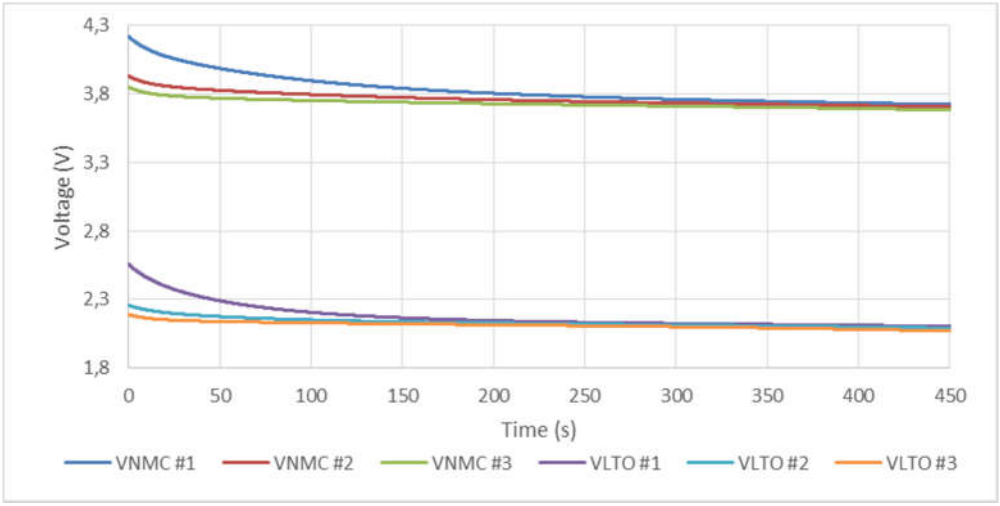

Figure 4.20: Simulation results of discharge mode operation.

Logic of the charge mode operation is inverse of the discharge mode operation as in this mode a source feeds the LTO cells. For the last simulations a load profile of

200 s, which includes 40 A charge, idle mode, 40 A discharge and 80 A discharge parts of 50 s each, is generated and used. The load profile is shown in Figure 4.21

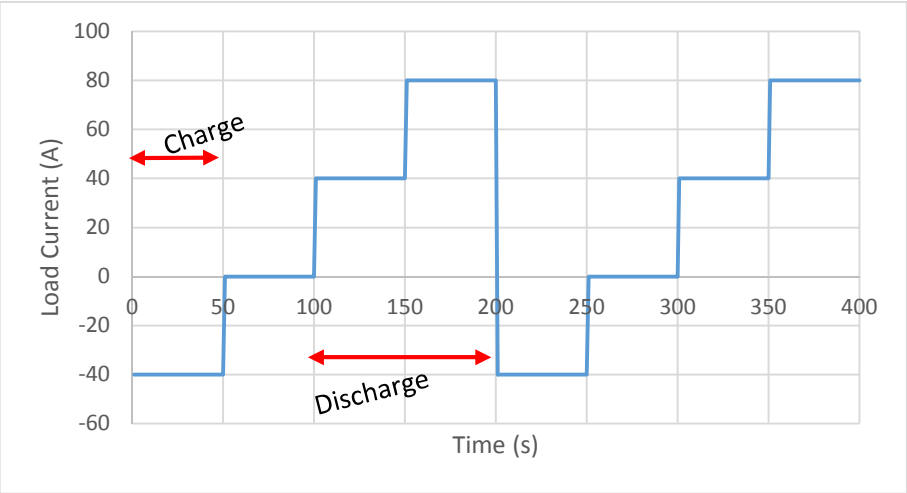

Figure 4.21: Load profile.

In this simulations NMC cells are fully charged where the voltage levels of LTO cells are set as: $V_{LTO_1} = 2.9506\ V$, $V_{LTO_2} = 2.6529\ V$, and $V_{LTO_3} = 2.5854\ V$. The results of the simulation is given in Figure 4.22.

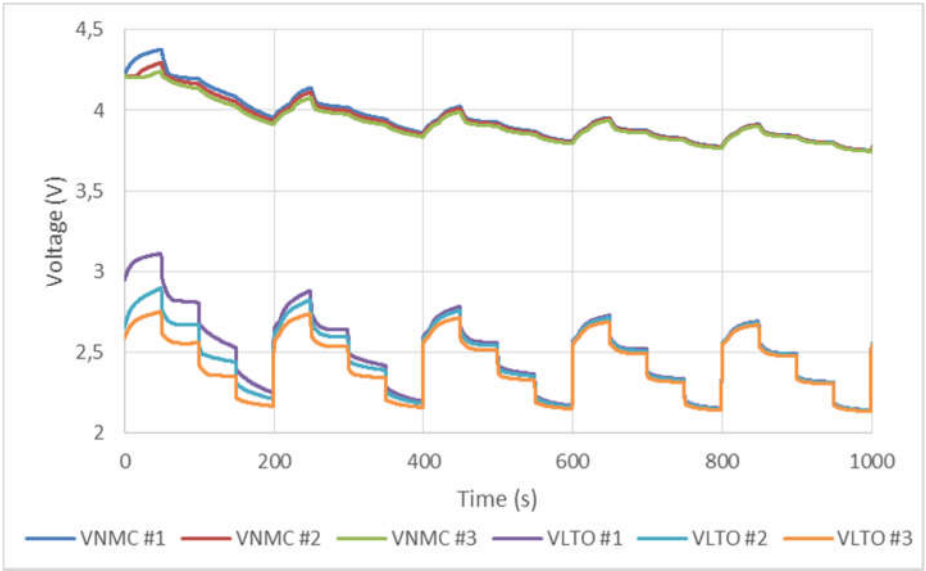

Figure 4.22: Simulation results under the load profile.

4.3.2.2. Experimental study

An experimental study is also done to validate system operation. Because of some limitations the system including two levels are implemented.

To test the system in the idle mode two different experiments are conducted. In the first one the energy transfer is in LTO-NMC direction. Battery voltages are set as: $V_{LTO_1} = 2.65\ V, V_{LTO_2} = 2.80\ V, V_{NMC_1} = 3.05\ V$, and $V_{NMC_2} = 3.25\ V$. The result of this experiment is given in Figure 4.23.

Later, the experiments are repeated, this time to observe the energy transfer in NMC-LTO direction. For this purpose battery voltages are arranged as: $V_{LTO_1} = 1.7\ V, V_{LTO_2} = 1.95\ V, V_{NMC_1} = 4.05\ V$, and $V_{NMC_2} = 4.2\ V$. The results are given in Figure 4.24

To test discharge mode operation several experiments with different constant load values are conducted. In the first experiment battery voltages are selected as, $V_{NMC_1} = 4\ V, V_{NMC_2} = 4.2\ V, V_{LTO_1} = 2.55\ V$, and $V_{LTO_2} = 2.75\ V$, and the load current is constant 10 A. The voltages are shown in Figure 4.25.

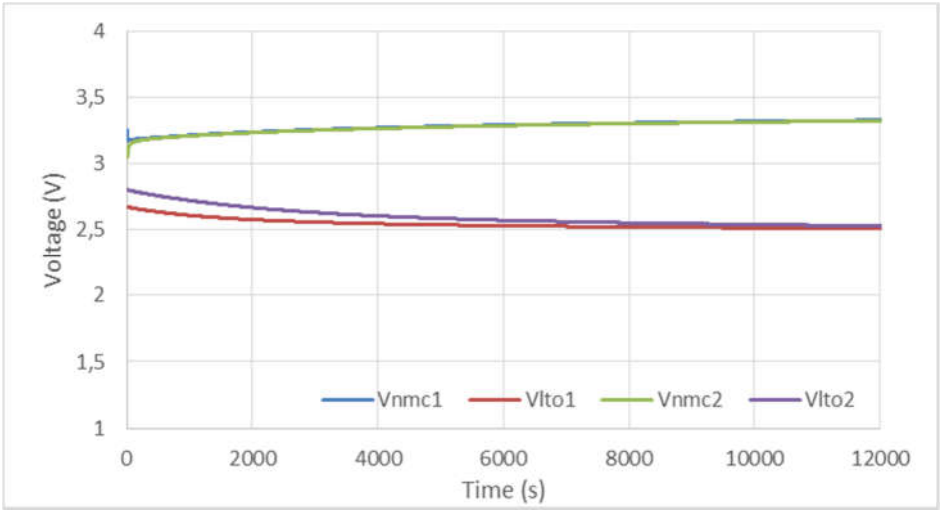

Figure 4.23: Experimental results for idle mode operation in LTO-NMC energy transfer direction.

For the second experiment battery voltages are selected as, $V_{NMC_1} = 4.18\ V, V_{NMC_2} = 4.23\ V, V_{LTO_1} = 2.50\ V$, and $V_{LTO_2} = 2.65\ V$, and the load current is constant 5 A. The voltages are shown in Figure 4.26.

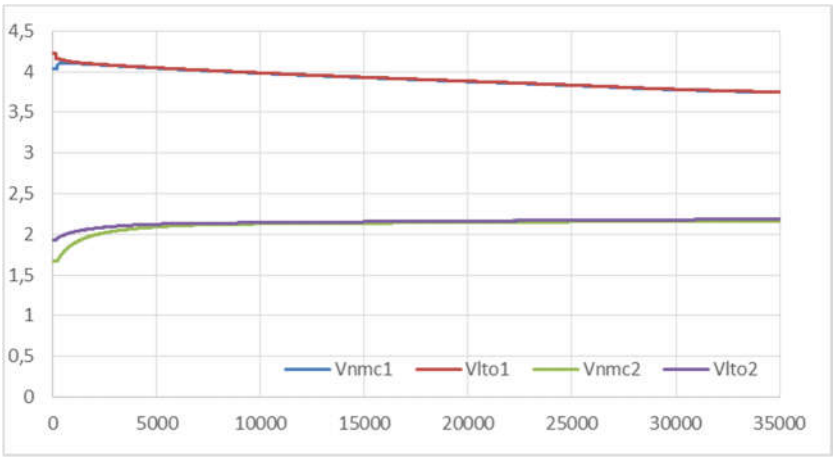

Figure 4.24: Experimental results for idle mode operation in NMC-LTO energy transfer direction.

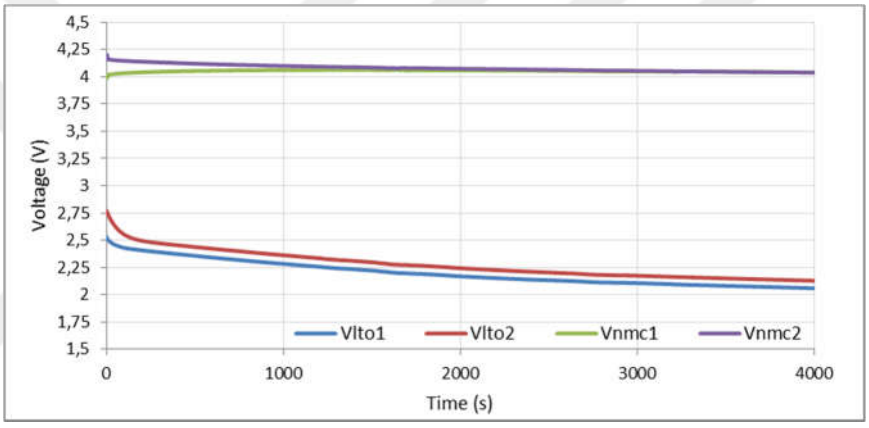

Figure 4.25: Experimental results for discharge mode operation under constant load of 10 A.

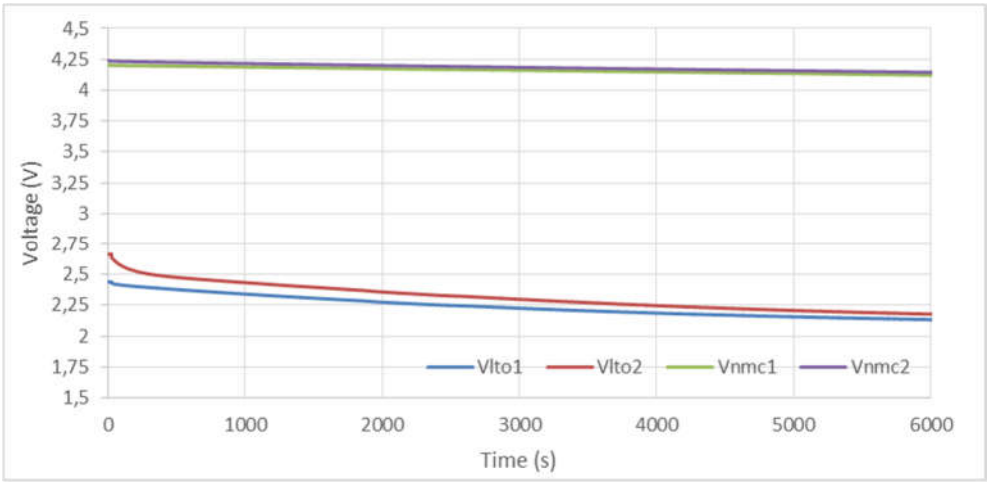

Figure 4.26: Experimental results for discharge mode operation under constant load of 5 A.

From Figure 4.25 and Figure 4.26 it can be seen that LTO cells can't be balanced under load.

For charge mode operation 10 A applied to the system. Battery voltages are arranged as, $V_{NMC_1} = 2.95\,V, V_{NMC_2} = 2.8\,V, V_{LTO_1} = 2.50\,V$, and $V_{LTO_2} = 2.70\,V$. The results are given in Figure 4.27.

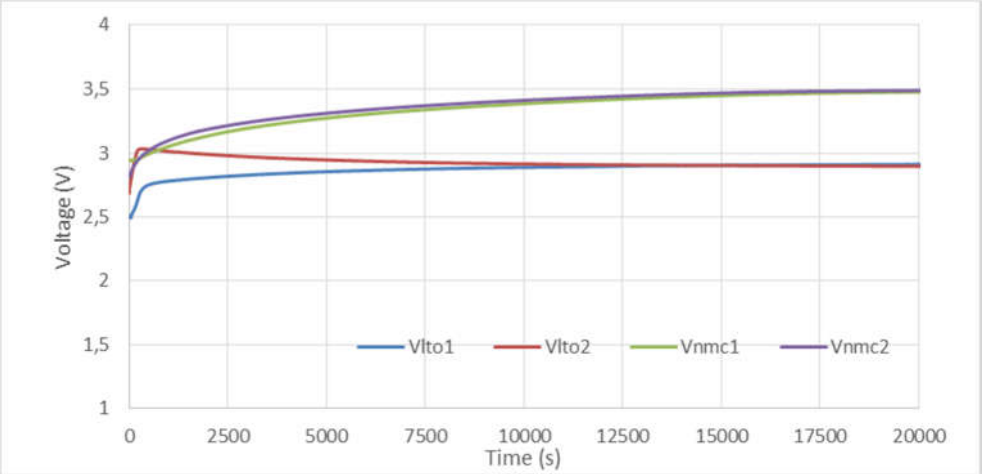

Figure 4.27: Results of the first experiments of charge mode operation under constant source.

Final experiments were conducted with different load conditions. Previously introduced scheme, which was given in Figure 2.9 is used as the load profile. The amplitude is used as half where the maximum current is 40 A. The results are given in Figure 4.28.

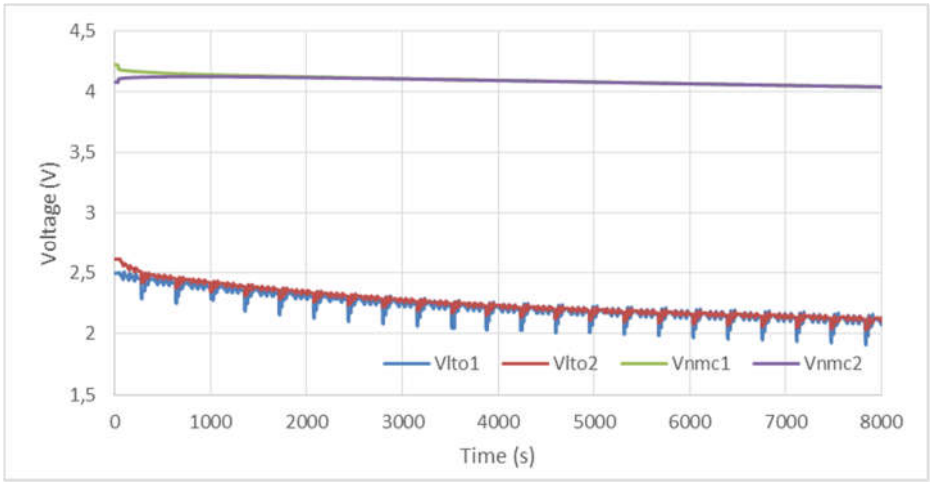

Figure 4.28. Experimental results under a variable load profile.

5. CONCLUSION AND FUTURE WORKS

5.1. Conclusion

The major subject of this study is Hybrid Battery System (HBS) which is a promising energy system alternative for battery electric vehicles (BEVs). In this work various topics related to HBS, including an analytical battery model which can also be used for SoC estimation, a relative capacity model for SoH estimation, a bidirectional DC/DC converter, and an energy management system has been investigated.

The first section of the thesis investigates environmental harms of fossil fuels and includes information about BEVs. A brief information about objectives of the thesis and the thesis layout is also presented in this section.

The second section is about battery modelling. In this section existing battery models are investigated. The achievements made about battery modelling in this thesis can be listed as follows.

- A previously introduced electric equivalent circuit battery model [17] is enhanced in order to reflect aging effects of the battery model. By this way this model became available to be used in SoH studies.
- A simple analytical battery modelling method is proposed. Model is validated with two different cell chemistries (NMC and LTO) and the success of the model is around 96%. This type of models may be used in analytical studies or heuristic methods. Furthermore the analytical model gives the consumed capacity in terms of load current and duration. Hence the model can also be used as a SoC model.

The third section is about battery state of health (SoH) estimation. Although SoH of a battery is not necessary for the energy management approach in this study, it is important to estimate SoH of a battery accurately for successful Battery Management (BMS) and Energy Management Systems (EMS), as most of battery parameters are directly correlated with available battery capacity. In this study SoH

is represented by using the relative capacity and capacity retention of the battery. Two different variations of this approach is methodized. Average errors for both methods are about 3%.

Main objective of this study is to design the new energy system, HBS. For this purpose in final chapter hybrid battery concept is introduced and two energy management systems are proposed. The main points of the study about HBS can be summarized as follows:

- Although both of the systems have deficiencies, they can be preferred in some applications depending on area of usage.
- Active EMS is operated with a constant duty ratio. Hence, unless a fault occurs, the system may be operated without need of any intervention. Thus the system may be accepted as a passive EMS.
- As seen from Figure 4.25, Figure 4.26, and Figure 4.28 NMC cell cannot support LTO cell as in desired level. This is because low energy transfer ratio between two cells in the same level. Main reason for this situation is the low efficiency depending on the losses of the transformer and converter circuit. Furthermore charging duration and voltage levels in Figure 4.27 also proves this suggestion.

5.2. Future Works

Efficiency of the active EMS may be increased. One of the methods for this purpose is to use planar magnetics. It is known that planar magnetics have low profile, greater surface area, greater magnetic cross-section area, smaller winding area, ability to use modified winding structures which enables fewer turns and interleaved windings (hence lower leakage inductance) and less AC winding resistance.

REFERENCES

[1] Sher E., (1998), "Environmental Aspects of Air Pollution". In: E. Sher, Editor, "Handbook of Air Pollution from Internal Combustion Engines: Pollutant Formation and Control", Boston: Academic Press.

[2] Kampa M., Castanas E., (2008), "Human health effects of air pollution", Environmental Pollution, 151 (2), 362-367.

[3] Web 1, (2016), https://people.hofstra.edu/geotrans/eng/ch8en/conc8en/ch8c1en.html, (Accessed 22/05/2016).

[4] Katsouyanni K., (2003), "Ambient air pollution and health", British Medical Bulletin, 68 (1), 143–156.

[5] Web 2, (2012), http://www.worldenergyoutlook.org/weo2012/, (Accessed 22/05/2016)

[6] Web 3, (2016), http://www.tuik.gov.tr/PreHaberBultenleri.do?id=21601. (Accessed: 22/05/2016).

[7] Web 4, (2015), http://www.tuik.gov.tr/PreHaberBultenleri.do?id=18744. (Accessed: 22/05/2016).

[8] Web 5, (2015), http://www.skdturkiye.org/tasitlardaenerjiverimliligi.pdf. (Accessed: 22/05/2016).

[9] Web 6, (2016), http://www.iea.org/evi/Global-EV-Outlook-2015-Update_1page.pdf, (Accessed: 22/05/2016).

[10] Web 7, (2016), http://www.odd.org.tr/folders/2837/categorial1docs/1414/basinbulteni7ocak2016.pdf, (Accessed22/05/2016).

[11] Ajanovic A., (2015), "The future of electric vehicles: prospects and impediments", Wiley Interdisciplinary Reviews: Energy and Environment, 4 (6), 521–536.

[12] Obreja V. V. N., (2008), "On the performance of supercapacitors with electrodes based on carbon nanotubes and carbon activated material—A review", Physica E: Low-Dimensional Systems and Nanostructures, 40 (7), 2596–2605.

[13] Omar N., Coosemans T., Martin J., Salminen J., Kortschak B., Van Mierlo J., Volker H., (2012), "SuperLib Project : Advanced Dual-Cell Battery Concept for Battery Electric Vehicles", EVS 26 International Battery, Hybrid and Fuel Cell Electric Vehicle Symposium, 1-6, Los Angeles, LA, USA, 6-9 May.

[14] Altairnano, (2012), "13 Amp Hour Cell, Nano Lithium-Titanate Battery Cell Specifications", Technical Report No: 3334206, Altair Nanotechnologies, USA.

[15] Kokam, (2009),"SLPB (Superior Lithium Polymer Battery) Technical Specification", Technical Report No: KD07-RE12-02, Kokam Co. Ltd., South Korea.

[16] Ceylan M., Sarikurt T., Balikci A., (2013), “Elektrikli araçlarda kullanilan lityum - iyon bataryalar için model geliştirilmesi”, 5. Enerji Verimliliği ve Kalitesi Kongresi, 82–87, Kocaeli, Türkiye, 23-24 May.

[17] Ceylan M., Sarikurt T., Balikci A., (2014), “A Novel Lithium-Ion-Polymer Battery Model for Hybrid / Electric Vehicles”, IEEE International Symposium on Industrial Electronics, ISIE, 366–369, Istanbul, Turkey, 1-4 June.

[18] Sarikurt T., Ceylan M., Balikci A., (2014), “A Hybrid Battery Model and State of Health Estimation Method for Lithium-Ion Batteries”, IEEE International Energy Conference, ENERGYCON, 1349–1356, Dubrovnik, Croatia, 13-16 May.

[19] Sarikurt T., Balikci A., (2015), “A novel battery system for electric vehicles”, In: I. Dincer, M. A. Ezan, C. O. Colpan, O. Kizilkan Editors, “Progress in Clean Energy, Volume 2, Novel Systems and Applications”, Springer International Publishing.

[20] Deng D., (2015), “Li-Ion batteries: basics, progress, and challenges”, Energy Science & Engineering, 3 (5), 385–418.

[21] Scrosati B., Garche J., (2010), “Lithium batteries: Status, prospects and future”, Journal of Power Sources, 195 (9), 2419–2430.

[22] Köhler U., Kümpers J., Ullrich M., (2002), “High performance nickel-metal hydride and lithium-ion batteries”, Journal of Power Sources, 105 (1), 139–144.

[23] Nazri G. A., Pistoia G., (2008), “Lithium Batteries, Science and Technology”, 1st Edition, Springer Science & Business Media.

[24] Sasaki T., Ukyo Y., Novák P., (2013), “Memory effect in a lithium-ion battery”, Nature Materials, 12 (6), 569–575

[25] Rao R., Vrudhula S., Rakhmatov D. N., (2003), “Battery modeling for energy aware system design”, Computer, 36 (12), 77–87.

[26] Rakhmatov D., (2009), ”Battery voltage modeling for portable systems”, ACM Transactions on Design Automation of Electronic Systems, 14 (2), 1–36.

[27] Jongerden, M., Haverkort, B., (2008), “Battery Modeling”, Technical Report No: BatteryRep4, Faculty of Electrical Engineering, Mathematics and Computer Science, University of Twente, Netherlands.

[28] Newman J., Thomas K. E., Hafezi H., Wheeler D. R., (2003), ”Modeling of lithium-ion batteries”, Journal of Power Sources, 119, 838–843.

[29] Fang W., Kwon O. J., Wang C. Y., (2010), “Electrochemical-thermal modeling of automotive Li-ion batteries and experimental validation using a three-electrode cell”, International Journal of Energy Research, 34 (2), 107–115.

[30] Stetzel K. D., Aldrich L. L., Trimboli M. S., Plett G. L., (2015), “Electrochemical state and internal variables estimation using a reduced-order physics-based model of a lithium-ion cell and an extended Kalman filter”, Journal of Power Sources, 278, 490–505.

[31] Li Y., Liao C., Wang L., Wang L., Xu D., (2014), “Subspace-based modeling and parameter identification of lithium-ion batteries”, International Journal of Energy Research, 38 (8), 1024–1038.

[32] Feinauer J., Brereton T., Spettl A., Weber M., Manke I., Schmidt V., (2015), “Stochastic 3D modeling of the microstructure of lithium-ion battery anodes via Gaussian random fields on the sphere”, Computational Materials Science, 109, 137–146.

[33] Yang X. G., Taenaka B., Miller T., Snyder K., (2010), “Modeling validation of key life test for hybrid electric vehicle batteries”, International Journal of Energy Research, 34 (2), 171–181.

[34] Dubarry M., Vuillaume N., Liaw B. Y., (2010), “Origins and accommodation of cell variations in Li-ion battery pack modelling”, International Journal of Energy Research, 34(2), 216–231.

[35] Xu L., Wang J., Chen Q., (2012), “Kalman filtering state of charge estimation for battery management system based on a stochastic fuzzy neural network battery model”, Energy Conversion and Management, 53 (1), 33–39.

[36] Doyle M., Fuller T. F., Newman J., (1993), “Modeling of galavanostatic charge and discharge of the lithium/polymer/insertion cell”, Journal of the Electrochemical Society, 140 (6), 1526–1533.

[37] Manwell J. F., McGowan J. G., (1994), “Extension of the Kinetic Battery Model for Wind/Hybrid Power Systems”, European Wind Energy Conference, 284–289, Thessaloniki, Greece, 10-14 October.

[38] Jongerden M., Haverkort B., (2009), “Which battery model to use?”, IET Software, 3 (6), 445-457.

[39] Kaj I., Konané V., (2016), “Modelling battery cells under discharge using kinetic and stochastic battery models”, Applied Mathematical Modelling, 40 (17) 1–15.

[40] Landstorfer M., Jacob T., (2013), “Mathematical modeling of intercalation batteries at the cell level and beyond”, Chemical Society Reviews, 42 (8), 3234–52.

[41] Ramadesigan V., Northrop P. W. C., De S., Santhanagopalan S., Braatz R. D., Subramanian V. R., (2012), “Modeling and Simulation of Lithium-Ion Batteries from a Systems Engineering Perspective”, Journal of the Electrochemical Society, 159 (3), 31–45.

[42] Andre D., Meiler M., Steiner K., Walz H., Soczka-Guth T., Sauer D. U., (2011), ” Characterization of high-power lithium-ion batteries by electrochemical impedance spectroscopy. II: Modelling”, Journal of Power Sources, 196 (12), 5349–5356.

[43] Chen M., Rincon-Mora G. A., (2006), “Accurate Electrical Battery Model Capable of Predicting Runtime and I – V Performance”, IEEE Transactions on Energy Conversion, 21 (2), 504–511.

[44] Dubarry M., Liaw B. Y., (2007), “Development of a universal modeling tool for rechargeable lithium batteries”, Journal of Power Sources, 174 (2), 856–860.

[45] Smith K., Kim G. H., Darcy E., Pesaran A., (2010), “Thermal/electrical modeling for abuse-tolerant design of lithium ion modules”, International Journal of Energy Research, 34 (2), 204–215.

[46] He H., Zhang X., Xiong R., Xu Y., Guo H., (2012), “Online model-based estimation of state-of-charge and open-circuit voltage of lithium-ion batteries in electric vehicles”, Energy, 39 (1), 310–318.

[47] Samadani E., Mastali M., Farhad S., Fraser R. A., Fowler M., (2015), “Li ion battery performance and degredation in electric vehicles under different usage scenarios”, International Journal of Energy Research, 31 (4), 135–147.

[48] Gomez J., Nelson R., Kalu E. E., Weatherspoon M. H., Zheng J. P., (2011), “Equivalent circuit model parameters of a high-power Li-ion battery: Thermal and state of charge effects”, Journal of Power Sources, 196 (10), 4826–4831.

[49] Sarikurt T., Ceylan M., Balikci A., (2014), “An Analytical Battery State of Health Estimation Method”, ”, IEEE International Symposium on Industrial Electronics, ISIE, 1605–1609, Istanbul, Turkey, 1-4 June.

[50] Doerffel D., Sharkh S. A., (2006), “A critical review of using the Peukert equation for determining the remaining capacity of lead-acid and lithium-ion batteries”, Journal of Power Sources, 155 (2), 395–400.

[51] Vetter J., Novák P., Wagner M. R., Veit C., Möller K. C., Besenhard J. O., Hammouche A., (2005), “Ageing mechanisms in lithium-ion batteries”, Journal of Power Sources, 147 (1-2), 269–281.

[52] Hatzell K. B., Sharma A., Fathy H. K., (2012), “A survey of long-term health modeling, estimation, and control of Lithium-ion batteries: Challenges and opportunities”, American Control Conference, 584–591, Montreal, Canada, 27-29 June.

[53] Berecibar M., Gandiaga I., Villarreal I., Omar N., Van Mierlo J., Van Den Bossche, P., (2016), “Critical review of state of health estimation methods of Li-ion batteries for real applications”, Renewable and Sustainable Energy Reviews, *56 (1),* 572–587.

[54] Fei Z., Guangjun L., Lijin F., (2009), “Battery state estimation using Unscented Kalman Filter”, IEEE International Conference on Robotics and Automation, ICRA ’09, 1863–1868, Kobe, Japan, 12-17 May.

[55] Lee S., Kim J., Lee J., Cho B. H., (2008), “State-of-charge and capacity estimation of lithium-ion battery using a new open-circuit voltage versus state-of-charge”, Journal of Power Sources, 185 (2), 1367–1373.

[56] Plett G. L., (2004), “Extended Kalman filtering for battery management systems of LiPB-based HEV battery packs, Part 3. State and parameter estimation”, Journal of Power Sources, 134 (2), 277–292.

[57] Remmlinger J., Buchholz M., Soczka-Guth T., Dietmayer K., (2013), “On-board state-of-health monitoring of lithium-ion batteries using linear parameter-varying models”, Journal of Power Sources, 239, 689–695.

[58] Kim I.-S., (2010), “A technique for estimating the state of health of lithium batteries through a dual-sliding-mode observer”, IEEE Transactions on Power Electronics, 25 (4), 1013–1022.

[59] Singh P., Reisner D., (2002), “Fuzzy logic-based state-of-health determination of lead acid batteries”, 24th Annual International Telecommunications Energy Conference, INTELEC, Montreal, Que., Canada, 29 September-3 October.

[60] Zenati A., Desprez P., Razik H., (2010), “Estimation of the SOC and the SOH of Li-ion batteries, by combining impedance measurements with the fuzzy logic inference”, IECON Proceedings (Industrial Electronics Conference), 1773–1778, Glendale, AZ, USA, 7-10 November.

[61] Schweiger H.-G., Obeidi O., Komesker O., Raschke A., Schiemann M., Zehner C., Birke P., (2010), “Comparison of several methods for determining the internal resistance of lithium ion cells”, Sensors, 10 (6), 5604–5625.

[62] Waag W., Fleischer C., Sauer D. U., (2014), “Critical review of the methods for monitoring of lithium-ion batteries in electric and hybrid vehicles”, Journal of Power Sources, 258, 321–339.

[63] Wei X., Zhu B., Xu W., (2009), “Internal resistance identification in vehicle power lithium-ion battery and application in lifetime evaluation”, International Conference on In Measuring Technology and Mechatronics Automation, ICMTMA’09, 388–392hangjiajie, China, 11-12 April.

[64] Blanke H., Bohlen O., Buller S., De Doncker R. W., Fricke B., Hammouche A., Sauer D. U., (2005), “Impedance measurements on lead–acid batteries for state-of-charge, state-of-health and cranking capability prognosis in electric and hybrid electric vehicles”, Journal of Power Sources, 144 (2), 418–425.

[65] Galeotti M., Giammanco C., Cinà L., Cordiner S., Di Carlo, A., (2015), “Synthetic methods for the evaluation of the State of Health (SOH) of nickel-metal hydride (NiMH) batteries”, Energy Conversion and Management, 92, 1–9.

[66] Kozlowski J. D., (2003), “Electrochemical Cell Prognostics using Online Impedance Measurements and Model-Based Data Fusion Techniques”, IEEE Aerospace Conference, 3257–3270, Big Sky, MT, USA, 8-15 March.

[67] Andre D., Meiler M., Steiner K., Wimmer C., Soczka-Guth T., Sauer D. U., (2011), “Characterization of high-power lithium-ion batteries by electrochemical impedance spectroscopy. I. Experimental investigation”, Journal of Power Sources, 196 (12), 5334–5341.

[68] Goebel K., Saha B., Saxena A., Celaya J. R., Christophersen J. P., (2008), “Prognostics in Battery Health Management”, IEEE Instrumentation Measurement Magazine, 11 (4), 33–40.

[69] Onori S., Spagnol P., Marano V., Guezennec Y., Rizzoni G., (2012), “A new life estimation method for lithium-ion batteries in plug-in hybrid electric vehicles applications”, International Journal of Power Electronics, 4 (3), 302-319.

[70] Feng X., Li J., Ouyang M., Lu L., Li J., He X., (2013), “Using probability density function to evaluate the state of health of lithium-ion batteries”, Journal of Power Sources, 232, 209–218.

[71] Ng K. S., Moo C. S., Chen Y. P., Hsieh Y. C., (2009), “Enhanced coulomb counting method for estimating state-of-charge and state-of-health of lithium-ion batteries”, Applied Energy, 86 (9), 1506–1511.

[72] Spotnitz R., (2003)”, Simulation of capacity fade in lithium-ion batteries”, Journal of Power Sources, 113, 72–80.

[73] Yang Y., Hu T., (2007), “A New Energy Management System of Directly-Driven Electric Vehicle with Electronic Gearshift and Regenerative Braking”, American Control Conference, 4419–4424, New York City, USA, 11-13 July.

[74] Sciaretta A., Guzzella L., (2007), “Control of Hybrid Electric Vehicles”, Control Systems, IEEE, 27 (2), 60–70.

[75] Gonder J., Markel T., (2007), “Energy Management Strategies for Plug-In Hybrid Electric Vehicles Distance”, SAE World Congress, 1–5, Detroit, MI, USA, 26-19 April.

[76] Musardo C., Rizzoni G., Guezennec Y., Staccia B., (2005), “A-ECMS: An Adaptive Algorithm for Hybrid Electric Vehicle Energy Management”, European Journal of Control, 11 (4-5), 509–524.

[77] Zhang R., Chen Y., (2001), “Control of Hybrid Dynamical Systems for Electric Vehicles” American Control Conference, 1–6, Arlington, VA, USA, 25-27 June.

[78] Barsali S., Miulli C., Possenti A., (2004), “A Control Strategy to Minimize Fuel Consumption of Series Hybrid Electric Vehicles”, IEEE Transactions on Energy Conversion, 19 (1), 187–195.

[79] Delprat S., Lauber J., Guerra T. M., Rimaux J., (2004), “Control of a Parallel Hybrid Powertrain: Optimal Control”, IEEE Transactions on Vehicular Technology, 53 (3), 872–881.

[80] Guzzella L., Sciarretta A., (2013), “Vehicle Propulsion Systems”, 3rd Edition, Springer Berlin Heidelberg.

[81] Baumann B. M., Washington G., Glenn B. C., Rizzoni G., (2000), “Mechatronic design and control of hybrid electric vehicles”, IEEE/ASME Transactions on Mechatronics, 5 (1), 58–72.

[82] Schouten N. J., Salman M. A., Kheir N. A., (2002), “Fuzzy logic control for parallel hybrid vehicles”, IEEE Transactions on Control Systems Technology, 10 (3), 460–468.

[83] Tate E. D., Boyd S. P., (1998), “Finding Ultimate Limits of Performance for Hybrid Electric Vehicles”, SAE Transactions, 109, 2884–2889.

[84] Hofman T., van Druten R., (2004), “Energy Analysis of Hybrid Vehicle Powertrains”, IEEE International Symposium of Vehicular Power Propulsion, 1–8, Paris, France, 6-8 October.

[85] Lin C., Peng H., Grizzle J. W., Kang J.-M., (2003), “Power management strategy for a parallel hybrid electric truck”, IEEE Transactions on Control Systems Technology, 11 (6), 839–849.

[86] Kolmanovsky I., Siverguina I., Lygoe B., (2002), “Optimization of powertrain operating policy for feasibility assessment and calibration: stochastic dynamic programming approach”, American Control Conference, 1425–1430, Anchorage, AK, USA, 8-10 May.

[87] Johnson, V., Wipke, K., Rausen, D., (2000), “HEV Control Strategy for Real-Time Optimization of Fuel Economy and Emissions”, SAE, Future Car Congress, 1677-1690, Arlington, VA, USA 2-6 April.

[88] Sciarretta A., Guzzella L., (2007), “Control of Hybrid Electric Vehicles”, IEEE Control Systems Magazine, 27(2), 60–70.

[89] Schouten N. J., Salman M. A., Kheir N. A., (2003), “Energy management strategies for parallel hybrid vehicles using fuzzy logic”, Control Engineering Practice, 11, 171–177.

[90] Back M., Simons M., Kirschaum F., Krebs V., (2002), “Predictive Control of Drivetrains”, IFAC Proceedings, 35(1), 241-246.

[91] Lin C., Pengl H., Grizzle J. W., (2004), “A Stochastic Control Strategy for Hybrid Electric Vehicles”, American Control Conference, 4710–4715, Boston, MA, USA, 30 June-2 July.

[92] Koot M., Kessels J. T. B. A., de Jager B., Heemels W. P. M. H., van den Bosch P. P. J., Steinbuch M., (2005), “Energy Management Strategies for Vehicular Electric Power Systems”, IEEE Transactions on Vehicular Technology, 54 (3), 771–782.

[93] Paganelli G., Ercole G., Brahma A., Guezennec Y., Rizzoni G., (2001), “General supervisory control policy for the energy optimization of charge-sustaining hybrid electric vehicles”, JSAE Review, 22 (4), 511–518.

[94] Arsie I., Graziosi M., Pianese C., Rizzo G., Sorrentino M., (2004), “Optimization of Supervisory Control Strategy for Parallel Hybrid Vehicle with Provisional Load Estimate”, AVEC04, 483–488, Arnhem, The Netherlands, 23-27 August.

[95] Jeon S., Jo S., Park Y., Lee J., (2002), “Multi-Mode Driving Control of a Parallel Hybrid Electric Vehicle Using Driving Pattern Recognition”, Journal of Dynamic Systems, Measurement, and Control, 124 (1), 141.

[96] Kleimaier A., Schroder D., (2002), “An approach for the online optimized control of a hybrid powertrain”, 7th International Workshop on Advanced Motion Control. Proceedings, 215–220, Maribor, Slovenia, 3-5 July.

[97] Burke A., (2000), “Ultracapacitors: why, how, and where is the technology”, Journal of Power Sources, 91 (1), 37–50.

[98] Kuperman A., Aharon I., (2011), “Battery-ultracapacitor hybrids for pulsed current loads: A review”, Renewable and Sustainable Energy Reviews, 15 (2), 981–992.

[99] Kuperman A., Aharon I., Kara A., Malki S., (2011), “A frequency domain approach to analyzing passive battery–ultracapacitor hybrids supplying periodic pulsed current loads”, Energy Conversion and Management, 52 (12), 3433–3438.

[100] Penella M. T., Gasulla M., (2010), “Runtime Extension of Low-Power Wireless Sensor Nodes Using Hybrid-Storage Units”, IEEE Transactions on Instrumentation and Measurement, 59 (4), 857–865.

[101] Dougal R. A., Liu S., White R. E., (2002), “Power and Life Extension of Battery – Ultracapacitor Hybrids”, IEEE Transactions on Components and Packaging Technologies, 25 (1), 120–131.

[102] Zheng J. P., Jow T. R., Ding M. S., (2001), “Hybrid Power Sources for Pulsed Current Applications”, IEEE Transactions on Aerospace and Electronic Systems, 37 (1), 288–292.

[103] Khaligh A., Li, Z., (2010), “Battery, Ultracapacitor, Fuel Cell, and Hybrid Energy Storage Systems for Electric, Hybrid Electric, Fuel Cell, and Plug-In Hybrid Electric Vehicles: State of the Art”, IEEE Transactions on Vehicular Technology, 59 (6), 2806–2814.

[104] Gao L., Dougal R. A., Liu S., (2005), “Power enhancement of an actively controlled battery/ultracapacitor hybrid”, IEEE Transactions on Power Electronics, 20 (1), 236–243.

[105] Govindaraj A., Lukic S. M., Emadi, A., (2009), “A novel scheme for optimal paralleling of batteries and ultracapacitors”, IEEE Energy Conversion Congress and Exposition, 1410–1416, San Jose, CA, USA, 20-24 September.

[106] Ortúzar M., Moreno J., Dixon J., (2007), “Ultracapacitor-based auxiliary energy system for an electric vehicle: Implementation and evaluation”, IEEE Transactions on Industrial Electronics, 54 (4), 2147–2156.

[107] Camara M. B., Gualous H., Gustin F., Berthon A., (2008), “Design and new control of DC/DC converters to share energy between supercapacitors and batteries in hybrid vehicles”, IEEE Transactions on Vehicular Technology, 57 (5), 2721–2735.

[108] Amjadi Z., Williamson S. S., (2010), “Power-Electronics-Based Solutions for Plug-in Hybrid Electric Vehicle Energy Storage and Management Systems”, IEEE Transactions on Industrial Electronics, 57 (2), 608-616.

[109] Gao Y., Ehsani, M., (2006), “Parametric design of the traction motor and energy storage for series hybrid off-road and military vehicles”, IEEE Transactions on Power Electronics, 21 (3), 749–755.

[110] Lu S., Corzine K. A., Ferdowsi M., (2007), “A new battery/ultracapacitor energy storage system design and its motor drive integration for hybrid electric vehicles”, IEEE Transactions on Vehicular Technology, 56 (4), 1516–1523.

[111] Solero L., Lidozzi A., Pomilio J. A., (2005), “Design of multiple-input power converter for hybrid vehicles”, IEEE Transactions on Power Electronics, 20 (5), 1007–1016.

[112] Schupbach R. M., Balda J. C., Zolot M., Kramer B., (2003), “Design Methodology of a Combined Battery-Ultracapacitor Energy Storage Unit for Vehicle Power Management”, Power Electronics Specialists Conference, PESC, 88–93, Acopulco, Mexico, 15-19 June.

[113] Zhang Y., Jiang Z., Yu X., (2008), “Control Strategies for Battery/Supercapacitor Hybrid Energy Storage Systems”, IEEE Energy 2030 Conference, 1–6. Atlanta, GA, USA, 17-18 November.

[114] Wang L., Li H., (2010), “Maximum fuel economy-oriented power management design for a fuel cell vehicle using battery and ultracapacitor”, IEEE Transactions on Industry Applications, 46 (3), 1011–1020.

[115] Jarvis L. P., Atwater T. B., J. Cygan P., (1999), “Fuel cell/electrochemical capacitor hybrid for intermittent high power applications”, Journal of Power Sources, 79 (1), 60–63.

[116] Atwater T. B., Cygan P. J., Leung F. C., (2000), “Man portable power needs of the 21st century I. Applications for the dismounted soldier . II . Enhanced capabilities through the use of hybrid power sources”, Journal of Power Sources, 91 (1), 27–36.

[117] Smith T. A., Mars J. P., Turner G. A., (2002), “Using supercapacitors to improve battery performance”, Power Electronics Specialists Conference, PESC, 124–128, Cairns, QLD, Australia, 23-27 June.

[118] Holland C. E., Weidner J. W., Dougal R. a., White R. E., (2002), “Experimental characterization of hybrid power systems under pulse current loads”, Journal of Power Sources, 109 (1), 32–37.

[119] Sikha G., White R. E., Popov B. N., (2005), “A Mathematical Model for a Lithium-Ion Battery/Electrochemical Capacitor Hybrid System”, Journal of the Electrochemical Society, 152 (8), 1682-1693.

[120] Michalczuk M., Grzesiak L. M., Ufnalski B., (2012), “A lithium battery and ultracapacitor hybrid energy source for an urban electric vehicle”, Przeglad Elektrotechniczny (Electrical Review), 88 (4), 158–162.

[121] Altemose G., Hellermann P., Mazz, T., (2011), “Active cell balancing system using an isolated share bus for Li-Ion battery management: Focusing on satellite applications”, IEEE Long Island Systems, Applications and Technology Conference, LISAT, 1-7, Farmingdale, NY, USA, 4 May.

[122] Caricchi F., Crescimbini F., Capponi F. G., Solero L., (1998), “Study of bi-directional buck-boost converter topologies for application in electrical vehicle motor drives”, APEC ’98 Thirteenth Annual Applied Power Electronics Conference and Exposition, 287-293, Anaheim, CA, USA, 15-19 February.

[123] Schupbach R. M., Balda J. C., (2003), “Comparing DC-DC converters for power management in hybrid electric vehicles”, Electric Machines and Drives Conference, IEMDC’03, 1369-1374, Madison, WI, USA, 1-4 June.

[124] Cuk S., (1983), “A New Zero-Ripple Switching DC-to-DC Converter and Integrated Magnetics”, IEEE Transactions on Magnetics, 19 (2), 57–75.

[125] Du Y., Lukic S., Jacobson B., Huang A., (2011), “Review of high power isolated bi-directional DC-DC converters for PHEV/EV DC charging infrastructure”, IEEE Energy Conversion Congress and Exposition, 553–560, Phoenix, AZ, USA, 17-22 September.

[126] Yoo H., Sul S.-K., Park Y., Jeong J., (2008), “System Integration and Power Flow Management for a Series Hybrid Electric Vehicle Using Super-capacitors and Batteries”, IEEE Transactions on Industry Applications, 44 (1), 108–114.

[127] Czogalla J., Li J. L. J., Sullivan C. R., (2003), “Automotive Application of Multi-Phase Coupled-Inductor DC-DC Converter”, 38th IAS Annual Meeting on Conference Record of the Industry Applications Conference, 1524–1529, Salt Lake City, UT, USA, 12-16 October.

[128] Waffler S., Kolar J. W., (2008), “A novel low-loss modulation strategy for high-power Bi-directional buck+Boost converters”, 7th International Conference on Power Electronics, ICPE’07, 889–894, Daegu, South Korea, 22-26 October.

[129] Khan M. A., Husain I., Sozer Y., (2012), “A bi-directional DC-DC converter with overlapping input and output voltage ranges and vehicle to grid energy transfer capability”, IEEE Journal of Emerging and Selected Topics in Power Electronics, 2 (3), 507-516.

[130] Khan M. A., Ahmed A., Husain I., Sozer Y., Badawy M., (2015), “Performance Analysis of Bidirectional DC – DC Converters for Electric Vehicles”, IEEE Transactions on Industry Applications, 51 (4), 3442–3452.

[131] Cuzner R. M., Bendre A. R., Faill P. J., Semenov B., (2007), “Implementation of a non-isolated three level DC/DC converter suitable for high power systems”, Conference Record - IAS Annual Meeting, 2001–2008, New Orleans, LA, USA, 23-27 September.

[132] Ruan X., Li B., Chen Q., Tan S. C., Tse C. K., (2008), “Fundamental considerations of three-level DC-DC converters: Topologies, analyses, and control”, IEEE Transactions on Circuits and Systems I: Regular Papers, 55 (11), 3733–3743.

[133] Yalamanchili K. P., Ferdowsi M., (2005), “Review of multiple input DC-DC converters for electric and hybrid vehicles”, IEEE Vehicle Power and Propulsion Conference, 552–555, Chicago, IL, USA, 7-9 September.

[134] Wang K., Lin C. Y., Zhu L., Qu D., Lee F. C., Lai J. S., (1998), “Bi-directional DC to DC converters for fuel cell systems”, Power Electronics in Transportation, 10, 47–51.

[135] Garcia O., Flores L. A., Oliver J. A., Cobos J., de la Pena J., (2005), “Bi-directional DC/DC Converter for Hybrid Vehicles”, IEEE 36th Conference on Power Electronics Specialists, 1881–1886, Recife, Brazil, 12-18 June.

[136] Zhu L., (2004), “A novel soft-commutating isolated boost full-bridge ZVS-PWM DC-DC converter for bi-directional high power applications”, IEEE Annual Power Electronics Specialists Conference, 2141–2146, Orlando, FL, USA, 17-21 June.

[137] Jang S.-J., Lee T. W., Lee W. C., Won C. Y., (2004), “Bi-directional dc-dc converter for fuel cell generation system”, Power Electronics Specialists Conference, PESC 04, 4722–4728, Aachen, Germany, 20-26 June.

[138] Li H. L. H., Peng F. Z., Lawler J. S., (2001), “A natural ZVS high-power bi-directional DC-DC converter with minimum number of devices”, IEEE Industry Applications Conference. 36th IAS Annual Meeting, 1874–1881, Chicago, IL, USA, 30 September-4 October.

[139] Inoue S., Akagi H., (2007), “A bidirectional DC-DC converter for an energy storage system with galvanic isolation”, IEEE Transactions on Power Electronics, 22 (6), 2299–2306.

[140] Morrison R., Egan M. G., (2000), “A new power-factor-corrected single-transformer UPS design”, IEEE Transactions on Industry Applications, 36 (1), 171–179.

[141] Xu X., Khambadkone A. M., Oruganti R., (2007), “A soft-switched back-to-back bi-directional DC/DC converter with a FPGA based digital control for automotive applications”, International Conference On Industrial Electronics Society, IECON, 262-267, Taipei, Taiwan, 5-8 November.

[142] Du Y., Zhou X., Bai S., Lukic S., Huang A., (2010), “Review of non-isolated bi-directional DC-DC converters for plug-in hybrid electric vehicle charge station application at municipal parking decks”, IEEE Applied Power Electronics Conference and Exposition, APEC, 1145–1151, Palm Springs, CA, USA, 21-25 February.

[143] Kumar L., Jain S., (2013), “Multiple-input DC/DC converter topology for hybrid energy system”, Power Electronics, IET, 6 (8), 1483–1501.

[144] Wei X. Z., Zhao X., Haifeng D., (2009), “The application of flyback DC/DC converter in Li-ion batteries active balancing”, 5th IEEE Vehicle Power and Propulsion Conference, VPPC ’09, 1654–1656, Dearborn, MI, USA, 7-11 September.

[145] Karnjanapiboon C., Jirasereeamornkul K., Monyakul V., (2010), “The high efficiency charge equalized system for serially connected VRLA battery string using synchronous flyback converter”, International Power Electronics Conference, ECCE Asia, IPEC, 1185–1188, Sapporo, Japan, 21-24 June.

[146] Lee J. J., Kwon J. M., Kim E. H., Choi W. Y., Kwon B. H., (2008), “Single-stage single-switch PFC flyback converter using a synchronous rectifier”, IEEE Transactions on Industrial Electronics, 55 (3), 1352–1365.

[147] Koo G.-B., (2006), “Application Note AN-4147 Design Guidelines for RCD Snubber of Flyback Converters”, Technical Report No: AN 4147, Fairchild Semiconductor.

BIOGRAPHY

Türev SARIKURT was born in İzmir in 1983. He received the B. Sc. degree in Electrical and Electronics Engineering from İstanbul University, İstanbul, in 2006. He has the M. Sc. degree from Department of Electronics Engineering, Graduate School of Natural and Applied Sciences, Gebze Institute of Technology in 2010. Between 2010 and 2016, he worked as research assistant in Department of Electronics Engineering, Gebze Technical University. Since 2016 he works as a specialist researcher on battery management systems in TÜBİTAK Marmara Research Centre.

APPENDICES

APPENDIX A: List of publications during this study.

Ceylan M., Sarikurt T., Balikci A., (2013). “Elektrikli araçlarda kullanilan lityum - iyon bataryalar için model geliştirilmesi”, 5. Enerji Verimliliği ve Kalitesi Kongresi, 82–87, Kocaeli, Türkiye, 23-24 May.

Ceylan M., Sarikurt T., Balikci A., (2014). “A Novel Lithium-Ion-Polymer Battery Model for Hybrid / Electric Vehicles”, IEEE International Symposium on Industrial Electronics, ISIE, 366–369, Istanbul, Turkey, 1-4 June.

Sarikurt T., Ceylan M., Balikci A., (2014), “An Analytical Battery State of Health Estimation Method”, ”, IEEE International Symposium on Industrial Electronics, ISIE, 1605–1609, Istanbul, Turkey, 1-4 June.

Sarikurt T., Ceylan M., Balikci A., (2014). “A Hybrid Battery Model and State of Health Estimation Method for Lithium-Ion Batteries”, IEEE International Energy Conference, ENERGYCON, 1349–1356, Dubrovnik, Croatia, 13-16 May.

Sarikurt T., Balikci A., (2015), “A novel battery system for electric vehicles”, In: I. Dincer, M. A. Ezan, C. O. Colpan, O. Kizilkan Editors, “Progress in Clean Energy, Volume 2, Novel Systems and Applications”, Springer International Publishing.